Universitat Autònoma de Barcelona

TESIS DOCTORAL

Vertically-aligned ZnO Nanostructures for excitonic Solar Cells

DEFENDED BY:

Irene González Valls

THESIS DIRECTOR:

Dra. Mónica Lira Cantú

TUTOR:

Dra. Maria Muñoz Tapia

PROGRAMA DE DOCTORAT EN CIÈNCIA DE MATERIALS

DEPTARTAMENT DE QUÍMICA

FACULTAT DE CIÈNCIES

2013

CIN2 CENTRE D'INVESTIGACIÓ EN NANOCIÈNCIA I NANOTECNOLOGIA

CSIC

Centre d'Investigació en Nanociència i Nanotecnologia CIN2 (CSIC-ICN)
Consejo Superior de Investigaciones Científicas
Campus UAB
08193 Bellaterra, Barcelona

Universitat Autònoma de Barcelona
Departament de Química
08193 Bellaterra, Barcelona

Memòria presentada per aspirar al Grau de Doctor per Irene González Valls:

Irene González Valls

Dra Mónica Lira-Cantu, responsable del grup Laboratory of Nanostructured Materials for Photovoltaic Energy, en el Centre d'Investigació en Nanociència i Nanotecnologia CIN2 (CSIC-ICN).

Certifica que el treball descrit en aquesta tesis titulada: **"Vertically-aligned ZnO nanostructures for Excitonic Solar Cells"** presentada per Irene González Valls per optar al grau de Doctor, ha estat realitzada sota la meva direcció.

Dra. Mónica Lira Cantú

Vist i plau de la Tutora de tesis:

Dra. Maria Muñoz Tapia

Bellaterra, 25 d' abril de 2013

Als meus pares, al Paco i l'Albert

"Learn from yesterday, live for today,
hope for tomorrow. The important thing is
not to stop questioning."

Albert Einstein

Contents

Abstract

Solar energy converts the sunlight into electricity and is one of the most encouraging renewable, CO_2-free and low cost alternative energy source to fossil fuels. Among the different photovoltaic devices the third-generation excitonic solar cells (XSCs), which include organic, hybrid and dye-sensitized solar cells, are promising devices for the achievement of the three main criteria that would lead to large scale commercialization: high efficiency, low cost and the possibility to apply simple and scalable fabrication techniques.

The application of ZnO in XSCs has been rising over the last few years due to its similarities with the most studied semiconductor oxide, TiO_2. ZnO presents comparable bandgap values and conduction band position as well as higher electron mobility than TiO_2. It can be synthesized in a wide variety of nanoforms applying straight forward and scalable synthesis methodologies. Specially, the application of vertically-aligned ZnO nanostructures it is thought to improve contact between the donor and acceptor material in organic solar cells (OSC), or improve electron injection in Dye sensitized solar cells (DSCs).

The present thesis focuses on the preparation and characterization of ZnO nanostructures: nanorods (NR), nanotrees (NTr) and core-shells (CS) and their application in DSCs and OSCs. The optimization of the solar cell parameters to enhance its performance is also presented here.

Abbreviations & Symbols

AAO	Anodic aluminum oxide
ACN	Acetonitrile
Ag	Silver
A-HM	Autoclave hydrothermal method
ALD	Atomic layer deposition
Ar	Argon
ATR-FTIR	Attenuated total reflectance infrared
BHJ	Bulk heterojunction
CB	Conduction band
CBD	Chemical bath deposition
CBE	Chemical beam epitaxy
CVD	Chemical vapor deposition
CE	Counter electrode
CS	Core-shell
DEA	Diethanolamine
DLE	Deep level emission
DLT	Dye-loading time
DSC	Dye-sensitized solar cell
e^-	Electron
EBPVD	Electron beam physical vapor deposition
EDS	Energy disperse x-ray spectroscopy
EDX	Energy disperse x-ray Spectroscopy
E_g	Band gap
EQE	External quantum efficiency
ETM	Electron transport material
FF	Fill factor (%)
FTO	Fluorinated indium tin oxide
η	efficiency
h	Hour
HMT	Hexamethylenetetramine
HT	Hydrothermal method
HTM	Hole transport material
HSC	Hybrid solar cell
In	Indium
IPCE	Incident photon to current efficiency
ISC	Inorganic solar cell
ITO	Indium-tin oxide
IV-curves	Current-Voltage curves
J_{sc}	Short-circuit current density ($mA\cdot cm^{-2}$)
JV-curves	Current density-Voltage curves
K_B	Boltzmann's constant
LCVD	Laser chemical vapor deposition
LHM	Light harvesting material
LT-HM	Low temperature hydrothermal method
min	Minute
MOCVD	Metal organic chemical vapor deposition
NBE	Near band edge
N719	dye $(Bu_4N)_2$ $Ru(debpyH)_2(NCS)$
NP	Nanoparticle
NR	Nanorod
ns	nanoseconds
NT	Nanotube
NTr	Nanotrees
NW	Nanowire
OAG	Oxide assisted growth
0-DCB	o-Dichlorobenzene
O_i	Oxygen intersticial defects
OPV	Organic photovoltaic cell
OSC	Organic solar cell
O_{vac}	Oxygen vacancy defects
PACVD	Plasma assisted chemical vapor deposition

PCE	Power conversion efficiency (%)
P_{in}	Power incident light
PL	Photoluminescence
PLD	Pulsed laser deposition
P_{max}	Power at the maximum power point
ps	picoseconds
PSC	Polymer solar cell
Pt	Platinum
PVD	Physical vapor deposition
rpm	Revolutions per minute
R_s	Series resistance
R_{sh}	Shunt resistance
QD	Quantum dot
QDSC	Quantum dot solar cell
QW	Quantum well
s	Second
S	Sulfur
SAED	Selected-area electron diffraction
SEM	Scanning electron microscopy
SILAR	Successive ion layer adsoption and reaction
^{t}BuOH	tert-Buthyl alcohol
ss-DSC	solid-state Dye-sensitized solar cell
T	Temperature
TCO	Transparent conductive oxide
TEM	Transmission electron microscopy
TGA	Thermogravimetric analysis
TRPL	Time resolved photoluminescence
UV	Ultraviolet
VB	Valence band
VLS	Vapor-liquid-solid
VPE	Vapor phase epitaxy
V_{oc}	Open-circuit voltage (V)
VS	Vapor –solid
VSS	Vapor-solid-solid
XRD	X-ray diffraction
XSC	Excitonic solar cell
Zn_i	Zinc intersticial defects
Zn_{vac}	Zinc vacancy defects

Synonyms

Dye-sensitized solar cells (DSC)	Grätzel cells
Efficiency	Power Conversion Efficiency
Electron Transport Material (ETM)	Acceptor material
Hole Transport Material (HTM)	Donor material
Isopropanol	2-propanol
IPCE	EQE
n-type material	Electron Transport Material (ETM)
Organic solar cells (OSC)	Organic photovoltaic cells (OPV)
Organic solar cells (OSC)	Polymer solar cells (PSC)
p-type material	Hole Transport Material (HTM)
Quantum dot (QD)	Quantum well (QW)
Solar Cell (SC)	Photovoltaic Cell (PV)
Dye loading time	Dye immersion time

List of Figures

List of Tables

Chapter 1
Introduction

1.1 Solar Energy

Interest in clean energy sources is growing nowadays due to the increasing energy demand, the climate change and to promote a sustainable scenario. Several renewable energy sources are being developed such as biomass, wind, hydroelectricity, geothermal and solar. Among them solar energy is an attractive source since it is available, abundant and CO_2-free.[1, 2] The world energy consumption, reported by the International Energy Agency in 2007[3] (see Figure 1.1), reveals that non-renewable energies encompass the ~87% of the total consumption, highly exceeding the reported 13% consumption from the renewable sources.[3] On the other hand, solar energy has a very small role on the overall energy scene (only 0.039 %). Nevertheless, recent published road-maps on energy for the year 2011, demonstrates a 2.5% increase on energy consumption respect to the previous reports, and a similar world energy consumption scenario. The use of oil and nuclear energies slightly decreased from 34.3% and 6.5%, to 32.8% and 5.8% respectively. Probably nuclear energy will further decrease in the following years after the catastrophic accident at the Fukushima Nuclear plant in Japan in 2011. However, the utilization of coal energy source incremented from 25.1% to 27.2% and the natural gas was maintained at 20.9%. Renewable energy sources slightly increased from 13.1% to 13.3%. A promising result is the increased use of solar energy, an increase of 86.3% (from 0.039% to 0.07%) respect the previous report, yet it is only a 0.07% of the total energy statistic value.[4, 5] Thus, an enormous effort is being invested nowadays in order to modify the world energy consumption trend and to increment the use of renewable sources, specially, in a near future where an increasing energy demand and the almost exhaustion of fossil fuels is envisaged.

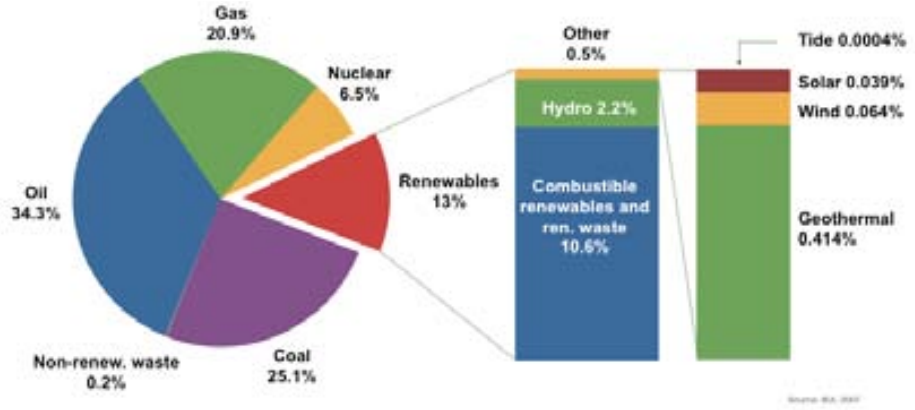

Figure 1.1 World Energy consumption of the different energy sources. Non-renewables: coal, oil, gas and nuclear and renewables: hydroelectricity, biomass, solar, wind and geothermal.[3]

1.1.1 Energy from the sun: the possibilities

The total energy consumption of the world is today ~14 TW (terawatts, TW = 14 x 10^{12} watts), and it has been calculated to increase up to 30 TW by the year 2050. Thus, renewable energy (Eolic, solar, etc.) is the best alternative for the future, being solar energy one of the most promising since it is a CO_2-free and abundant source of energy. The Sun radiates on the surface of the earth more than 120 000 TW/year, or an amount of ~13 TW/h, that equals the total energy consumption on the planet in only one year. G. Knies reports that in only 6h the deserts receive more energy from the sun than the energy consumption of the world in one year. Assuming the use of only 1% of the desert or semi-desert areas of the world, the potential for electric energy generation with solar energy (thermal and photovoltaic) should be enough to embrace the annual demand of energy of the world.[6, 7]

1.1.2 Renewable Energy at European level: 20% by 2020

At European level different initiatives have been established in order to reduce greenhouse gas emissions and increase renewable energy use. Besides confronting the climate change, there is a growing concern to reduce the dependence of imported energy and secure our energy supply for the future. In 2007, the 27 EU members adopted the target of 20 % use of renewable energy by the year 2020.[8, 9]

For Spain, the 20% target implies that 45 % of the electricity must come from renewable sources by 2020 (including biofuels). Recent studies revealed that Spain potential to generate this level of energy can be achieved with the efficient combined use of wind and solar energy. The estimation for a baseline scenario is 74750 MW of wind power (59800 MW onshore), 3000 MW of solar PV, and 500 MW of solar thermoelectric.[10, 11]

1.1.3 The cost of Solar Energy

Unfortunately, the cost of solar energy is still too high. Among the different technologies to convert solar energy into electricity, the photovoltaic has a lower price compared to, for example, the hybrid gas-solar technology. The cost of the photovoltaic technology is ~121 €/MWh, while the gas-solar hybrid technology is ~332 €/MWh. Nevertheless, the photovoltaic technology should be reduced in order to be competitive with the conventional energy sources (~61 €/MWh).[12, 13] Thus, current research efforts are being directed towards the production of low-cost, highly efficient and stable photovoltaic devices.[1, 2]

The solution is then, the cost reduction of the current PV technology options. For this, we have to understand that the cost of solar photovoltaics is calculated on the cost of Si-based solar cell technology which is the current technology on the marketplace. Emerging photovoltaic alternatives are being developed in order to cope with lower prices, and their difference with respect to Si-based photovoltaic is the way these technologies adsorb the photon from sunlight. In Si-based solar cells the absorption of light leads to the direct formation of free electron–hole pairs in the bulk of the material and the direct production of charge carriers.[14, 15] In XSCs, the presence of organic semiconductors implies that the absorption of photons from sunlight produces an exciton, a tightly bound electron–hole pair, which must be split for charge generation. Exciton dissociation takes place at the interface between the constituent semiconductors. Thus, XSCs encompass photovoltaic systems largely dependent on interfacial processes. The reliance on the crystallinity of the materials for photovoltaic response indicates that while highly crystalline and chemically pure materials are required for ISCs (e.g. silicon), less pure and therefore less expensive compounds can be applied in XSCs (e.g. TiO_2).[15, 16]

1.1.4 Solar Cell Generations

Current photovoltaic technology can be classified by generations, based on the materials and production used for their fabrication as:

- *First generation*: crystalline silicon (c-Si), which is the 85-90% of the global annual market at present (2011).
- *Second generation:* thin films, currently are present on the 10-15% of the commercial modules (2011). They are subdivided into three groups:
    a) Amorphous Silicon (a-Si)
    b) Cadmium-Telluride (CdTe)
    c) Copper-Indium-Diselenide (CIS) and Copper-Indium-Gallium-Diselenide (CIGS).
- *Third generation:* an emerging technology that uses organic semiconductors. These cells include polymer solar cells, dye-sensitized solar cells and small molecule solar cells, among others. They are also called *excitonic solar cells (XSC)* due to its charge generation mechanism based on to the formation of an exciton.

Figure 1.2 shows the comparison between power efficiency and module cost of the different types of solar cells.[17] *First generation* solar cells require highly pure and highly crystalline silicon to achieve their highest power conversion efficiency, ~20%. The application of different materials than silicon in *second generation* devices permitted a slight cost reduction. However, the inorganic materials from thin films, *second generation,* cells (indium, cadmium, gallium…etc.) are not abundant on the planet and toxic. On the other hand, *third generation* solar cells also reduce the cost of the module preparation due to the application of organic materials that can be less crystalline.

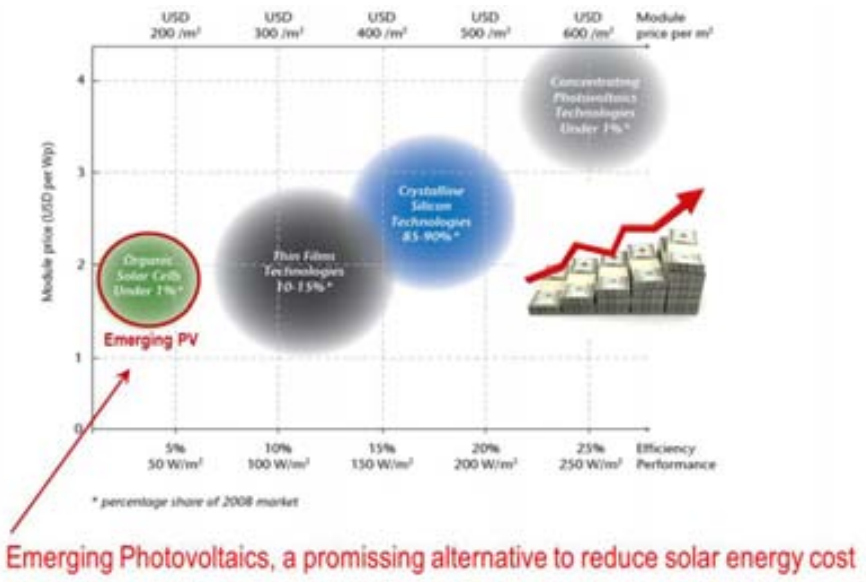

Figure 1.2 Efficiency performance Vs. the module cost of the different types of solar cells.[17]

1.1.5 Solution processing low-temperature water-based techniques for XSC

Emerging solar cells have many other advantages such as large variety of organic materials with different chemical structures easily to be modified by synthesis procedures, can be deposited by simple techniques on flexible substrates and can also be transparent. All those advantages make them very appealing for different applications.[18-22] Some of these applications are the production of textile utilities or for building integration. Yet, the potential for the low cost of these emerging solar cells resides not only on the low price of the materials applied, but due to the low-temperature printing techniques used for their fabrication. The possibility to fabricate XSCs by scalable and low-cost printing techniques makes these devices very attractive, since this is unachievable nowadays on crystalline silicon solar cells. The application of printing techniques like screen printing, roll-to-roll, gravure, offset, lithography, inject, etc., as well as the reduction of the cost, permits the integration of other printing electronic devices such as lighting or batteries to form a complete system (Figure 1.3).[23] The current solar cell cost is 3.2€/W (first generation) and 2.2€/W (second generation). The fabrication cost of the third generation solar cells is constantly decreasing and are estimated to be in 2020 at around 0.5€/W.[17] Thus, *third generation* solar cells are promising alternatives to silicon solar cells and thus, the study of different types of excitonic solar cells are presented in this thesis.

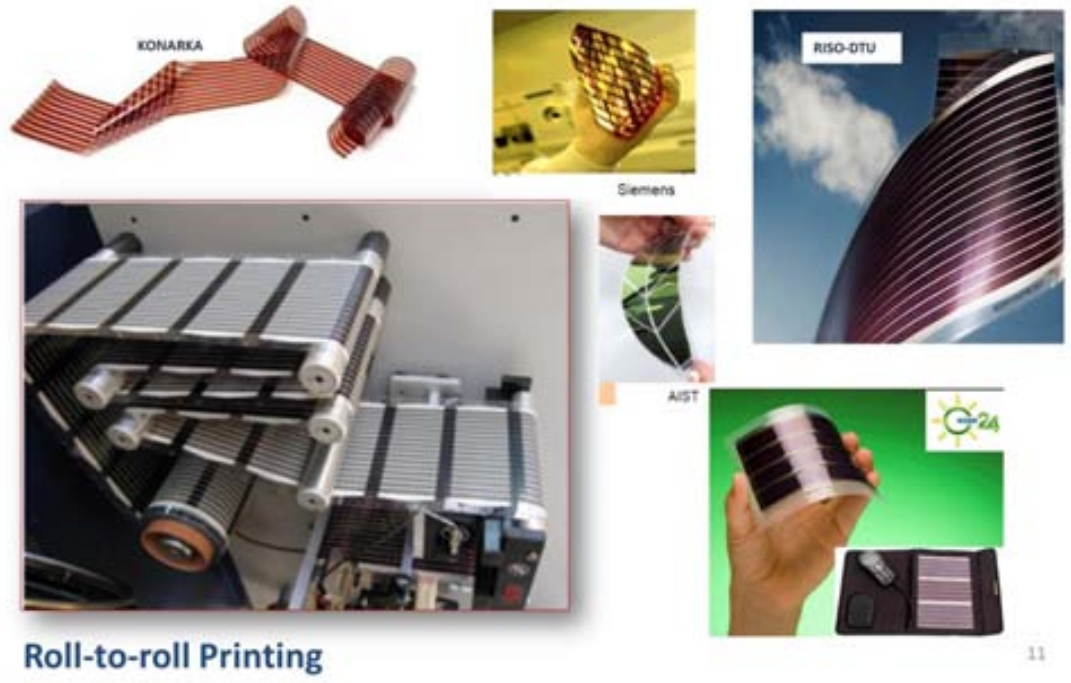

Figure 1.3 Flexible solar cells from different companies and the roll-to-roll equipment to fabricate them.

1.2 Photovoltaic energy conversion

The photovoltaic devices produce electrical power from the solar photons. All the processes involved in the production of energy will be explained in this section: the solar photon source, photoconversion mechanism of the different solar cells, semiconductor and other materials.

1.2.1 The photovoltaic effect

Since the discovery of the photovoltaic effect by Edmund Becquerel in 1839 from a silver coated platinum electrode immersed in electrolyte, other researchers reported materials with the same photovoltaic effect. Some of these materials are selenium with platinum[24, 25], selenium with gold[26] and copper-copper oxide thin films in lead sulphide and thallium sulphide. All these cells were thin film Schottky barrier devices that present a barrier to current flow.[27] The Schottky barrier is a semiconductor-metal diode system that exhibits an electron or hole barrier. The latter effect is caused by an electric dipole charge

distribution associated to the contact potential difference of the semiconductor and metal materials. The current can pass through the diode in one direction but not in the other.[28, 29]

However, the production of useful power with photovoltaic cells was not achieved until the development of good quality silicon wafers in 1954 by Chapin, Fuller and Pearson.[30] The fabrication of *p*-n junctions in single-crystal silicon converted the sunlight into electricity with an efficiency of about 6%, six times higher than the previous cells. Nevertheless, the high cost of this technology (~$200 per Watt) permitted only the use of solar cells in space applications until mid-70s. This high price is due to the complex production steps involved in the silicon wafers fabrication to have a high level of purity.[31] The oil-crisis in 1973 started a growth of interest and investment in alternative sources of energy. Attempts to lower the cost of solar cells were carried out using polycrystalline silicon, amorphous silicon, and other thin film materials and organic semiconductors.

1.2.2 Solar light irradiation

The intensity of the solar radiation that reaches the atmosphere of the Earth is around 1.367 $W \cdot m^{-2}$. This intensity is measured in function of the distance between the Sun and our planet when the radiation is perpendicular to the Earth and it is known as *solar constant.* However, when the solar radiation enters the Earth's atmosphere this intensity is attenuated by reflection and scattering from air molecules and also for their absorption, in particular from oxygen, ozone, water vapor and carbon dioxide. Therefore, the solar spectrum intensity is lower when reaches the Earth's surface. Figure 1.4 represents the solar irradiance spectrum at the top of the Atmosphere and the Earth's surface. The solar spectrum is similar to one produced by a black body at a temperature of about 5800 K that corresponds with the surface temperature of the Sun. The solar spectrum emits infrared, visible and ultraviolet light (Figure 1.4). The higher peak intensities of the solar irradiation are in the visible region, around 400-700 nm.[32, 33]

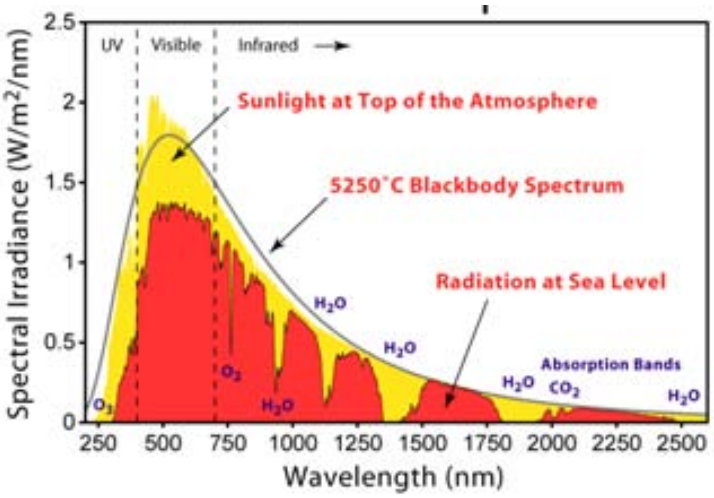

Figure 1.4 Solar spectrum of the light irradiated at the top of the atmosphere and surface of the Earth.[34]

The atmosphere attenuation of the solar spectrum can be quantified by the *Air Mass*, which is the optical path length that the sunlight must travel through the atmosphere to reach the Earth's surface (Figure 1.5). For the standard terrestrial sunlight spectrum, *Air Mass 1.5* (AM1.5), the angle θ is 48° and the light intensity defined at 1000 W·m^{-2} also called 1 Sun irradiation at these conditions.[34] The sun simulation lamps for the solar cell characterization have to be calibrated at AM1.5 and 1000 W·m^{-2} light intensity (which is the higher sunlight intensity at noon and on a cloudless day).[27, 33]

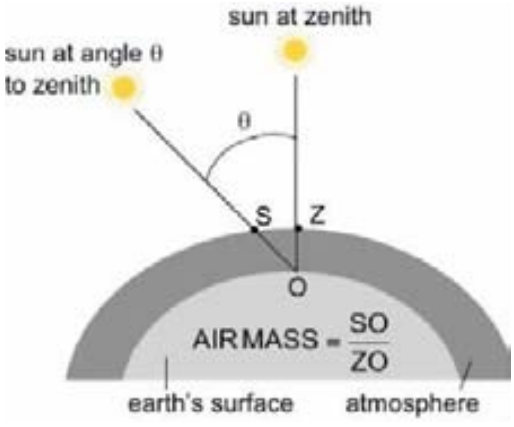

Figure 1.5 Representation of the Air Mass calculation for a given irradiation angle to the zenith (θ).

1.2.3 Operation mechanism

Photovoltaic cells (PV) can be represented as a one-diode equivalent circuit model (Figure 1.6) where a current (I_L) is generated by the illumination of incident light. When no load exist in the system (infinite external load, $R_L=\infty$) and the terminals of the cell are isolated, the voltage generated is the *open circuit voltage* (V_{oc}), which is the maximum possible voltage across a solar cell when no current is flowing. If a load is applied but there is no external resistance ($R_L=0$) the current formed is the *short circuit current* (I_{sc}), the highest that a cell can produce, there is no voltage and no work is done in the device. The current depends on the area of the cell and thus, the short circuit current density (J_{sc}) is an important parameter. [35-37]

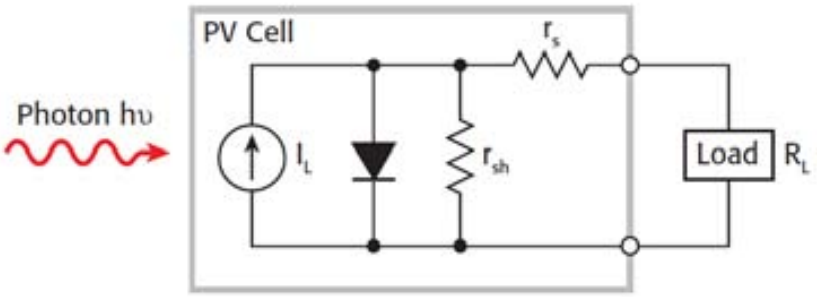

Figure 1.6 Schematic representation circuit of a photovoltaic cell.[35, 36]

The introduction of a load with external resistance (R_L) between 0 and infinite in the device creates a voltage (V) between 0 and V_{oc} and a current (I) defined as $V=I\cdot R_L$ that can be measured from the IV- curves (or JV-curves) under illumination. Figure 1.7 represents a IV-curve where are represented all the important parameters for the calculation of the power conversion efficiency (PCE); maximum power point (P_{max}), maximum current point (I_{max}), maximum voltage point (V_{max}), open circuit voltage (V_{oc}), short circuit current (I_{sc}) and the maximum power area that it is called fill factor (FF). The power conversion efficiency (η or PCE) can be determined following the equation (1.1) and using all the parameters extracted from the IV-curves (P_{in} is the power of incident light).[38]

$$\eta = \frac{P_{max}}{P_{in}} = \frac{V_{max} \cdot I_{max}}{P_{in}} = \frac{V_{oc} \cdot I_{sc} \cdot FF}{P_{in}} \qquad (1.1)$$

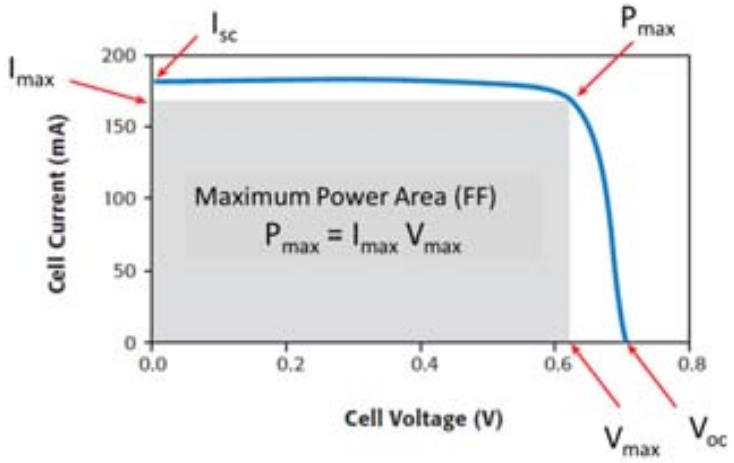

Figure 1.7 Example of a typical IV-curve for a solar cell.[35, 38]

PV cells have recombination processes due to the existence of series (R_s) and shunt resistances (R_{sh}) which reduce the FF value from the devices, an ideal device would have a 100% FF. Series resistance (R_s) is related to the resistance of the metal contacts, ohmic losses in the front surface of the cell, impurity concentrations and junction depth. Shunt resistance (R_{sh}) represents internal losses, such as recombination in the interface oxide/dye for the oxide surface defects.[27, 39, 40] An ideal cell should have a R_s=0 Ω and the R_{sh} should be infinite. As higher the value of R_{sh} and lower the value of R_s higher the solar cell performance (Figure 1.8). The values of R_{sh} and R_s in this thesis were measured from the IV-curves of the cells under illumination and defined as: $R_{sh}=dV/dI_{(V=0)}$ and $R_s=dV/dI_{(I=0)}$.[41, 42]

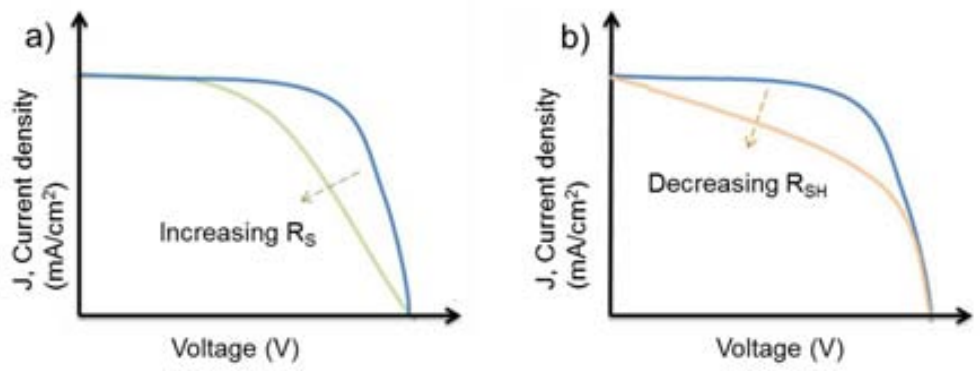

Figure 1.8 Effect of the modification of series resistance (a) and shunt resistance (b) in JV-curves of a solar cell.[27, 43]

The dark IV-curve measurement of the PV devices provides information of significant performance parameters and is more sensitive than illuminated IV-curves. The information that can be extracted from dark IV-curves is the series resistance, diode factor and diode saturation currents. All these parameters can be calculated applying a voltage from 0 to a determined value and measuring the current at the applied voltage when the cell is in the dark.[44-47] The current density produced in the dark conditions (J_{dark}) has an opposite direction than the current density obtained when the cell is illuminated. This dark current can be defined as equation (1.2), where J_0 is a constant, k_B is the Boltzmann's constant, T is temperature and m an ideality factor for a non-ideal diode equation.[1, 27]

$$J_{dark}(V) = J_0(e^{\frac{qV}{mK_BT}} - 1) \qquad (1.2)$$

The net current density in the cell can be calculated with the equation (1.3), using the sign convention that determines the photocurrent positive.

$$J\,(V) = J_{sc} - J_{dark}(V) \qquad (1.3)$$

The combination of equation (1.2) and (1.3) provides the equation (1.4) for the net current in the cell.

$$J\,(V) = J_{sc} - J_0(e^{\frac{qV}{mK_BT}} - 1) \qquad (1.4)$$

Another technique to characterize the solar cells is the external quantum efficiency (EQE) or incident photon to current efficiency (IPCE, it includes losses by reflection and transmission). The latter techniques measure the I_{sc} as a function of the incident illumination power P_{in} at different λ following the equation (1.5).

$$\mathrm{EQE}\ (\lambda) = \frac{h \cdot c}{q \cdot \lambda} \frac{I_{sc}\ (\lambda)}{P_{in}\ (\lambda)} \qquad (1.5)$$

The internal quantum efficiency (IQE) considers only the processes involving absorbed photons. IQE corrects the EQE by the spectral reflectance R (λ), equation (1.6).

$$IQE\ (\lambda) = \frac{EQE\ (\lambda)}{R\ (\lambda)} \qquad (1.6)$$

1.2.4 Photoconversion mechanism

The process taking place in a solar cell to produce electrical power follow three basic steps:

a) Solar Light absorption generating an electron-hole pair
b) Charge separation
c) Charge transport and extraction to an external circuit.

First, the solar cells need to absorb solar photons above a certain minimum energy, called *band gap* (E_g), and then generate an electron-hole pair state. The materials capable to perform the latter process are the *semiconductors*. These materials have their electrons distributed in a lower energy band completely filled called *valence band* (VB). When the electrons are excited with energy higher than the band gap jump to the *conduction band* (CB) and produce a hole in the VB (Figure 1.9). Depending on the E_g, a semiconductor can absorb light at different portions of the solar spectrum. The band gap can be modified by changing the particle size or doping the semiconductor. Semiconductors can also have atomic irregularities in the lattice structure, known as defects that act as electron traps avoiding the electrons to reach the electrodes and decreasing the efficiency of the device. Therefore, the properties of the semiconductors are very important and these materials need to be carefully characterized to understand their behavior.[1, 48]

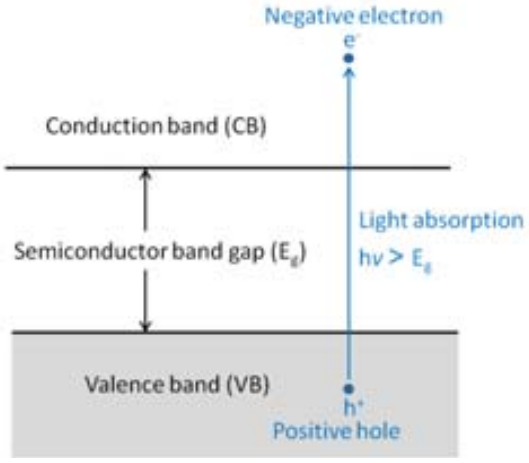

Figure 1.9 Excitation of an electron in a semiconductor material.

After the electron-hole pair generation, the following step is the charge separation by a driving force that avoids the recombination of the excited electron and the relaxation of the system to its initial state. This driving force is produced due to the presence of a *p-n junction* that is the contact of a *p-type* and *n-type* semiconductor materials (or the same semiconductor divided in two areas that are doped to present a p-type and n-type behavior as in silicon solar cells, see section 1.3.2). P-type semiconductors are electron rich materials in the conduction band when they are excited by light photons and thus, are also known as donors or hole transport materials (HTM). On the other hand, n-type semiconductors are known as acceptors or electron transport materials (ETM) due to the facility they present to accept electrons and also have high electron conductivity. Figure 1.10 represents the main materials in a XSC. The electron and hole transport material (ETM and HTM) are in contact through the interface only in some cases are separated by a light-harvesting material (LHM) such a dye or quantum dot. Thus, the LHM is the responsible for photon absorption when is present or sometimes the HTM has a dual function acting as the light absorber and hole transport material.[49]

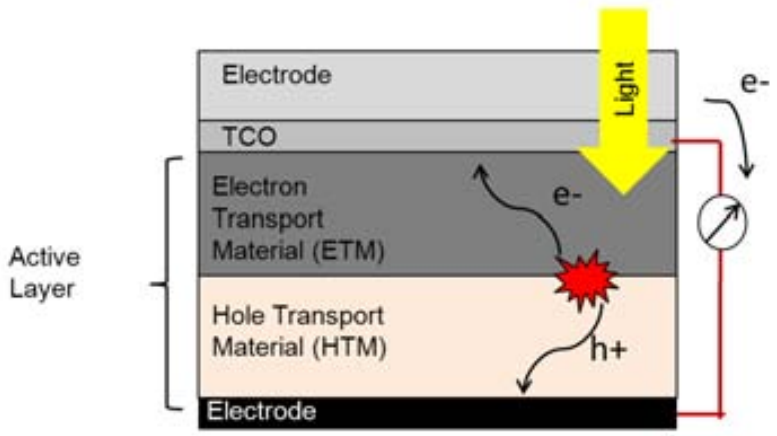

Figure 1.10 Schematic representation of an excitonic solar cell (XSC) showing the active materials hole transport (HTM) and electron transport materials (ETM).

In the inorganic solar cells (ISC) (conventional first generation cells), the electron-hole pair is formed directly in the bulk of the material and the charge separation is instantaneously produced. This is the main difference with the third generation cells, the presence of organic semiconductors (e.g., dyes, small molecules, organic polymers) imply the formation of an electron-hole pair tightly bound called *exciton*. For this reason, third

generation cells are also known as excitonic solar cells (XSC). The driving force in ISCs is a build-up potential generated at the p-n junction in the bulk material. Therefore, bulk properties such as crystallinity and chemical purity control the efficiency of conventional solar cells and make them more expensive than XSCs as commented in section 1.1 (Figure 1.2). In the case of XSC, the exciton formed need to be split, this dissociation takes place at the interface between the semiconductors, thus, these cells are largely dependent on interfacial processes.[15, 49, 50] A strategy to improve the efficiency of XSCs is the control of the interfaces through materials nanostructuration that will be explained in section 1.4.3.

The charge extraction is through the two electrically conductive electrodes. In XSCs, one electrode is generally a glass covered with a transparent conductive oxide (TCO) that permits the sunlight to spread within the solar cell device. TCO can be indium-tin oxide (ITO) or fluorinated indium-tin oxide (FTO). The back electrode normally is a metal such as silver, gold or platinum. Other extra components can be added in the XSC that offer benefits to the device, for example, oxide buffer layers (ZnO or TiO_2) to easily extract the electrons or polymers, for example, PEDOT:PSS to help the hole extraction (Figure 1.10).

1.3 Excitonic solar cells (XSC)

Third generation solar cells also known as excitonic solar cells (XSC) can be classified depending on the material applied or the type of p-n junction in the final device. The main components of XSCs are the electron transport material (ETM), hole transport material (HTM) and light harvesting material (LHM), Figure 1.10. Both types of classification are strongly interconnected and can lead to confusion since the same XSC can have two different nomenclatures.[49]

1.3.1 Classification by type of material

Excitonic solar cells can be classified by the type of the semiconductor applied: organic or inorganic. The inorganic semiconductors act as ETM due to their electronic properties, some examples of the most used materials are TiO_2, ZnO or CdSe among others. Many different organic semiconductors can be applied in XSC such as dyes, polymers, quantum dots or small organic molecules. These organic materials have properties of ETM (such as

PCBM), HTM (polymers), LHM (dyes) or both HTM+LHM at the same time (for example the polymer P3HT that absorbs light and transports the holes). XSCs classified by type of material are divided in three categories: dye-sensitized solar cells (DSC), organic solar cells (OSC) and hybrid solar cells (HSC). Quantum dot solar cells (QDSC) are another type of solar cell that have a similar configuration to DSCs or OSCs and are also explained in this section.

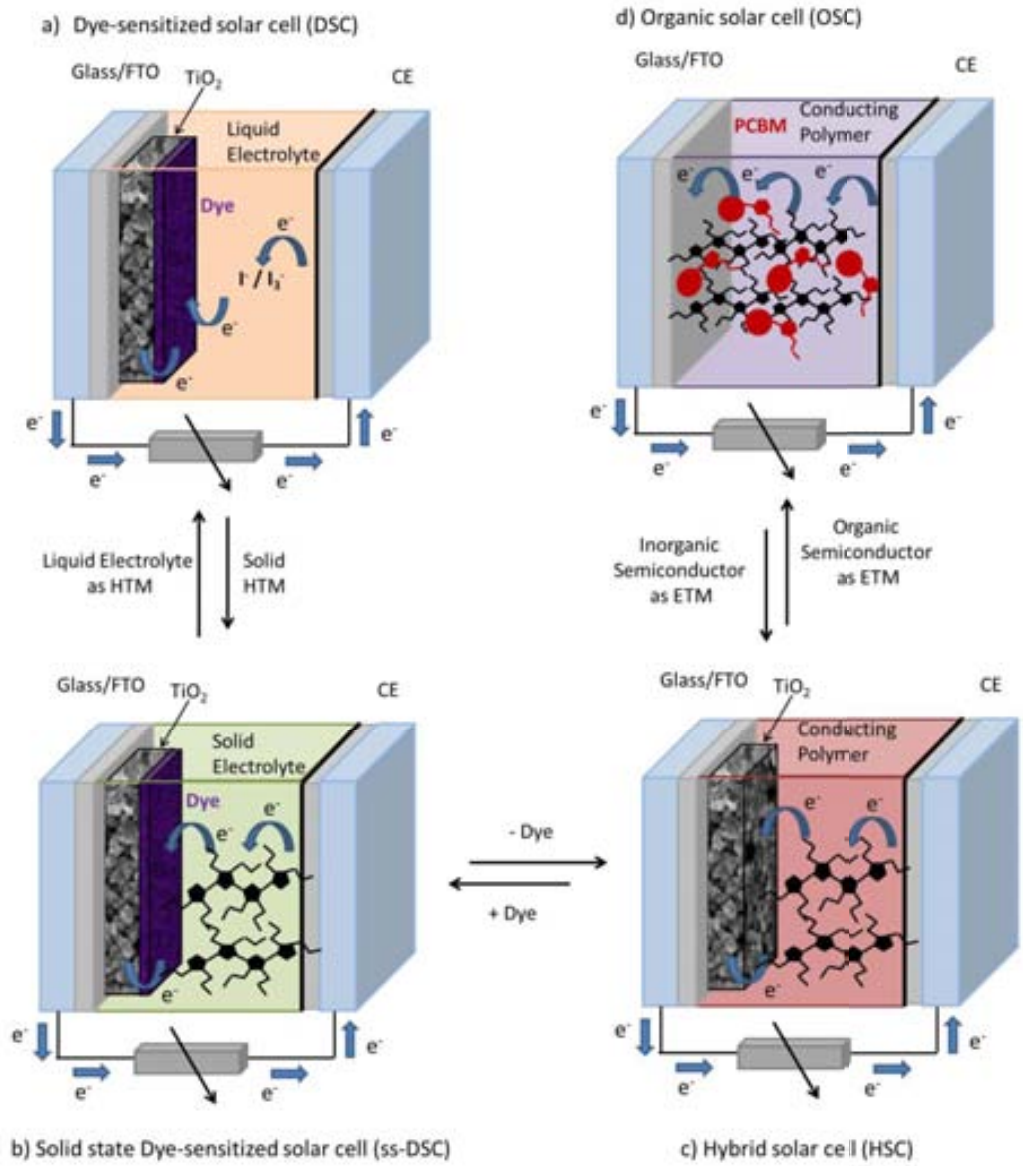

Figure 1.11 Schematic representation of XSCs by the type of material applied, a) dye-sensitized solar cells (DSC), b) solid state DSC, c) hybrid solar cells (HSC) and d) Organic solar cells (OSC).

Figure 1.11 represents the different XSCs depending on the type of the materials applied. The modification of these materials transforms the cell into another type. Thus, when the liquid electrolyte is substituted for a solid state electrolyte then the dye-sensitized solar cell (DSC) is a solid-state DSC. The replacement of the dye (LHM) and electrolyte (HTM) from the DSC for a single organic material, such a polymer, transforms this XSC in a hybrid solar cell (HSC). Finally, when the inorganic oxide from the HSC is exchanged by an organic semiconductor as electron transport material (ETM), the cell is an organic solar cell (OSC). These different types of XSCs are explained in more detail:

1.3.1.1 Dye-sensitized solar cells (DSC)

Dye-sensitized solar cells consist of an inorganic semiconductor oxide layer on a TCO electrode, usually TiO_2, but others can be also applied like ZnO that act as ETM. Then, a dye is anchored on the oxide surface, as the LHM, and a liquid electrolyte containing a redox couple is applied, as the HTM. The most used electrolyte is iodide/triiodide in an organic solvent. Finally a counter electrode, normally platinum, completes the device (Figure 1.11a).[51-53] The dye is the light harvesting material (LHM) that absorbs the photons from the sunlight and subsequently the exciton is formed at the interface between the dye and semiconductor oxide. When the exciton splits into electron and hole, the electrons are injected into the conduction band of the oxide and transported through the nanoparticle or other nanostructure network. Then, the holes travel along the electrolyte to the counter electrode. A successive regeneration of the dye is done by the electrolyte that after is also regenerated by the counter electrode (Figure 1.12). The voltage obtained from the DSC under illumination corresponds to the difference between the Fermi level of the semiconductor oxide and the redox potential of the electrolyte. Recently, DSCs with solid-state electrolytes have been reported in order to overcome some problems presented with the liquid electrolytes, for example, solvent evaporation or electrode corrosion. The latter cells are known as solid-state dye-sensitized solar cells (ss-DSC) (Figure 1.11b).[16, 54-56]

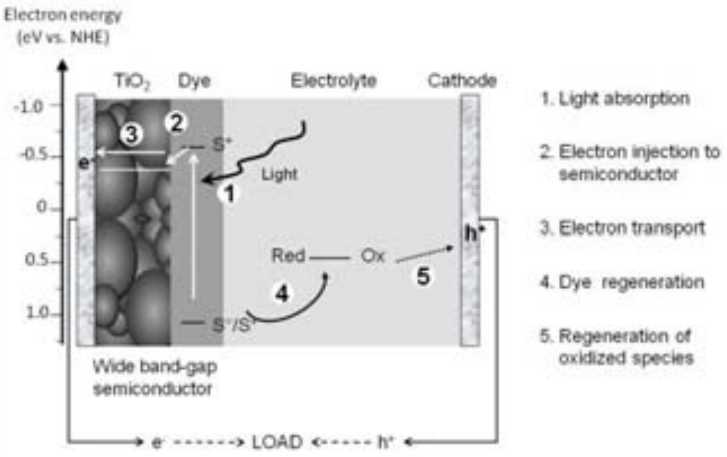

Figure 1.12 Schematic representation of a DSC and all the processes that take place in the photovoltaic energy conversion: (1) light absorption, (2) electron injection to semiconductor, (3) electron transport, (4) dye regeneration and (5) regeneration of the electrolyte.

1.3.1.2 Organic solar cells (OSC)

Organic solar cells have two organic semiconductors one ETM and the other HTM. Both organic materials are usually mixed in a bulk heterojunction configuration in the active layer in order to have the maximum contact between them and thus, enhance the solar cell performance (Figure 1.11d).[23, 57-59] The light-harvesting component, usually a polymer (HTM), absorbs photons from the sunlight and then, an exciton is formed at the interface between HTM and ETM. The ETM can be another conjugated polymer, but, up to now the best material is a soluble C_{60} derivative, PCBM. OSCs are also called polymer solar cells (PSC) due to the usually application of organic polymers in these types of solar cells. These cells have two different configurations depending on the application of PEDOT:PSS or a layer of inorganic semiconductor oxide (Figure 1.13). The *conventional configuration* has a thin film of PEDOT:PSS placed between the transparent conducting oxide (TCO) and the active blend material. The holes, in this configuration, formed in the active interface are transported toward the PEDOT:PSS electrode and the electrons to the other electrode. On the other hand, in *inverted configuration* an inorganic oxide layer is placed now on the TCO electrode that forces the movement of the electrons to this electrode and a PEDOT:PSS layer is also deposited on top of the other electrode to collect the holes (Figure 1.13). Lower photovoltaic performances have been observed in inverted OSCs, though, the lifetime of these devices improved.[21, 59, 60]

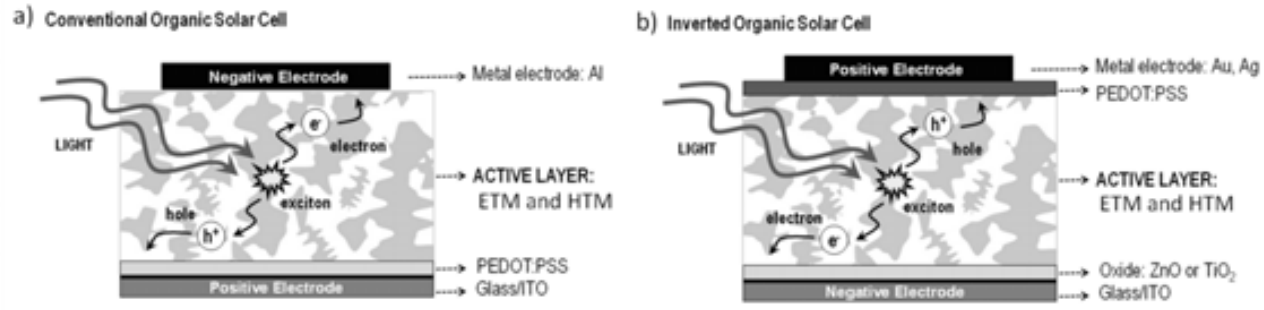

Figure 1.13 Schematic representation of OSCs with a) conventional and b) inverted configuration.

1.3.1.3 Hybrid solar cells (HSC)

Hybrid solar cells are similar to OSCs with the same conventional and inverted configurations but applying an inorganic semiconductor as ETM, for example oxides such as TiO_2, ZnO, Nb_2O_5 or other inorganic semiconductors like CdS, CdSe. The active layer of an HSC is a mixture of the inorganic ETM and the organic HTM that also act as LHM (usually a polymer). Both materials are in direct physical contact and the exciton is formed at the interface between them (Figure 1.11c).[61-64] This interface can be enhanced applying a bulk heterojunction blend configuration like in OSCs but other active layer configurations can be used in these cells such as bilayer. The different active layer configurations will be explained in the following solar cell classification by type of p-n junction (section 1.3.2).

1.3.1.4 Quantum dot solar cells (QDSC)

Quantum dots (QD) or also known as quantum wells (QW) are very small particle semiconductors that due to quantum mechanics their band gaps can be easily tunable changing the particle size. This ability to modify their band gap is very attractive for solar cell applications to be applied as light harvesters.[65] The use of different QDs permits to absorb higher-energy and lower-energy photons reducing the heat loss due to carrier relaxation via phonon emission.[66, 67] These PV devices can be prepared in three different configurations:

- Dye-sensitized solar cells (DSC): the dye is replaced by the QDs, which act as the light harvesting material (LHM)[68] - Figure 1.14a

- Hybrid solar cells (HSC): the QDs are dispersed within a polymer blend solution and/or organic fullerene material, in this case they act as the light absorber and/or hole transport material (HTM)[69] - Figure 1.14b

- Inorganic solar cells: the QDs act as intermediate band (IB) gap material within the p-n semiconductor to allow more light absorption[70] - Figure 1.14c

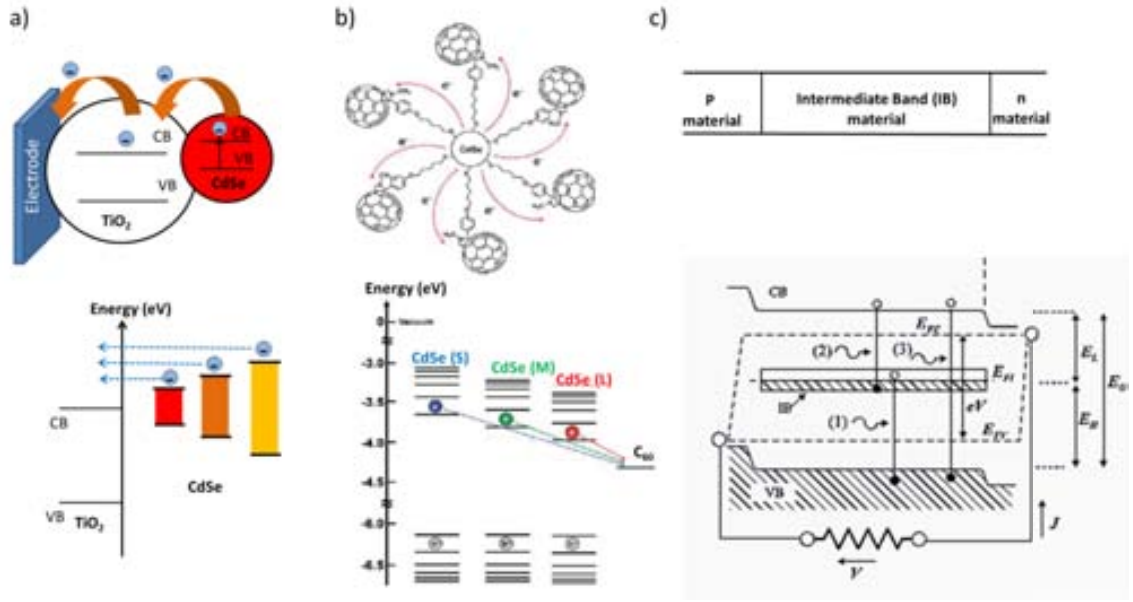

Figure 1.14 Schematic representation of the band gap energy levels when QDs are applied in a) Dye-sensitized solar cells (DSCs)[68], b)Hybrid solar cells (HSC)[69] and c) Inorganic solar cells (ISCs)[70].

1.3.2 Classification by type of junction

The photovoltaic energy conversion is produced in the solar cell junction, where the charge separation takes place (see section 1.2.4). The latter charge separation process occurs due to the electrostatic force originated when two electronically different materials are in contact. The contact area of these two materials is the solar cell junction. In this section the different types of junctions between semiconductors materials are presented.

1.3.2.1 The p-n junction

The p-n junction is the standard model of an inorganic solar cell (ISC). This junction is created when the same semiconductor is doped differently in two separate regions. One region of the latter semiconductor presents a p-type behavior and the other an n-type (Figure 1.15a).[27] The p-type region is rich of free charge carriers (holes) in the valence band, where the n-type region is electron rich. In the case of conventional silicon solar cells can be doped with trivalent atoms such as boron, aluminum or gallium to produce the p-type region and doped with pentavalent atoms such as antimony, arsenic or phosphorous to obtain an n-type region.[71]

The p-n junction acts as a selective barrier to charge carrier flow, providing the asymmetry in resistance which is necessary for photovoltaic conversion. The control of the doping process produces large potential barriers which allow large photovoltages.[27]

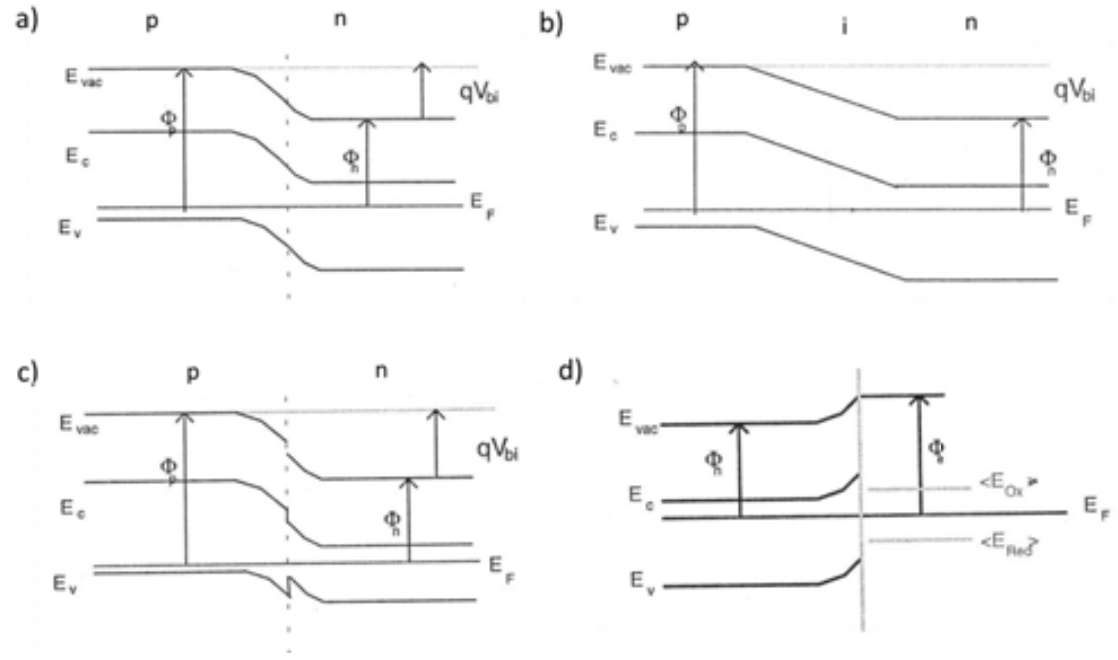

Figure 1.15 Band profiles in equilibrium of a) p-n junction, b) p-i-n junction, c) p-n heterojunction and d) electrochemical junction. E_{vac} = vacuum level, E_F= Fermi level, E_c= conduction band, E_v = valence band, E_{red} = reduction band, E_{ox} = oxidation band, V_{bi} = built in bias potential, ϕ_n = work function of n-type material, ϕ_p = work function of n-type material and ϕ_n = work potential of the electrolyte.[27]

1.3.2.2 The p-i-n junction

The p-i-n junction is a variation of the classical p-n junction. This junction has an undoped or intrinsic (i) layer of semiconductor between the p- and n- regions. The charge carriers photogenerated in the i-region are driven to the contacts by the electric field and they can survive for a large distance than in p-n junctions (Figure 1.15b). However, this junction has also some disadvantages: a) the i-region is less conductive, thus introduces series resistances, b) it produces recombination at forward bias conditions, where the electron and hole are in similar number and c) if the intrinsic i-region has impurities the electric field fall to zero.

1.3.2.3 The p-n heterojunction

The p-n heterojunction uses two different semiconductor materials with different band gaps. Now at the junction appears a discontinuity in the conduction and valence band

edges due to the change in the band gap. These discontinuities built charge barriers which enhance the recombination processes (Figure 1.15c). Thus, the interface between both materials is a critical parameter.

Excitonic solar cells (XSC) have this type of junction. In the photoconversion of the XSCs and exciton (electron-hole bound together) in the active layer is formed and diffuses to reach the interface of the two different materials. In this interface the charge generation takes place. Thus, the interface is a critical parameter that needs to be optimized. If the active layer is too thick, then the exciton can be recombined. For this reason, a thickness optimization of the p-n heterojunction is crucial since the exciton diffusion length depends on the materials applied. An exciton diffusion length between 10-20 nm was measured in polymers and up to 1 μm in high-quality small molecule films. Moreover, the p-n heterojunction must maximize the volume of available interface between the semiconductors to increase the charge separation process.[49] Therefore, different p-n heterojunctions emerged to improve the solar cell performance represented in Figure 1.16: bilayer, bulk-heterojunction and electrochemical junction.

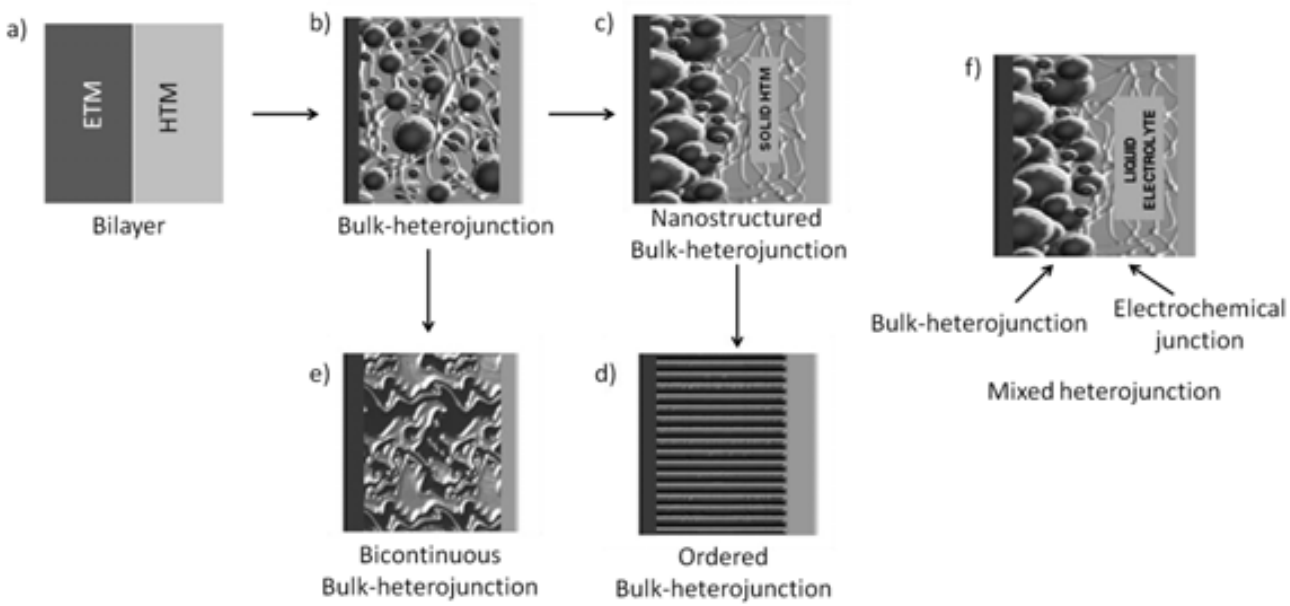

Figure 1.16 Schematic representation of p-n heterojunctions found in XSCs: a) bilayer, b) bulk-heterojunction, c) nanostructured bulk-heterojunction, d) ordered bulk-heterojunction, e) bicontinuous bulk-heterojunction and f) Mixed heterojunction (bulk-heterojunction and electrochemical junction).

Bilayer p-n heterojunction

The most basic p-n heterojunction is a bilayer (Figure 1.16a). The bilayer presents a smooth flat interface between the ETM and HTM. Since the organic semiconductors have a short diffusion lifetime, the length of this p-n heterojunction is limited to about ~10 nm only.[72] This restriction reduces the amount of LHM in contact with the ETM and thus, decreases the power conversion efficiency of the device. For this reason, other p-n heterojunctions were developed. This configuration was usually applied in HSCs.

Bulk heterojunction

In a bulk-heterojunction (BHJ) layer, the ETM and the HTM are mixed homogeneously in a blend within the active layer (Figure 1.16b). In this way, the contact between ETM and HTL increases and allows a thicker active layer of about ~100 nm.[73] The first reported BHJ was in polymer-fullerene OSCs achieving enhanced efficiencies.[74] Other studies of the BHJ morphology observed an improvement on the cell performance when thermal treatments were applied. The latter permits a better contact between ETM and HTM due to a crystal organization in the active layer. The resulting p-n heterojunction after the thermal treatment is known as bicontinuous bulk-heterojunction (Figure 1.16e).[75, 76] Another type, the nanostructured BHJ, is a mixture between a bilayer and BHJ, where a layer of nanoparticles presents a larger surface area compared with the bilayer to increase the amount of LHM at the interface (Figure 1.16c). The nanostructured BHJ can also be well ordered, by the application of vertically-aligned nanorods, nanowires, nanotubes…etc. (Figure 1.16d). This well ordered structure avoids the drawback that have the BHJ layers, where the active materials are randomly distributed and in some parts can be isolated not achieving exciton dissociation. The introduction of well-ordered ETM nanostructures allows a direct electron path to the electrode, reducing the recombination.

1.3.2.4 The electrochemical junction

The electrochemical junction is a variation of the p-n heterojunction, where a liquid electrolyte is in contact with a semiconductor material. The charge transport in these junctions is performed by a redox couple included in the electrolyte. The redox couple are two ionic species of different state of charge (oxidized and reduced species), which

determine the energy levels of its conduction and valence band (Figure 1.15d). The combination of a bulk-heterojunction with an electrochemical junction represents the configuration of the DSC active layer, where the BHJ is made of the TiO_2 and the light harvesting dye which are in contact with a liquid electrolyte (Figure 1.16f).

1.4 ZnO semiconductor

Zinc Oxide (ZnO) is a well-known semiconductor for its advantageous properties that make it a suitable material for a wide range of devices: photodetectors, biomedical and chemical sensors, transparent thin-film transistors, light-emitting diodes, laser diodes, among others.[77, 78] In this section, all the ZnO properties are presented. Moreover, different ZnO synthesis techniques are explained and some of the different reported ZnO nanostructures are showed. Finally, the application of ZnO in XSC is presented.

1.4.1 ZnO properties

General physical properties of ZnO are depicted in Table 1.1. The crystalline structure, optical properties, defects, electrical conductivity, wettability and chemical properties are explained in detail in this section.

Table 1.1 General properties of ZnO semiconductor material

Property	Symbol (units)	Value	Reference
Molecular weight	M_w ($mol \cdot g^{-1}$)	81.39	[79]
Density	ρ ($g \cdot cm^{-3}$)	5606	[79]
Melting point	mp (°C)	1975	[79]
Enthalpy of formation	ΔH_f ($J \cdot mol^{-1}$)	$6.5 \cdot 10^5$	[80]
Entropy of formation	ΔS ($J \cdot mol^{-1} \cdot K^{-1}$)	100	[81]
Heat capacity	C_p ($J \cdot mol^{-1} \cdot K^{-1}$)	41	[81]
Electron mobility	($cm^2 \cdot V^{-1} \cdot s^{-1}$)	200	[82]
Carrier concentration	(cm^{-3})	$8 \cdot 10^{13}$	[82]
Refractive index	n_D	2.008-2.029	[79]
Water solubility	(mg/L)	1.6 (at 29 ºC)	[79]

1.4.1.1 Crystal and surface structure

The ZnO can crystallize in three different structures: hexagonal wurtzite, cubic zinc blende and cubic rocksalt. Under ambient conditions ZnO presents hexagonal wurtzite crystalline structure that belongs to the spacial group $P6_3mc$ (C^4_{6v}) (Figure 1.17c). Wurtzite is the most stable phase since the ionicity of Zn^{2+} and O^{2-} is between covalent and ionic, thus, the wurtzite structure maintain both atoms as far as possible. The wurtzite lattice parameters are a=3.25 Å and c=5.21 Å, it lacks of a symmetry center and thus, is a good piezoelectric and pyroelectric material (Figure 1.18).[83, 84] The other two ZnO crystalline structures, zinc blende and rocksalt can only be obtained under special synthesis conditions. The zinc blende structure is only stabilized when the ZnO growth is on cubic substrates (for example, ZnS, GaAs/ZnS, Pt/Ti/SiO_2/Si) and the rocksalt structure is only obtained at high pressures, above 10 GPa (Figure 1.17a). Polar surfaces of ZnO are another important characteristic. The most common polar surface is the basal plane, which presents a normal dipole moment and spontaneous polarization along the c-axis, direction [0001]. This polar surface is the responsible of the nanorod or nanocolumn growth of ZnO along this c-axis.

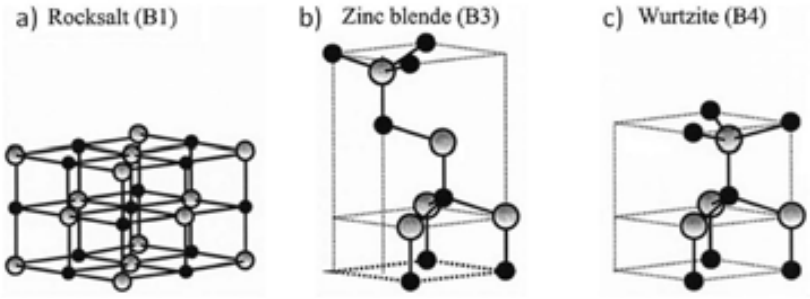

Figure 1.17 Crystalline structures of ZnO semiconductor, a) rocksalt, b) zinc blende and c) wurtzite.

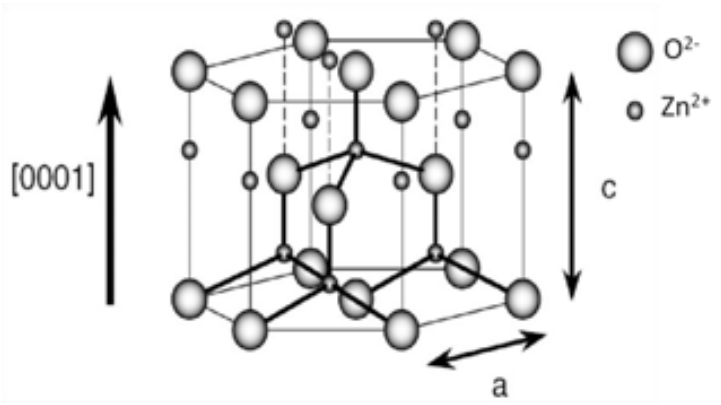

Figure 1.18 Wurtzite hexagonal crystalline structure of ZnO.

In this work, the wurtzite crystalline structure of ZnO is represented by a four-index Miller indices (*h l i k*), related to the hexagonal system. Many papers report the crystalline structure of ZnO with a three index system (*h' l' k'*), Miller indices, and also the majority of the X-rays patterns. The latter system is not erroneous but the four-index system is more accurate in hexagonal crystalline structures due to lower symmetry of this structure compared to cubic systems and gives many different reciprocal lattice planes.[85] To convert the three index Miller indices into four-index indices we use this expression:

$$h = h', \quad l = l', \quad i = -(h'+l'), \quad k = k'$$

1.4.1.2 Optical properties and defects

ZnO is a II-VI semiconductor transparent to visible light with a wide band gap of 3.37 eV and high exciton binding energy of 60 meV.[86, 87] This high excitation binding energy permits efficient excitonic emission at room temperature and Ultraviolet (UV) luminescence.[88, 89] Therefore, the optical properties of ZnO have been studied by photoluminescence (PL) spectroscopy.[87] The PL analysis spectrum provides information about defects on the surface and core of the ZnO material. Depending on the ZnO nanostructure, the PL spectra present different bands. Typically consist of a UV emission around 380 nm related to the Near Band Edge (NBE) and related to the electronic transition from near conduction band to valence band of the ZnO. Moreover, the PL presents one or more visible bands related to defects or/impurities around 650 nm (orange band) or also called deep level emission (DLE) band. The orange visible emission band presents different contributions: known as green (550 nm), yellow (600 nm) and red (700 nm) emission bands which are related to the ZnO defects such as oxygen vacancies (O_{vac}), oxygen interstitial (O_i), Zn vacancies (Zn_{vac}), Zn interstitial (Zn_i) or other surface defects like capping hydroxide ($Zn(OH)_2$). The exact defect that origins each band (yellow, green and orange-red) is still not clear and it is a controversial subject.[72, 90-93] The energy levels of the different ZnO defects within the band gap have been measured and are shown in Figure 1.19. The donor defects are zinc interstitial (Zn_i^{2+}, Zn_i^{+}, Zn_i^{0}) and oxygen vacancies (O_{vac}^{2+}, O_{vac}^{+}, O_{vac}^{0}) and the acceptor defects are zinc vacancies (Zn_{vac}^{2-}, Zn_{vac}^{-}).[78] It was reported that depending on the availability of the oxygen in the synthesis of ZnO NRs, the PL spectra will show a green or orange emission band.[91] For low oxygen ZnO NR

synthesis a green band was observed and was attributed to O_{vac} defects.[94] Some groups associated the orange-red band centered at ~640-650 nm wavelength to the excess of oxygen in the sample obtained using hydrothermal, electrochemical, laser deposition and spray pyrolysis techniques having O_i defects, surface dislocations or Zn_i defects.[91, 95]

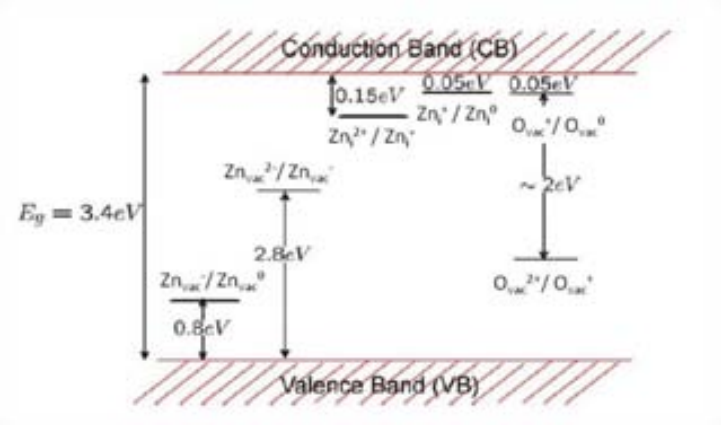

Figure 1.19 Representation of the energy levels of different defects in ZnO: zinc interstitial (Zn_i), zinc vacancy (Zn_{vac}) and oxygen vacancy (O_{vac}).[78]

1.4.1.3 Electrical conductivity

Most of the synthesis techniques produce ZnO n-type semiconductor initially attributed to native point defects, such as zinc interstitial (Zn_i), oxygen vacancies (O_{vac}) or antisites.[96-98] However, more recent studies demonstrated that native point defects are not the responsible of the ZnO n-type behavior but rather the unintentionally incorporation of impurities. Incorporation of hydrogen was reported to act as shallow donor causing the ZnO n-type conductivity since hydrogen is present in all the ZnO growth techniques. Figure 1.20 represents a calculated model of the possible sites where the hydrogen can be introduced in ZnO and this hydrogen incorporation was also observed experimentally.[77, 99-102] Many efforts are being developed to control the ZnO electrical conductivity to achieve a p-type behavior.[77, 83] Doping the ZnO is one strategy to obtain the latter, yet, it is difficult to succeed due to be few candidate shallow acceptors for ZnO and the low solubility of the dopant elements in the ZnO material. Attempts on doping ZnO with group-I elements (Li, Na, K, Cu and Ag) to fill the zinc vacancies were not successful. Despite the reports of some research groups on ZnO p-type behavior doping with group-V elements (N, P, As and Sb) in the oxygen vacancies, reliability and reproducibility are still big issues.[103-106]

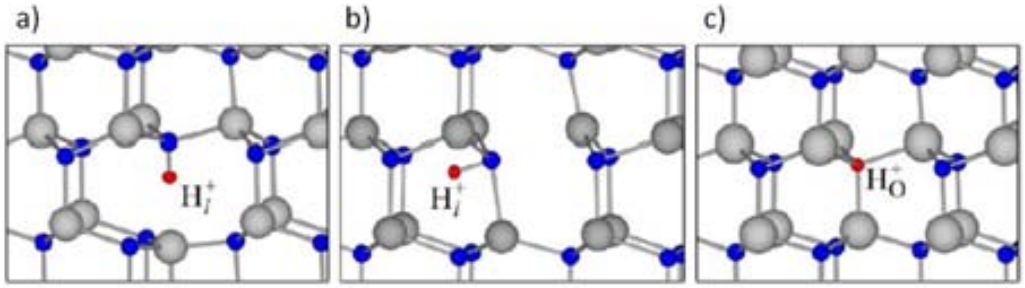

Figure 1.20 Representation of a calculation model for the possible hydrogen incorporation into the ZnO structure: a) interstitial site, b) antibonding site and c) substitutional oxygen site.[77]

Electrical mobility of ZnO is strongly dependent on the quality of the ZnO material and the temperature. The highest room-temperature electron mobility for a bulk ZnO single crystal material grown by vapor-phase transport method was measured to be 205 $cm^2 \cdot V^{-1} \cdot s^{-1}$ with a carrier concentration of $6 \cdot 10^{16}$ cm^{-3} (Table 1.1).[83] For ZnO nanorods or nanowires the electron mobility obtained was as high as 80 $cm^2 \cdot V^{-1} \cdot s^{-1}$.[58]

1.4.1.4 Wettability

Another relevant ZnO property is the surface wettability, which it is known to be easily modified by humidity conditions or UV irradiation.[64, 107, 108] In XSCs is important that the organic semiconductor material reach the whole surface area of the other semiconductor, ZnO in this case, and this is more emphasized when ZnO nanostructures are applied. Thus, the wettability surface of ZnO is a key factor for a good solar cell performance. Some groups observed properties of superhydrophobicity and superhydrophilicity on ZnO under different conditions. The alternation of UV irradiation and dark storage switched the latter properties that can be controlled selectively depending on the different applications.[109-112]

1.4.1.5 Chemical properties

ZnO has a high energy radiation stability that makes it attractive for space applications and also suitable for the preparation of small-size devices due to be easily etched with all

kind of acids and some bases. Nevertheless, the low stability of ZnO in acidic media is not a desirable property for XSCs applications and in particular, on DSCs, where the most used dyes have carboxylic groups, –COOH, to attach to the oxide surface. These acidic groups from the dye dissolves and precipitates the ZnO as a [Dye-Zn^{2+}] complex.[113-115] Therefore, several strategies to improve the ZnO stability in XSCs are currently being investigated (see section 1.4.4.4).

1.4.2 ZnO synthesis techniques

A large variety of different synthesis techniques have been reported to obtain ZnO nanostructured materials. The ZnO properties depend to a great extent on the preparation conditions. However, the relationship between the growth technique, native defects concentration and properties it is difficult to be established since many other factors play an important role on the ZnO preparation and the XSC performance such as humidity.[50, 86] The synthesis techniques can be classified in two groups: high temperature (chemical and physical vapor deposition that are vacuum-based techniques) and low temperature methods (<100°C like hydrothermal or electrochemical depositions). In this section, the vapor phase, hydrothermal and electrochemical deposition growth methods for the preparation of one dimensional ZnO nanostructures such as nanorods or other ZnO nanostructures are explained.

1.4.2.1 Towards low temperature solution processing and water-based fabrication of ZnO

The commercialization maturity of the excitonic solar cell technology (organic, hybrid, dye sensitized solar cells) can only be accomplished by maximizing device efficiency and lifetime, while minimizing fabrication costs. The printing of active layers from solution applying large-scale manufacturing technologies (i.e. roll-to-roll, slot-dye, gravure/ flexographic) is being slowly established as the best alternative for competitive-cost device fabrication. ZnO is an important material for the printed electronics and the photovoltaic industry.[50, 86, 116] The fabrication of vertically-aligned ZnO electrodes can be carried out by the low-temperature hydrothermal synthesis method (LT-HM), also known

as the chemical bath deposition (CBD). This synthesis method has received enormous attention in recent years due to the possibility to be carried out at low temperatures, on almost any substrate and in large areas. The later makes the technique highly attractive for the scale-up fabrication of ZnO electrodes useful in many flexible optoelectronic devices, like dye sensitized solar cells (DSCs).[50]

1.4.2.2 Hydrothermal synthesis (HT) or chemical bath deposition (CBD)

Hydrothermal synthesis (HT) or also known as chemical bath deposition (CBD) is a low-cost aqueous technique. Some groups reported HT synthesis at temperature between 100-1000°C and under pressure between 1 MPa-1GPa in a sealed autoclave reactor.[117, 118] However, the advantages of a simple ZnO synthesis at low temperature (< 100°C) in aqueous solution and under atmospheric pressure expanded the publication of a large number of HT papers with low-cost conditions.[91, 119-122] Figure 1.21 shows the formation of ZnO nanorods on ITO substrates from an initial ZnO nanoparticles layer.

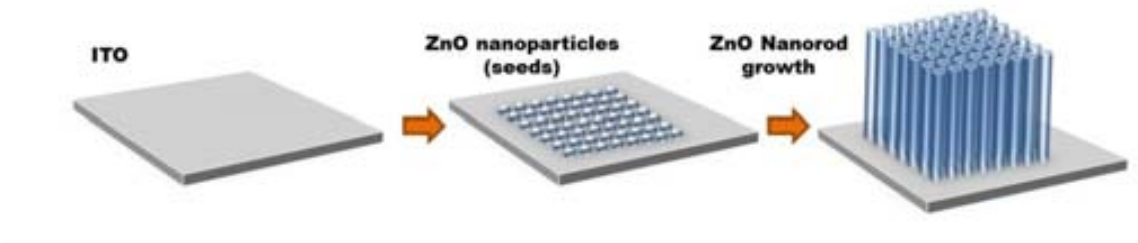

Figure 1.21 Schematic representation of the growth of ZnO nanorods on ITO substrates using the HT synthesis from an initial ZnO nanoparticles layer.

The HT technique consists on the formation of ZnO from the hydrolysis of Zn^{2+} salts in a basic aqueous solution. The basic media is essential for the formation of ZnO nanostructures and can be formed using strong or weak alkalis. Normally, the most used base is hexamethylenetetramine (HMT, $C_6H_{12}N_4$), that acts as pH buffer to control the pH value at 6-7 to slowly supply anions of OH^- (equation 1.7 and 1.8).[91, 120, 123-125] Other bases applied in HT synthesis are NaOH, KOH or NH_4^+.[126-128] When the concentration of Zn^{2+} and OH^- exceeds a critical value and the solution is heated, the precipitation of ZnO starts (equation 1.9 and 1.10). Then, the obtained ZnO in the solution begin the nucleation on top of the substrates with ZnO nanoparticles (NP) that are up-side down in the solution

forming ZnO NRs. The ZnO NPs act as seeds for the nucleation of the ZnO generated in the solution to allow the formation of ZnO NRs.[120] All the chemical reactions involved in the HT synthesis are described in equations 1.7-1.10.[124, 125]

$$(CH_2)_6N_4 + 6H_2O \rightarrow 6HCHO + 4NH_3 \qquad (1.7)$$

$$NH_3 + H_2O \leftrightarrow NH_4^+ + OH^- \qquad (1.8)$$

$$Zn^{2+} + 2OH^- \rightarrow Zn(OH)_2 \qquad (1.9)$$

$$Zn(OH)_2 \rightarrow ZnO + H_2O \qquad (1.10)$$

The final ZnO nanorod dimensions and quality depend on the HT synthesis conditions, like zinc concentration in solution, growth time or growth temperature. Furthermore, the solution reaction should be changed after certain time to renew the precursor materials within the solution reaction.

1.4.2.3 Vapor phase methods (VP)

Vapor phase methods have been widely applied for the ZnO nanostructures preparation.[77, 129, 130] Usually, a tubular furnace is used to carry out the thermal evaporation, which is done at high temperature (around 1000°C) and most of the times under vacuum conditions (Figure 1.22). The morphology and phase structure of the obtained ZnO nanostructures depend on the source materials and the reaction conditions. These conditions are temperature, pressure, carrier gas, substrate and evaporation time period and they should be controlled. The vapor phase process consist on the evaporation of the starting material (gas phase) by heating above the material eutectic temperature and the transport of this vapor with a carrier gas to another part of the furnace where the temperature is lower and a substrate is placed (Figure 1.22). Then, the vapor is condensed into solid material on top of the desired substrate. Some examples to obtain ZnO with a vapor phase method use ZnO power mixed with graphite and Ar as carrier gas[131-133] or pure Zn powder as starting source combined with O_2 carrier gas.[130, 134]

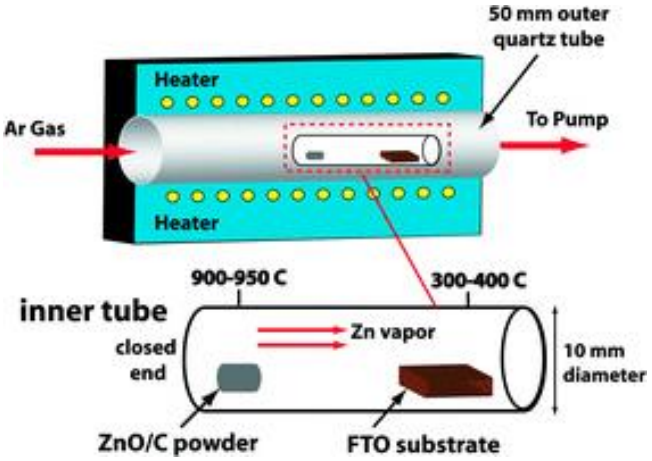

Figure 1.22 Schematic representation of an example of ZnO NRs vapor phase deposition method on a transparent conductive substrate.[135]

There are many different variations of vapor phase deposition methods and can be classified in two groups: physical vapor deposition (PVD) and chemical vapor deposition (CVD). While in PVD the target material is only evaporated and condensed back to solid state, in CVD the starting material reacts on the surface of the substrate to form the desired solid material. Many different deposition techniques are classified in the group of PVD such as sputtering, pulsed laser deposition (PLD)[136], vapor phase epitaxy (VPE)[129], electron beam physical vapor evaporation (EBPVD) among others. On the other hand, there are also many different types of CVD techniques such as plasma assisted CVD (PACVD), chemical beam epitaxy (CBE), laser CVD (LCVD), metal organic chemical deposition (MOCVD)[129, 137] and atomic layer deposition (ALD).[138] Moreover, these methods are also known by the mechanism involved: vapor-liquid-solid (VLS), vapor-solid (VS), vapor-solid-solid (VSS) and oxide assisted growth (OAG). As an example of VLS is a reaction with ZnO powder as starting material (with graphite) and Au droplets on the substrate, used as catalyst. In the latter reaction, the ZnO is evaporated and transported to the substrate, where the catalyst droplet (liquid phase) directs the NR growth defining its diameter.[137]

1.4.2.4 Electrochemical deposition synthesis (ED)

Electrochemical deposition (ED) is a low temperature technique in an aqueous growth solution. The standard ED reaction uses a three electrode setup, normally with an Ag/AgCl reference electrode and a Pt electrode as the counter-electrode (Figure 1.23).[139, 140] The working electrode is the substrate where the deposition of ZnO is produced.[118, 129, 141] The reaction system is controlled by a constant voltage source to maintain a constant driving force or by a constant current to keep a constant reaction rate. In the aqueous solution it is needed a dissolved Zn^{2+} salt and also an oxygen source that can be O_2 or NO_3^-. The latter oxygen sources are transformed to OH^- by the chemical reactions in equations 1.11 or 1.12 respectively. Then, the production of ZnO proceeds by the reactions from equations 1.9 and 1.10.[141-143] The oxygen source can also be directly introduced by adding alkaline precursors.

$$O_2 + 2\ H_2O + 4\ e^- \rightarrow 4\ OH^- \qquad (1.11)$$

$$NO_3^- + H_2O + 2\ e^- \rightarrow NO_2^- + 2\ OH^- \qquad (1.12)$$

The ZnO formation rate depends on the concentration of the precursors and the voltage or current applied in the reaction. The combination of ED with templates such as anodic aluminum oxide (AAO) is a synthesis method known as templated growth. This permits the control of the dimensions of the obtained ZnO nanostructures.[141]

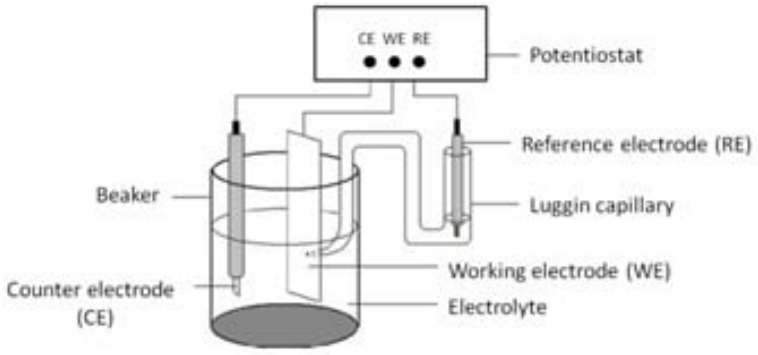

Figure 1.23 An schematic representation of a three electrode setup for the electrochemical deposition synthesis (ED).[118]

1.4.3 ZnO nanostructures

The nanostructuration of ZnO in XSCs confers unique and novel properties to the cells due to the advantage of controlling the interface at the nanoscale level. The interfaces between the ETM and HTM play an important role on the XSCs performance, as was mentioned in section 1.2.4. Thus, the increase of the interfacial area is beneficial in these devices. Additionally, the nanostructure can improve the charge transport due to a more direct electron way to the electrode through the semiconductor. In this section we discuss the different ZnO nanostructures with their advantageous properties.

1.4.3.1 Nanostructures for high surface area: nanoparticles and nanoaggregates

The nanoparticles (NP) and nanoaggregates form a porous interconnected network in which the specific surface area is increased by more than 1000 times when compared with bulk materials. These high surface-area-to-volume nanostructures have a large interface in contact with the light harvesting material (LHM) such as the dye in DSCs so they can adsorb a high quantity of LHM.[116] Figure 1.24 shows and schematic representation of an electrode with ZnO NPs and some examples of ZnO NPs obtained in literature.

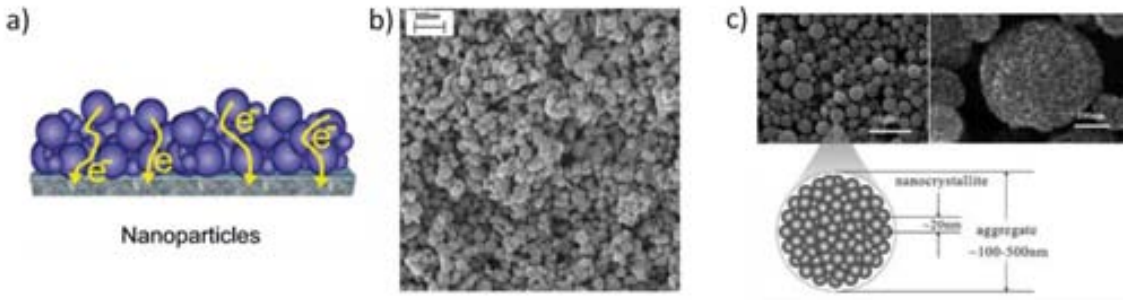

Figure 1.24 a) Schematic representation of the possible electron path taking place on a ZnO NP electrode, b) SEM image of ZnO NPs[113] and c) SEM image of ZnO NP aggregates.[144]

1.4.3.2 Nanostructures for high electron transport: nanorods, nanowires, nanotips and nanotubes

The 1-dimensional nanostructures: nanorods (NR), nanowires (NW), nanotips and nanotubes (NT) allow a highly efficient electron transport pathway compared to ZnO nanoparticles (NP) that are limited by grain boundaries between each nanoparticle shown

in Figure 1.24a.[50] These grain boundaries are electron traps that produce the charge recombination. The recombination has been found to be a limiting factor that causes energy loss and reduces the final power conversion efficiency in the XSCs.[55] Therefore, the 1-D nanostructures have been widely studied in the past few years.[120, 145-150] Figure 1.25 shows and schematic representation of an electrode with ZnO NRs and some examples of ZnO nanowires and nanotubes obtained in literature. The only difference between NRs and NWs is the aspect ratio, which is the length divided by the diameter. The NWs are known to be longer and thinner than the NRs. Some groups defined the NRs when the aspect ratio is between 1 and 20 and NWs when the aspect ratio is greater than 20 (nanoparticles present an aspect ratio of 1).[151-154] However, the definitions NRs and NWs are often used arbitrary in the reported papers.[155] A bibliographic review of the application of ZnO NRs and NWs in DSCs is presented at the beginning of chapter 2 (Table 2.1).

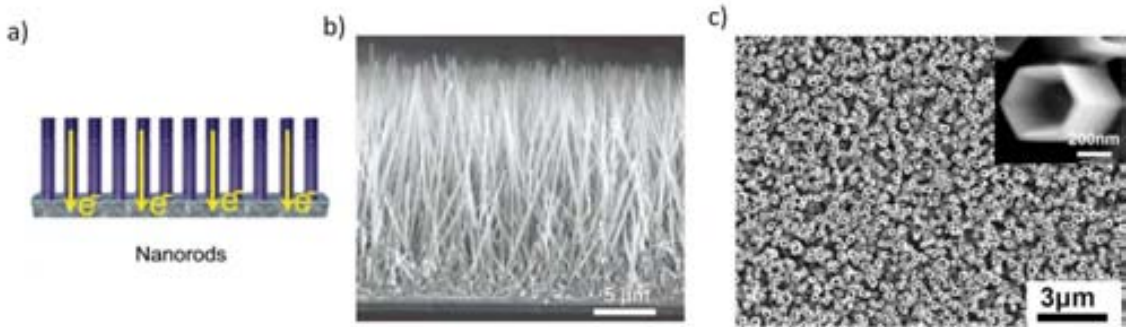

Figure 1.25 a) Schematic representation of the possible electron path taking place on a ZnO NR electrode, b) SEM image of ZnO nanowires[145] and c) SEM image of ZnO nanotubes.[153]

1.4.3.3 Sophisticated ZnO nanostructures: nanotrees, core-shell, nanosheets and nanoflowers

Other more sophisticated nanostructures such as branched NRs could introduce beneficial improvements combining the properties of the NRs, which have good electron transport qualities and the increased surface area when the branches are added (Figure 1.26a).[156] A porous single crystal structure is another reported option to enhance the XSC performance. The highly nanoporous semiconductor ensures an ideal oxide-light harvesting material interaction, in addition to an up-standing with interconnected channels of crystalline ZnO not completely vertical to improve surface area and charge collection (Figure 1.26d).[157, 158] Several types of these ZnO nanostructures have been

obtained: branched nanorods, nanocombs, nanorings, nanospirals, tetrapods, nanoflowers among many others.[116, 159-162] Recently, hierarchical ZnO nanostructures are attracting much attention due to the exhibited highly power conversion efficiencies in DSCs. These reported hierarchical structures comprise nanosheets, nanoplates, dislike nanostructures, spindle-shaped particles, aggregates, etc.[119, 144, 163-169] Some examples of the latter ZnO nanostructures reported in literature are shown in Figure 1.26. A bibliographic review of the different ZnO nanostructures applied in DSCs is presented at the beginning of chapter 3 (Table 3.1).

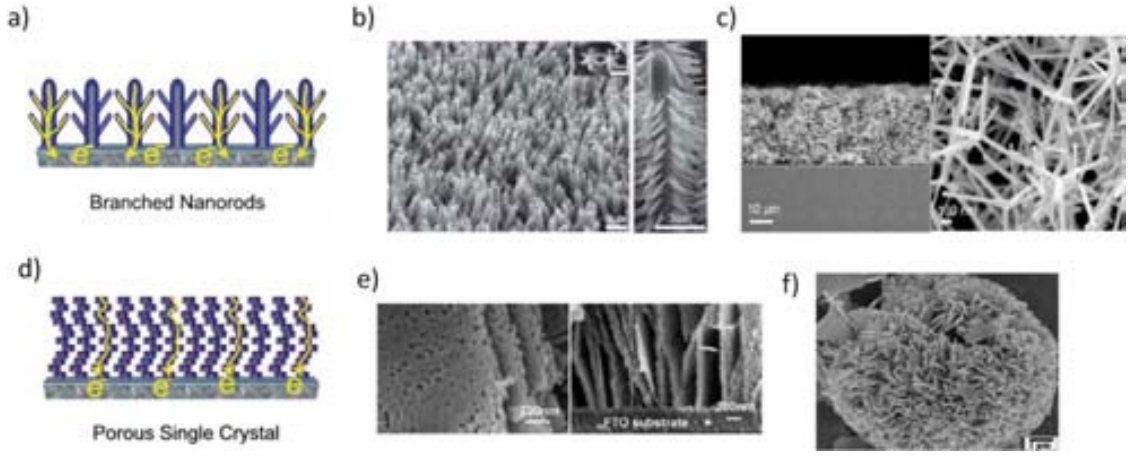

Figure 1.26 Schematic representation of the possible electron path taking place on a)branched NRs and d) Nanoporous electrodes and SEM images of different hierarchical ZnO nanostructures: b) Nanotrees,[170] c) nanotetrapods,[171] e) nanosheets,[172] and f) nanoplates.[119]

1.4.4 Application of ZnO in XSCs

ZnO is a promising material for XSCs due to their similarities of the ZnO properties and other advantages over TiO_2, the most applied semiconductor in XSCs. Here we present the comparison of ZnO properties with TiO_2, a review of the power conversion efficiencies obtained with different ZnO nanostructures; ZnO doped nanostructures and some limitations of ZnO XSCs.

1.4.4.1 Comparison with TiO_2

The band gap of the ZnO is similar to the band gap of TiO_2 and the conduction band edge is located at approximately the same level.[50, 115] A significant advantage over TiO_2 is that ZnO

can be prepared by a wide range of synthesis techniques and easily obtained in a large variety of different morphologies (see section 1.4.2 and 1.4.3). Several of these synthesis methods are low-cost, scalable for large production and suitable for many different substrates.[91] The ZnO nanorods introduce direct electron pathways and avoid the grain boundaries that are electron traps and produce electron recombination as occurs when nanoparticles are used.[50] The ZnO nanostructuration also permits to control the interface between the ETL and LHM or HTL that is an important factor in XSCs (see section 1.4.3). Moreover, ZnO has higher electron mobility and longer electron lifetimes than TiO_2, and even longer when ZnO nanorods were applied.[173, 174] The latter ZnO nanorods improvement was due to a faster and more efficient electron transport. Both properties are very promising for the improvement of XSCs. The latter means that ZnO has lower charge recombination, however, up to now ZnO achieved a lower solar cell performance. Therefore, a careful control of the solar cell parameters must be achieved to overcome these problems. For all these reasons, we decided to study and optimize the preparation of vertically nanostructured ZnO electrodes and its application in XSCs.

1.4.4.2 Nanostructures Vs. Power conversion efficiency

Different ZnO nanostructures were applied in XSCs reporting power conversion efficiencies up to 7.5% for ZnO nanocrystallites.[175] Figure 1.27 shows the reported DSCs power conversion efficiencies values when applying different ZnO nanorods (for details see Table 2.1 and Table 3.1). We can see in Figure 1.27 that many different PCE values were obtained for the same ZnO nanostructure. Thus, the relation concerning performance and the ZnO nanostructure is difficult to be determined since other factors also affect the cell performance such as the ZnO layer thickness, the dye used, the type of platinum counter-electrode, humidity, etc. Therefore, the specification of all the applied XSC conditions is crucial to compare the cell performance.

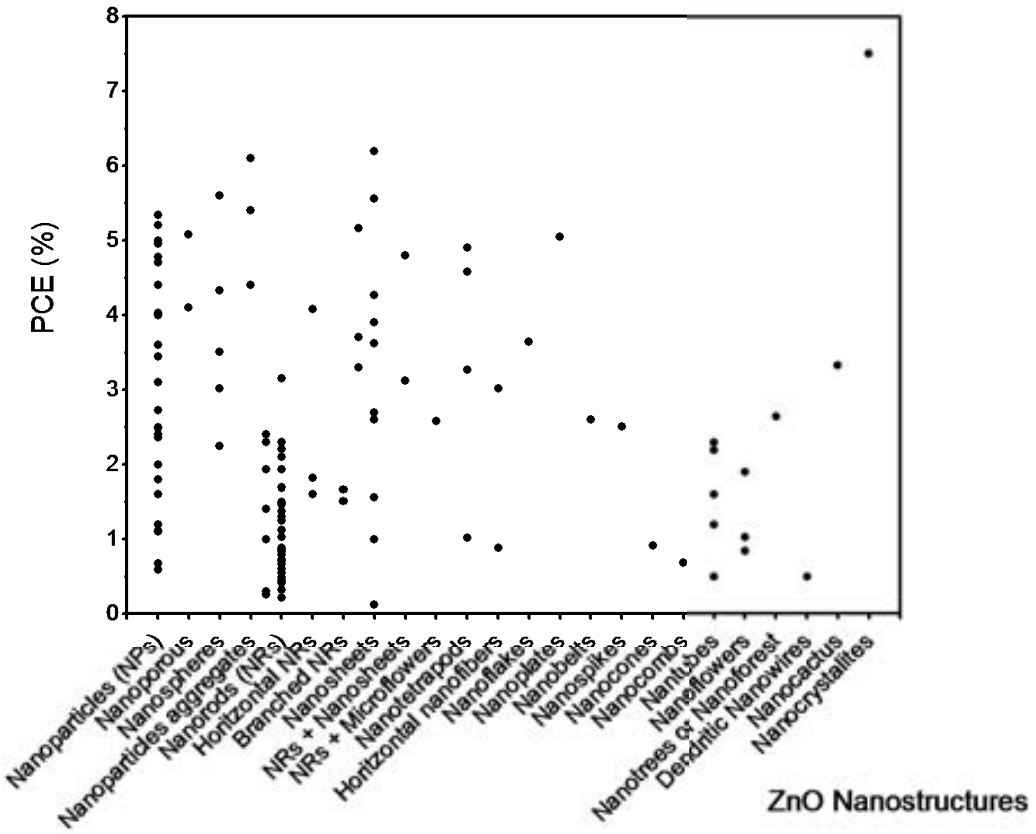

Figure 1.27 Power conversion efficiency (PCE) of DSCs applying different ZnO nanostructures.

1.4.4.3 ZnO doped nanostructures

Doped ZnO nanostructures with appropriate lattice elements are being analyzed to modify the physical and chemical properties of the ZnO semiconductor. The dopant elements can control the band gap and absorption properties or tailor the conductivity of the original material. Many efforts on doping the ZnO have been done in order to modify its conductivity from n-type behavior to a p-type with unsuccessful results as commented in section 1.4.1.3. Many other research groups doped the ZnO with transition elements such as Mn, Fe, Cu, Co or others like Ga, Mg, Sn, Al, etc., to modify its band gap or improve its electron transport properties.[89, 176-181] The doped semiconductor, $Zn_{1-x}M_xO$, applied in XSCs enhanced the charge generation mechanism,[176] increase electrical conductivity[180] and charge carrier density[179] achieving higher efficiencies. Table 1.2 shows some examples from literature of XSC applying doped-ZnO nanostructures. Several groups are studying the properties of doped-ZnO films for Organic solar cells (OSC) in order to replace the transparent conductive layer (TCO).

Table 1.2 Literature examples of XSCs applying doped-ZnO nanostructures. *ECG= Enhance charge generation, IEC= Increase electrical conductivity, ICCD= Increase charge carrier density,*

Type of XSC	ZnO Nanostruct.	Doping agent	Doping agent function	Dye or active blend	Light Intensity (mW/cm^2)	V_{oc} (V)	J_{sc} ($mA \cdot cm^{-2}$)	FF (%)	PCE (%)	Ref.
DSC	Nanoflowers	Au	ECG	N3	100	0.50	15.0	33	2.5	[182]
DSC	Nanorods	Al	IEC	N719	100	0,48	8.9	32	1.3	[180]
DSC	Nanotips	Ga	IEC	N719	100	-	-	55	1.1	[183]
DSC	Nanoparticles	Sn	ICCD	N719	100	0.64	9.2	65	3.8	[179]
OSC	Nanoparticles	Nb	IEC	P3HT:PCBM	120	-	13.9	-	3.6	[184]
OSC	Nanoparticles	Ga	IEC	P3HT:PCBM	100	0.52	8.5	32	1.4	[185]
OSC	Nanoparticles	Ga	IEC	P3HT:PCBM	100	0.42	11.7	40	1.9	[186]
OSC	Nanoparticles	Al	ICCD	P3HT:PCBM	100	0.50	8.9	45	2.0	[187]

1.4.4.4 Limitations of ZnO in Excitonic solar cells (stability)

Up to now, electrodes made of 1D-nanostructures of ZnO have never reach power conversion efficiencies in DSCs comparable its homologue TiO_2 oxide, ZnO around 6-7%[144, 188] and TiO_2-based DSCs 11.3%.[189] Some causes have been related to the low surface area of ZnO NRs, which indicates the need for long NR lengths, only obtainable after long reaction times and time-consuming synthesis and the lower electron injection efficiency for ZnO, an order of magnitude lower than TiO_2.[173, 190] The acidic media of the Dyes employed for DSC is also unfavourable due to the chemical instability of the oxide.[50, 191] Different strategies have been implemented in order to overcome these limitations. For example, the synthesis of branched nanorods (nanoforest, nanotrees) have been applied in order to increase surface area[118, 192] neutral organic Dyes are being applied to reduce ZnO solubility and stability problems[193-196] or the application of different nanoforms (nanosheets[118, 192, 197], nanoflowers[198]), the decoration of the NR with nanoparticles,[199, 200] the application of different electrolytes[201, 202] or the use of core-shell nanostructures[203-210] where a thin layer of an inorganic semiconductor shapes an outer protective layer against corrosion or as electron barrier to enhance the electron transport to the electrode and reduce the recombination.

1.5 Objectives of the thesis

1.5.1 General objective

The general objective of this work is the synthesis and characterization of vertically-aligned ZnO nanostructures and their application in excitonic solar cells (XSC), such as dye sensitized solar cells (DSCs) and organic solar cells (OSCs).

Vertically-aligned nanostructures (nanorods, NRs, nanowires, NWs, nanotubes, NTs, etc.) has been chosen since they present several advantages over the nanoparticle or nanoaggregate structures: they confer faster and more efficient electron transport, avoid grain boundaries (less electron recombination), increase the superficial area and permit the control of the solar cell interface.

The work encompasses the synthesis of different ZnO nanostructures, their characterization, electrode formation and complete solar cell fabrication. A final objective is the comparison between these nanostructures in order to find the relationship between materials properties and device performance.

1.5.2 Specific objectives

1.5.2.1 Synthesis of vertically-aligned ZnO nanostructures

A specific objective of this work is the synthesis of the ZnO nanostructures by the hydrothermal synthesis (or chemical bath deposition) or a modification of the same. This specific synthesis methodology has been selected among others due to its particular characteristics: it is a low-cost synthesis technique with the possibility to be carried out at low-temperature and under water or alcohol solvents. Additionally, the technique permits the formation of ZnO nanostructures on almost any substrate and at large scale (cm scale). The later permits the compatibility of the synthesis method with large-scale fabrication, by solution processing techniques, for the final ZnO electrodes.

A further specific objective is the control the ZnO morphology and dimensions, such as diameter or length. For the latter, several synthesis parameters are optimized: thickness of nucleation seeds layer, distance between the substrate and the bottom of the flask, concentration and growth time, pressure, temperature, among others.

1.5.2.2 Characterization of vertically-aligned ZnO electrodes

An extra specific objective is the characterization of the ZnO NRs and electrodes by several techniques: a) Electron microscope techniques, SEM and TEM, show the ZnO morphologies. These morphologies are important to improve the interface area and also the infiltration of the organic material within the ZnO nanostructure. B) XRD and high resolution TEM present the ZnO crystalline structure. A good crystallinity of the ZnO semiconductor is a relevant factor to achieve high power conversion efficiency due to have less electron traps and present faster electron transport properties. C) The optical quality of the resulting ZnO NRs can be measured by photoluminescence (PL), which reveal the ZnO surface defects. A high concentration of surface defects produces more electron recombination in solar cells and lower power conversion efficiency. The time-resolved PL (TRPL) can determine the electron lifetime for the different ZnO nanostructured electrodes.

1.5.2.3 Complete solar cell fabrication and characterization

Finally, the excitonic solar cells (XSC) under investigation in this work are dye-sensitized solar cells (DSC) and polymer solar cells (PSC). The vertically-aligned ZnO nanostructures can be good candidates to enhance the power conversion efficiencies due to the improvement of the contact between the dye or polymer harvesting materials and the direct electron pathways can reduce the electron recombination processes in these cells.

1.6 Scope of the work

The different vertically-aligned ZnO nanostructures are presented in different chapters (2, 3, 4 and 5). At the beginning of each of these chapters have a short introduction and a literature review of the reported solar cells using similar ZnO nanostructures. Then, it follows a description of the results and finally the conclusions and references.

Chapter 1: The introduction described in this chapter provides a brief overview about the motivation behind this research work. The goal of this chapter is to give a global perspective on the increasing need of renewable energy, the target requirements at

European and National level to cope their implementation by the year 2020 and how our research work can contribute, from the research point of view, to reach these targets.

Chapter 2: Presents the synthesis, preparation and characterization of vertically-aligned ZnO nanorods (NR) electrodes by low-temperature hydrothermal method and their application in Dye sensitized solar cells, DSCs. Several synthesis parameters are optimized and the study of the effect of many factors on the DSCs is also included.

Chapter 3: This chapter describes a modified hydrothermal synthesis method applying an autoclave reactor that is used to prepare vertically-aligned ZnO nanostructured electrodes. The comparison of the ZnO nanostructures obtained by the low-temperature and the autoclave hydrothermal methods and the application in DSCs is presented in this chapter. Besides, a new ZnO nanostructure, ZnO nanotrees, were obtained and characterized.

Chapter 4: The vertically-aligned ZnO nanostructures were covered with a new semiconductor, Indium sulfide, to enhance its properties and increase the power conversion efficiencies of the DSCs. The preparation, characterization of the ZnO/In_xS_y core-shell structure is presented and applied in DSCs.

Chapter 5: All the vertically-aligned ZnO electrodes prepared in chapter 2, 3 and 4 were applied now in polymer solar cells (PSC). The study of the effect of their different morphologies and the polymer blend infiltration within the nanostructures is presented here.

Chapter 6: This chapter describes the experimental procedures: materials, synthesis techniques, solar cells preparation and characterization instruments for all the ZnO nanostructures from chapter 2, 3, 4 and 5.

Chapter 7: The general conclusions of this work are discussed.

1.7 References

1. N. S. Lewis and G. Crabtree, "Basic research needs for solar energy utilization". US Department of Energy Office of Basic Energy Sciences: http://www.sc.doe.gov/bes/reports/files/SEU_rpt.pdf., **2005**.
2. H. Larsen and L. S. Petersen, "Ris Energy Report 9. Non-fossil energy technologies in 2050 and beyond. ". RisØ - DTU: **2010**.
3. "Renewabes in global energy supply". International Energy Agency http://www.iea.org/papers/2006/renewable_factsheet.pdf, **2007**.
4. "BP Statistical Review of World Energy". http://www.bp.com/assets/bp_internet/globalbp/globalbp_uk_english/reports_and_publications/statistical_energy_review_2011/STAGING/local_assets/pdf/statistical_review_of_world_energy_full_report_2012.pdf, **2012**.
5. "Key world energy statistics". International Energy Agency: http://www.iea.org/textbase/nppdf/free/2011/key_world_energy_stats.pdf, **2011**.
6. G. Knies, "Global energy and climate security through solar power from deserts". http://www.desertec.org/downloads/deserts_en.pdf, **2006**.
7. S. Herron, "Solar Irradiation and Energy from Deserts". http://large.stanford.edu/courses/2010/ph240/herron2/, **2010**.
8. "Renewable Energy Technology Roadmap 20% by 2020". European Renewable Energy Council (EREC): http://www.erec.org/fileadmin/erec_docs/Documents/Publications/Renewable_Energy_Technology_Roadmap.pdf, **2007**.
9. "Renewable Energy Technology Roadmap up to 2020". European Renewable Energy Council (EREC): http://www.erec.org/fileadmin/erec_docs/Documents/Publications/EREC-Technoloy_Roadmap_def1.pdf, **2006**.
10. Antonio Gómez, Javier Zubizarreta, Cesar Dopazo and N. Fueyo, "Spanish Energy Roadmap to 2020: Socioeconomic implications of renewable targets". http://www.unizar.es/dopazo/PUBS/Refereed%20Conferences/62%20Spanish%20energy%20roadmap.pdf, **2007**.
11. N. Fueyo, "Renewable hydrogen: Cost and impacts". http://www.climate-change-solutions.co.uk/pictures/content691/09_-_norberto_fueyo_-_1103-aicpe-birmingham_v1_for_web.pdf.
12. "Plan de enegías renovables 2011-2020". IDAE, instituto para la diversificación y ahorro de energía: http://www.idae.es/index.php/mod.documentos/mem.descarga?file=/documentos_11227_PER_2011-2020_def_93c624ab.pdf, **2011**.
13. I. Lafont, "Iberdrola pide que se detenga la inversión en energías renovables". *El País* **2012**.
14. C. J. Brabec, J. A. Hauch, P. Schilinsky and C. Waldauf, "Production aspects of organic photovoltaics and their impact on the commercialization of devices". *Mrs Bulletin* **2005,** 30 (1), 50-52.
15. B. A. Gregg and Ea, "The photoconversion mechanism of excitonic solar cells". *Mrs Bulletin* **2005,** 30 (1), 20-22.
16. M. Gratzel, "Dye-sensitized solid-state heterojunction solar cells". *Mrs Bulletin* **2005,** 30 (1), 23-27.
17. "Technology Roadmap. Solar photovoltaic energy". International Energy Agency: http://www.iea.org/papers/2010/pv_roadmap.pdf, **2010**.
18. S. E. Shaheen, D. S. Ginley, G. E. Jabbour and Ea, "Organic-based photovoltaics. toward low-cost power generation". *Mrs Bulletin* **2005,** 30 (1), 10-19.
19. E. Bundgaard and F. C. Krebs, "Low band gap polymers for organic photovoltaics". *Solar Energy Materials and Solar Cells* **2007,** 91 (11), 954-985.
20. T. L. Benanti and D. Venkataraman, "Organic solar cells: An overview focusing on active layer morphology". *Photosynthesis Research* **2006,** 87 (1), 73-81.

21. F. C. Krebs, S. A. Gevorgyan and J. Alstrup, "A roll-to-roll process to flexible polymer solar cells: model studies, manufacture and operational stability studies". *Journal of Materials Chemistry* **2009,** 19 (30), 5442-5451.
22. C. J. Brabec, A. Cravino, D. Meissner, N. S. Sariciftci, T. Fromherz, M. T. Rispens, L. Sanchez and J. C. Hummelen, "Origin of the open circuit voltage of plastic solar cells". *Advanced Functional Materials* **2001,** 11 (5), 374-380.
23. C. J. Brabec, U. Scherf and V. Dyakonov, "Organic photovoltaics. Materials, Device Physics, and Manufacturing Technologies". Publisher: Wiley-VCH: Book published in Weinheim, **2008**; ISBN: 978-3-527-31675-5.
24. William Adams, "Solar heat A substitute for fuel in tropical countries for heating steam boilers, and other purposes ". Publised in Bombay : printed at the Education Society's Press, Byculla., **1878**.
25. W.G. Adams and R.E. Day, "The Action of Light on Selenium". *Proceedings of the Royal Society (London)* **1877,** A25, 313-349.
26. C.E. Fritts, "On a New Form of Selenium Photocell". *Proceedings of the American Association for the Advancement of Science* **1883,** 33, 97.
27. J. Nelson, "The Physics of Solar Cells". Imperial College press: **2003**; 978-1-86094-340-9.
28. Q. Huang, R. Huang, Z. Wang, Z. Zhan and Y. Wang, "Schottky barrier impact-ionization metal-oxide-semiconductor device with reduced operating voltage". *Applied Physics Letters* **2011,** 99 (8), 083507-3pp.
29. W. Schottky, "For the theory of semiconductor junction and peak rectifier". *Zeitschrift Fur Physik* **1939,** 113 (5-6).
30. D. M. Chapin, C. S. Fuller and G. L. Pearson, "A new silicon p-n junction photocell for converting solar radiation into electrical power ". *Journal of Applied Physics* **1954,** 25 (5).
31. A. Shah, P. Torres, R. Tscharner, N. Wyrsch and H. Keppner, "Photovoltaic technology: The case for thin-film solar cells". *Science* **1999,** 285 (5428).
32. M. Pidwirny, "The encyclopedia of Earth". http://www.eoearth.org/article/Solar_radiation, **2012**.
33. J. Halme. Dye-sensitized nanostructured and organic photovoltaic cells: technical review and preliminary tests. Helsinki University of Technology, **2002**.
34. "ASTM G159-98 Standard Tables for References Solar Spectral Irradiance at Air Mass 1.5". American Society for Testing and Materials (ASTM) http://www.astm.org/Standards/G159.htm, **2005**.
35. "Photovoltaic Measurements: Testing the Electrical Properties of Today's Solar Cells". Keithley Instruments: http://www.keithley.com/events/semconfs/webseminars, **2009**.
36. "Making I-V and C-V Measurements on Solar/Photovoltaic Cells Using the Model 4200-SCS Semiconductor Characterization System"; Keithley Instruments: **2007**.
37. "The basic physics and design of iii-v multijunction solar cells nrel". NREL: http://photochemistry.epfl.ch/EDEY/NREL.pdf.
38. "Guide To Interpreting I-V Curve Measurementsof PV Arrays". Solmetric: http://www.solmetric.com, **2011**.
39. C. Bauer, G. Boschloo, E. Mukhtar and A. Hagfeldt, "Electron injection and recombination in Ru(dcbpy)(2)(NCS)(2) sensitized nanostructured ZnO". *Journal of Physical Chemistry B* **2001,** 105 (24), 5585-5588.
40. J. Nissfolk, K. Fredin, A. Hagfeldt and G. Boschloo, "Recombination and transport processes in dye-sensitized solar cells investigated under working conditions". *Journal of Physical Chemistry B* **2006,** 110 (36), 17715-17718.
41. S. S. Hegedus and W. N. Shafarman, "Thin-film solar cells: Device measurements and analysis". *Progress in Photovoltaics* **2004,** 12 (2-3), 155-176.
42. K.-i. Ishibashi, Y. Kimura and M. Niwano, "An extensively valid and stable method for derivation of all parameters of a solar cell from a single current-voltage characteristic". *Journal of Applied Physics* **2008,** 103 (9).
43. "Part II – Photovoltaic Cell I-V Characterization. Theory and LabVIEW Analysis Code". National Instruments: www.ni.com, **2009**; Vol. 7230.

44. D. L. King, B. R. Hansen, J. A. Kratochvil, M. A. Quintana and Ieee "Dark current-voltage measurements on photovoltaic modules as a diagnostic or manufacturing tool", *26th IEEE Photovoltaic Specialists Conference*, Anaheim, Ca, Sep 29-Oct 03; Anaheim, Ca, **1997**.
45. L. D. Nielsen, "Distributed series resistance effects in solar-cells". *Ieee Transactions on Electron Devices* **1982,** 29 (5).
46. G. L. Araujo, A. Cuevas and J. M. Ruiz, "The effect of distributed series resistance on the dark and illuminated current voltage characteristics of solar-cells ". *Ieee Transactions on Electron Devices* **1986,** 33 (3).
47. A. G. Aberle, S. R. Wenham, M. A. Green and Ieee "A new method for accurate measurements of the lumped series resistance of solar-cells ", *23rd IEEE Photovoltaic Specialists Conference*, Louisville, Ky, May 10-14; Louisville, Ky, **1993**.
48. V. Subramanian, "Nanostructured semiconductor composites for solar cells". *The electrochemical society* **2007**, 32-36.
49. M. Lira-Cantu and I. Gonzalez-Valls, "Nanomaterials for Excitonic Solar Cells". In *Encyclopedia of Nanotechnology*, B. Bushan, Ed. Springer: Ohio, **2012**; pp 1609-1620
50. I. Gonzalez-Valls and M. Lira-Cantu, "Vertically-aligned nanostructures of ZnO for excitonic solar cells: a review". *Energy & Environmental Science* **2009,** 2 (1), 19-34.
51. B. O'Regan and M. Gratzel, "A low-cost, high-efficiency solar-cell based on dye-sensitized colloidal TiO2 films". *Nature* **1991,** 353 (6346), 737-740.
52. M. Gratzel, "Photoelectrochemical cells". *Nature* **2001,** 414 (6861), 338-344.
53. A. Hagfeldt, G. Boschloo, L. Sun, L. Kloo and H. Pettersson, "Dye-Sensitized Solar Cells". *Chemical Reviews* **2010,** 110 (11).
54. C. Xu, J. Wu, U. V. Desai and D. Gao, "High-Efficiency Solid-State Dye-Sensitized Solar Cells Based on TiO2-Coated ZnO Nanowire Arrays". *Nano Letters* **2012,** 12 (5), 2420-2424.
55. H. J. Snaith, R. Humphry-Baker, P. Chen, I. Cesar, S. M. Zakeeruddin and M. Gratzel, "Charge collection and pore filling in solid-state dye-sensitized solar cells". *Nanotechnology* **2008,** 19 (42).
56. G. Q. Wang, L. A. Wang, S. P. Zhuo, S. B. Fang and Y. A. Lin, "An iodine-free electrolyte based on ionic liquid polymers for all-solid-state dye-sensitized solar cells". *Chemical Communications* **2011,** 47 (9), 2700-2702.
57. S. Gunes, H. Neugebauer and N. S. Sariciftci, "Conjugated polymer-based organic solar cells". *Chemical Reviews* **2007,** 107 (4), 1324-1338.
58. P. C. Chang, Z. Y. Fan, D. W. Wang, W. Y. Tseng, W. A. Chiou, J. Hong and J. G. Lu, "ZnO nanowires synthesized by vapor trapping CVD method". *Chemistry of Materials* **2004,** 16 (24), 5133-5137.
59. F. C. Krebs, "Polymer Photovoltaics. A practical approach". Washington, **2008**; 978-0-8194-6781-2.
60. T. Tromholt, A. Manor, E. A. Katz and F. C. Krebs, "Reversible degradation of inverted organic solar cells by concentrated sunlight". *Nanotechnology* **2011,** 22 (22).
61. M. Lira-Cantu, F. C. Krebs, P. Gomez-Romero and S. Yanagida, "Conjugated polymers as part of multifunctional organic/inorganic hybrid materials for photovoltaic applications". *Organic/Inorganic Hybrid Materials - 2007* **2008,** 1007, 249-257.
62. J. A. Ayllon and M. Lira-Cantu, "Application of MEH-PPV/SnO2 bilayer as hybrid solar cell". *Applied Physics a-Materials Science & Processing* **2009,** 95 (1), 249-255.
63. W. J. E. Beek, M. M. Wienk and R. A. J. Janssen, "Efficient hybrid solar cells from zinc oxide nanoparticles and a conjugated polymer". *Advanced Materials* **2004,** 16 (12), 1009-+.
64. M. Lira-Cantu and F. C. Krebs, "Hybrid solar cells based on MEH-PPV and thin film semiconductor oxides (TiO2, Nb2O5, ZnO, CeO(2)and CeO2-TiO2): Performance improvement during long-time irradiation". *Solar Energy Materials and Solar Cells* **2006,** 90 (14), 2076-2086.
65. A. H. Ip, S. M. Thon, S. Hoogland, O. Voznyy, D. Zhitomirsky, R. Debnath, L. Levina, L. R. Rollny, G. H. Carey, A. Fischer, K. W. Kemp, I. J. Kramer, Z. Ning, A. J. Labelle, K. W. Chou, A. Amassian and E. H. Sargent, "Hybrid passivated colloidal quantum dot solids". *Nature Nanotechnology* **2012,** 7 (9).
66. A. J. Nozik, "Quantum dot solar cells". *Physica E-Low-Dimensional Systems & Nanostructures* **2002,** 14 (1-2), 115-120.

67. V. Aroutiounian, S. Petrosyan, A. Khachatryan and K. Touryan, "Quantum dot solar cells". *Journal of Applied Physics* **2001,** 89 (4).
68. P. V. Kamat, "Quantum Dot Solar Cells. Semiconductor Nanocrystals as Light Harvesters". *Journal of Physical Chemistry C* **2008,** 112 (48), 18737-18753.
69. J. H. Bang and P. V. Kamat, "CdSe Quantum Dot-Fullerene Hybrid Nanocomposite for Solar Energy Conversion: Electron Transfer and Photoelectrochemistry". *Acs Nano* **2011,** 5 (12), 9421-9427.
70. A. Luque and A. Marti, "The Intermediate Band Solar Cell: Progress Toward the Realization of an Attractive Concept". *Advanced Materials* **2010,** 22 (2), 160-174.
71. C. J. Brabec, N. S. Sariciftci and J. C. Hummelen, "Plastic solar cells". *Advanced Functional Materials* **2001,** 11 (1), 15-26.
72. A. F. Kohan, G. Ceder, D. Morgan and C. G. Van de Walle, "First-principles study of native point defects in ZnO". *Physical Review B* **2000,** 61 (22), 15019-15027.
73. R. A. J. Janssen, J. C. Hummelen, N. S. Saricifti and Ea, "Polymer-fullerene bulk heterojunction solar cells". *Mrs Bulletin* **2005,** 30 (1), 33-36.
74. G. Yu, J. Gao, J. C. Hummelen, F. Wudl and A. J. Heeger, "Polymer Photovoltaic Cells - Enhanced efficiencies via a network of internal donor-acceptor heterojunctions". *Science* **1995,** 270 (5243), 1789-1791.
75. S. D. Oosterhout, M. M. Wienk, S. S. van Bavel, R. Thiedmann, L. J. A. Koster, J. Gilot, J. Loos, V. Schmidt and R. A. J. Janssen, "The effect of three-dimensional morphology on the efficiency of hybrid polymer solar cells". *Nature Materials* **2009,** 8 (10), 818-824.
76. S. S. van Bavel, E. Sourty, G. de With and J. Loos, "Three-Dimensional Nanoscale Organization of Bulk Heterojunction Polymer Solar Cells". *Nano Letters* **2009,** 9 (2), 507-513.
77. A. Janotti and C. G. Van de Walle, "Fundamentals of zinc oxide as a semiconductor". *Reports on Progress in Physics* **2009,** 72 (12).
78. L. Schmidt-Mende and J. L. MacManus-Driscoll, "ZnO - nanostructures, defects, and devices". *Materials Today* **2007,** 10 (5), 40-48.
79. " ZnO CAS no: 1314-13-2". CAS database: http://www.chemicalbook.com/ChemicalProductProperty_EN_CB3853034.htm.
80. "CRC Handbook of Chemistry and Physics". 67Th ed.; CRC Press, Inc.: Florida, **1986**.
81. "TAPP: Thermomechanical and Physical Properties". In *Base de datos*, ESM software: **1998**.
82. J. Nause and B. Nemeth, "Pressurized melt growth of ZnO boules". *Semiconductor Science and Technology* **2005,** 20 (4).
83. U. Ozgur, Y. I. Alivov, C. Liu, A. Teke, M. A. Reshchikov, S. Dogan, V. Avrutin, S. J. Cho and H. Morkoc, "A comprehensive review of ZnO materials and devices". *Journal of Applied Physics* **2005,** 98 (4).
84. H. Morkoc and U. Ozgur, "Zinc Oxide: Fundamentals, materials and device technology". Wiley-VCH: Weinheim, **2009**; 978-3-527-40813-9.
85. P. E. Champness, "Electron diffraction in the transmission electron microscope". **2001**; Vol. 47, p 170 1859961479, 9781859961476.
86. A. B. Djurisic, X. Chen, Y. H. Leung and A. M. C. Ng, "ZnO nanostructures: growth, properties and applications". *Journal of Materials Chemistry* **2012,** 22 (14).
87. A. B. Djurisic and Y. H. Leung, "Optical properties of ZnO nanostructures". *Small* **2006,** 2 (8-9).
88. O. Lupan, T. Pauporte and B. Viana, "Low-Voltage UV-Electroluminescence from ZnO-Nanowire Array/p-GaN Light-Emitting Diodes". *Advanced Materials* **2010,** 22 (30), 3298-+.
89. O. Lupan, T. Pauporte, T. Le Bahers, B. Viana and I. Ciofini, "Wavelength-Emission Tuning of ZnO Nanowire-Based Light-Emitting Diodes by Cu Doping: Experimental and Computational Insights". *Advanced Functional Materials* **2011,** 21 (18), 3564-3572.
90. A. B. Djurisic, Y. H. Leung, K. H. Tam, Y. F. Hsu, L. Ding, W. K. Ge, Y. C. Zhong, K. S. Wong, W. K. Chan, H. L. Tam, K. W. Cheah, W. M. Kwok and D. L. Phillips, "Defect emissions in ZnO nanostructures". *Nanotechnology* **2007,** 18, 095702.
91. L. E. Greene, M. Law, J. Goldberger, F. Kim, J. C. Johnson, Y. F. Zhang, R. J. Saykally, P. D. Yang and Qp, "Low-temperature wafer-scale production of ZnO nanowire arrays". *Angewandte Chemie-International Edition* **2003,** 42 (26), 3031-3034.

92. J. P. Liu, X. T. Huang, Y. Y. Li, X. X. Ji, Z. K. Li, X. He and F. L. Sun, "Vertically aligned 1D ZnO nanostructures on bulk alloy substrates: Direct solution synthesis, photoluminescence, and field emission". *Journal of Physical Chemistry C* **2007,** 111 (13), 4990-4997.
93. Z. Qin, Q. L. Liao, Y. H. Huang, L. D. Tang, X. H. Zhang and Y. Zhang, "Effect of hydrothermal reaction temperature on growth, photoluminescence and photoelectrochemical properties of ZnO nanorod arrays". *Materials Chemistry and Physics* **2010,** 123 (2-3), 811-815.
94. A. van Dijken, E. A. Meulenkamp, D. Vanmaekelbergh and A. Meijerink, "Identification of the transition responsible for the visible emission in ZnO using quantum size effects". *Journal of Luminescence* **2000,** 90 (3-4), 123-128.
95. X. Liu, X. H. Wu, H. Cao and R. P. H. Chang, "Growth mechanism and properties of ZnO nanorods synthesized by plasma-enhanced chemical vapor deposition". *Journal of Applied Physics* **2004,** 95 (6), 3141-3147.
96. S. E. Harrison, "Conductivity and hall effect of ZnO at low temperatures ". *Physical Review* **1954,** 93 (1).
97. A. R. Hutson, "Hall effect studies of doped Zin Oxide single crystals ". *Physical Review* **1957,** 108 (2).
98. K. I. Hagemark, "Defect structure of Zn-doped ZnO". *Journal of Solid State Chemistry* **1976,** 16 (3-4).
99. C. G. Van de Walle, "Hydrogen as a cause of doping in zinc oxide". *Physical Review Letters* **2000,** 85 (5).
100. A. Janotti and C. G. Van de Walle, "Native point defects in ZnO". *Physical Review B* **2007,** 76 (16).
101. S. F. J. Cox, E. A. Davis, S. P. Cottrell, P. J. C. King, J. S. Lord, J. M. Gil, H. V. Alberto, R. C. Vilao, J. P. Duarte, N. A. de Campos, A. Weidinger, R. L. Lichti and S. J. C. Irvine, "Experimental confirmation of the predicted shallow donor hydrogen state in zinc oxide". *Physical Review Letters* **2001,** 86 (12).
102. Y. M. Strzhemechny, H. L. Mosbacker, D. C. Look, D. C. Reynolds, C. W. Litton, N. Y. Garces, N. C. Giles, L. E. Halliburton, S. Niki and L. J. Brillson, "Remote hydrogen plasma doping of single crystal ZnO". *Applied Physics Letters* **2004,** 84 (14).
103. A. Tsukazaki, A. Ohtomo, T. Onuma, M. Ohtani, T. Makino, M. Sumiya, K. Ohtani, S. F. Chichibu, S. Fuke, Y. Segawa, H. Ohno, H. Koinuma and M. Kawasaki, "Repeated temperature modulation epitaxy for p-type doping and light-emitting diode based on ZnO". *Nature Materials* **2005,** 4 (1).
104. D. C. Look, D. C. Reynolds, C. W. Litton, R. L. Jones, D. B. Eason and G. Cantwell, "Characterization of homoepitaxial p-type ZnO grown by molecular beam epitaxy". *Applied Physics Letters* **2002,** 81 (10).
105. C. H. Park, S. B. Zhang and S. H. Wei, "Origin of p-type doping difficulty in ZnO: The impurity perspective". *Physical Review B* **2002,** 66 (7).
106. S. Limpijumnong, S. B. Zhang, S. H. Wei and C. H. Park, "Doping by large-size-mismatched impurities: The microscopic origin of arsenic- or antimony-doped p-type zinc oxide". *Physical Review Letters* **2004,** 92 (15).
107. M. Lira-Cantu, K. Norrman, J. W. Andreasen, F. C. Krebs and Nw, "Oxygen release and exchange in niobium oxide MEHPPV hybrid solar cells". *Chemistry of Materials* **2006,** 18 (24), 5684-5690.
108. M. Lira-Cantu, K. Norrman, J. W. Andreasen, N. Casan-Pastor and F. C. Krebs, "Detrimental effect of inert atmospheres on hybrid solar cells based on semiconductor oxides". *Journal of the Electrochemical Society* **2007,** 154 (6), B508-B513.
109. S. N. Das, J. H. Choi, J. P. Kar and J. M. Myoung, "Tunable and reversible surface wettability transition of vertically aligned ZnO nanorod arrays". *Applied Surface Science* **2009,** 255 (16), 7319-7322.
110. X. J. Feng, L. Feng, M. H. Jin, J. Zhai, L. Jiang and D. B. Zhu, "Reversible super-hydrophobicity to super-hydrophilicity transition of aligned ZnO nanorod films". *Journal of the American Chemical Society* **2004,** 126 (1), 62-63.

111. G. Kenanakis, E. Stratakis, K. Vlachou, D. Vernardou, E. Koudoumas and N. Katsarakis, "Light-induced reversible hydrophilicity of ZnO structures grown by aqueous chemical growth". *Applied Surface Science* **2008,** 254 (18), 5695-5699.
112. R. D. Sun, A. Nakajima, A. Fujishima, T. Watanabe and K. Hashimoto, "Photoinduced surface wettability conversion of ZnO and TiO2 thin films". *Journal of Physical Chemistry B* **2001,** 105 (10), 1984-1990.
113. K. Keis, C. Bauer, G. Boschloo, A. Hagfeldt, K. Westermark, H. Rensmo and H. Siegbahn, "Nanostructured ZnO electrodes for dye-sensitized solar cell applications". *Journal of Photochemistry and Photobiology a-Chemistry* **2002,** 148 (1-3), 57-64.
114. H. Horiuchi, R. Katoh, K. Hara, M. Yanagida, S. Murata, H. Arakawa and M. Tachiya, "Electron injection efficiency from excited N3 into nanocrystalline ZnO films: Effect of (N3-Zn2+) aggregate formation". *Journal of Physical Chemistry B* **2003,** 107 (11), 2570-2574.
115. I. Gonzalez-Valls and M. Lira-Cantu, "Dye sensitized solar cells based on vertically-aligned ZnO nanorods: effect of UV light on power conversion efficiency and lifetime". *Energy & Environmental Science* **2010,** 3 (6), 789-795.
116. Q. F. Zhang, C. S. Dandeneau, X. Y. Zhou and G. Z. Cao, "ZnO Nanostructures for Dye-Sensitized Solar Cells". *Advanced Materials* **2009,** 21 (41), 4087-4108.
117. A. Elkhidir Suliman, Y. Tang and L. Xu, "Preparation of ZnO nanoparticles and nanosheets and their application to dye-sensitized solar cells". *Solar Energy Materials and Solar Cells* **2007,** 91 (18), 1658-1662.
118. F. Xu and L. T. Sun, "Solution-derived ZnO nanostructures for photoanodes of dye-sensitized solar cells". *Energy & Environmental Science* **2011,** 4 (3), 818-841.
119. Y. C. Qiu, W. Chen and S. H. Yang, "Facile hydrothermal preparation of hierarchically assembled, porous single-crystalline ZnO nanoplates and their application in dye-sensitized solar cells". *Journal of Materials Chemistry* **2010,** 20 (5), 1001-1006.
120. L. Vayssieres, "Growth of arrayed nanorods and nanowires of ZnO from aqueous solutions". *Advanced Materials* **2003,** 15 (5), 464-466.
121. Y. Wang and M. Li, "Hydrothermal synthesis of single-crystalline hexagonal prism ZnO nanorods". *Materials Letters* **2006,** 60 (2), 266-269.
122. W. X. Zhang and K. Yanagisawa, "Hydrothermal synthesis of zinc hydroxide chloride sheets and their conversion to ZnO". *Chemistry of Materials* **2007,** 19 (9), 2329-2334.
123. M. Guo, P. Diao, S. M. Cai and Bg, "Hydrothermal growth of well-aligned ZnO nanorod arrays: Dependence of morphology and alignment ordering upon preparing conditions". *Journal of Solid State Chemistry* **2005,** 178 (6), 1864-1873.
124. Q. Ahsanulhaq, A. Umar and Y. B. Hahn, "Growth of aligned ZnO nanorods and nanopencils on ZnO/Si in aqueous solution: growth mechanism and structural and optical properties". *Nanotechnology* **2007,** 18 (11), 115603.
125. Q. C. Li, V. Kumar, Y. Li, H. T. Zhang, T. J. Marks and R. P. H. Chang, "Fabrication of ZnO nanorods and nanotubes in aqueous solutions". *Chemistry of Materials* **2005,** 17 (5), 1001-1006.
126. B. Cheng and E. T. Samulski, "Hydrothermal synthesis of one-dimensional ZnO nanostructures with different aspect ratios". *Chemical Communications* **2004,** (8), 986-987.
127. C. H. Lu, L. M. Qi, J. H. Yang, L. Tang, D. Y. Zhang, J. M. Ma and Wa, "Hydrothermal growth of large-scale micropatterned arrays of ultralong ZnO nanowires and nanobelts on zinc substrate". *Chemical Communications* **2006,** (33), 3551-3553.
128. K. W. Sue, K. Kimura, M. Yamamoto and K. Arai, "Rapid hydrothermal synthesis of ZnO nanorods without organics". *Materials Letters* **2004,** 58 (26), 3350-3352.
129. M. Willander, O. Nur, Q. X. Zhao, L. L. Yang, M. Lorenz, B. Q. Cao, J. Z. Perez, C. Czekalla, G. Zimmermann, M. Grundmann, A. Bakin, A. Behrends, M. Al-Suleiman, A. El-Shaer, A. C. Mofor, B. Postels, A. Waag, N. Boukos, A. Travlos, H. S. Kwack, J. Guinard and D. L. Dang, "Zinc oxide nanorod based photonic devices: recent progress in growth, light emitting diodes and lasers". *Nanotechnology* **2009,** 20 (33).
130. Z. L. Wang, "Zinc oxide nanostructures: Growth, properties and applications". *Journal of Physics Condensed Matter* **2004,** 16 (25).
131. M. H. Huang, Y. Wu, H. Feick, N. Tran, E. Weber and P. Yang, "Catalytic growth of zinc oxide nanowires by vapor transport". *Advanced Materials* **2001,** 13 (2), 113-116.

132. H. T. Ng, J. Han, T. Yamada, P. Nguyen, Y. P. Chen and M. Meyyappan, "Single crystal nanowire vertical surround-gate field-effect transistor". *Nano Letters* **2004,** 4 (7), 1247-1252.
133. E. C. Greyson, Y. Babayan and T. W. Odom, "Directed growth of ordered arrays of small-diameter ZnO nanowires". *Advanced Materials* **2004,** 16 (15 SPEC. ISS.), 1348-1352.
134. T. K. Shing, H. H. Pan, I. C. Chen and C. I. Kuo, "Growth and patterning of ZnO nanowires on silicon and LiNbO3 substrates". *Tamkang Journal of Science and Engineering* **2004,** 7 (3), 135-138.
135. D. S. Yu, T. Trad, J. T. McLeskey, V. Craciun and C. R. Taylor, "ZnO Nanowires Synthesized by Vapor Phase Transport Deposition on Transparent Oxide Substrates". *Nanoscale Research Letters* **2010,** 5 (8), 1333-1339.
136. J. H. Choi, H. Tabata and T. Kawai, "Initial preferred growth in zinc oxide thin films on Si and amorphous substrates by a pulsed laser deposition". *Journal of Crystal Growth* **2001,** 226 (4), 493-500.
137. M. Ahmad and J. Zhu, "ZnO based advanced functional nanostructures: synthesis, properties and applications". *Journal of Materials Chemistry* **2011,** 21 (3).
138. S. M. George, "Atomic Layer Deposition: An Overview". *Chemical Reviews* **2010,** 110 (1).
139. T. Pauporte and D. Lincot, "Heteroepitaxial electrodeposition of zinc oxide films on gallium nitride". *Applied Physics Letters* **1999,** 75 (24), 3817-3819.
140. T. Yoshida, J. B. Zhang, D. Komatsu, S. Sawatani, H. Minoura, T. Pauporte, D. Lincot, T. Oekermann, D. Schlettwein, H. Tada, D. Wohrle, K. Funabiki, M. Matsui, H. Miura and H. Yanagi, "Electrodeposition of Inorganic/Organic Hybrid Thin Films". *Advanced Functional Materials* **2009,** 19 (1), 17-43.
141. S. Xu and Z. L. Wang, "One-dimensional ZnO nanostructures: Solution growth and functional properties". *Nano Research* **2011,** 4 (11).
142. J. Elias, R. Tena-Zaera and C. Lévy-Clément, "Electrochemical deposition of ZnO nanowire arrays with tailored dimensions". *Journal of Electroanalytical Chemistry* **2008,** 621 (2), 171-177.
143. A. Goux, T. Pauporte, J. Chivot and D. Lincot, "Temperature effects on ZnO electrodeposition". *Electrochimica Acta* **2005,** 50 (11), 2239-2248.
144. Q. F. Zhang, C. S. Dandeneau, S. Candelaria, D. W. Liu, B. B. Garcia, X. Y. Zhou, Y. H. Jeong and G. Z. Cao, "Effects of Lithium Ions on Dye-Sensitized ZnO Aggregate Solar Cells". *Chemistry of Materials* **2010,** 22 (8), 2427-2433.
145. L. E. Greene, B. D. Yuhas, M. Law, D. Zitoun and P. D. Yang, "Solution-grown zinc oxide nanowires". *Inorganic Chemistry* **2006,** 45 (19), 7535-7543.
146. M. Law, L. E. Greene, J. C. Johnson, R. Saykally and P. D. Yang, "Nanowire dye-sensitized solar cells". *Nature Materials* **2005,** 4 (6), 455-459.
147. Y. W. Heo, D. P. Norton, L. C. Tien, Y. Kwon, B. S. Kang, F. Ren, S. J. Pearton and J. R. LaRoche, "ZnO nanowire growth and devices". *Materials Science & Engineering R-Reports* **2004,** 47 (1-2), 1-47.
148. Y. W. Heo, L. C. Tien, D. P. Norton, B. S. Kang, F. Ren, B. P. Gila and S. J. Pearton, "Electrical transport properties of single ZnO nanorods". *Applied Physics Letters* **2004,** 85 (11), 2002-2004.
149. O. Lupan, V. M. Guerin, I. M. Tiginyanu, V. V. Ursaki, L. Chow, H. Heinrich and T. Pauporte, "Well-aligned arrays of vertically oriented ZnO nanowires electrodeposited on ITO-coated glass and their integration in dye sensitized solar cells". *Journal of Photochemistry and Photobiology a-Chemistry* **2010,** 211 (1), 65-73.
150. C. Badre, T. Pauporte, M. Turmine and D. Lincot, "A ZnO nanowire array film with stable highly water-repellent properties". *Nanotechnology* **2007,** 18 (36).
151. C. J. Murphy and N. R. Jana, "Controlling the aspect ratio of inorganic nanorods and nanowires". *Advanced Materials* **2002,** 14 (1).
152. M. Tsuji, K. Matsumoto, P. Jiang, R. Matsuo, X.-L. Tang and K. S. N. Karnarudin, "Roles of Pt seeds and chloride anions in the preparation of silver nanorods and nanowires by microwave-polyol method". *Colloids and Surfaces a-Physicochemical and Engineering Aspects* **2008,** 316 (1-3), 266-277.

153. B. Cheng, W. S. Shi, J. M. Russell-Tanner, L. Zhang and E. T. Samulski, "Synthesis of variable-aspect-ratio, single-crystalline ZnO nanostructures". *Inorganic Chemistry* **2006,** 45 (3), 1208-1214.
154. G. W. Slawinski and F. P. Zamborini, "Synthesis and alignment of silver nanorods and nanowires and the formation of pt, pd, and Core/Shell structures by galvanic exchange directly on surfaces". *Langmuir* **2007,** 23 (20), 10357-10365.
155. G. Cao and Y. Wang, "Nanostructures And Nanomaterials: Synthesis, Properties & Applications". **2011**; p 600 ISBN-13: 978-9814324557
156. C. Y. Jiang, X. W. Sun, G. Q. Lo, D. L. Kwong, J. X. Wang and Fc, "Improved dye-sensitized solar cells with a ZnO-nanoflower photoanode". *Applied Physics Letters* **2007,** 90 (26), 263501.
157. T. Yoshida, M. Iwaya, H. Ando, T. Oekermann, K. Nonomura, D. Schlettwein, D. Wohrle and H. Minoura, "Improved photoelectrochemical performance of electrodeposited ZnO/EosinY hybrid thin films by dye re-adsorption". *Chemical Communications* **2004,** (4), 400-401.
158. T. Yoshida, K. Terada, D. Schlettwein, T. Oekermann, T. Sugiura and H. Minoura, "Electrochemical self-assembly of nanoporous ZnO/eosin Y thin films and their sensitized photoelectrochemical performance". *Advanced Materials* **2000,** 12 (16), 1214-1217.
159. Z. L. Wang, "Nanostructures of zinc oxide". *Materials Today* **2004,** 7 (6), 26-33.
160. V. V. Kislyuk and O. P. Dimitriev, "Nanorods and nanotubes for solar cells". *Journal of Nanoscience and Nanotechnology* **2008,** 8 (1), 131-148.
161. Q. Zhang and G. Cao, "Nanostructured photoelectrodes for dye-sensitized solar cells". *Nano Today* **2011,** 6 (1), 91-109.
162. C. Magne, T. Moehl, M. Urien, M. Graetzel and T. Pauporte, "Effects of ZnO film growth route and nanostructure on electron transport and recombination in dye-sensitized solar cells". *Journal of Materials Chemistry A* **2013,** 1 (6), 2079-2088.
163. C. K. Xu, P. Shin, L. L. Cao and D. Gao, "Preferential Growth of Long ZnO Nanowire Array and Its Application in Dye-Sensitized Solar Cells". *Journal of Physical Chemistry C* **2010,** 114 (1), 125-129.
164. J. X. Wang, C. M. L. Wu, W. S. Cheung, L. B. Luo, Z. B. He, G. D. Yuan, W. J. Zhang, C. S. Lee and S. T. Lee, "Synthesis of Hierarchical Porous ZnO Disklike Nanostructures for Improved Photovoltaic Properties of Dye-Sensitized Solar Cells". *Journal of Physical Chemistry C* **2010,** 114 (31), 13157-13161.
165. H. M. Cheng and W. F. Hsieh, "High-efficiency metal-free organic-dye-sensitized solar cells with hierarchical ZnO photoelectrode". *Energy & Environmental Science* **2010,** 3 (4), 442-447.
166. Y. T. Shi, C. Zhan, L. D. Wang, B. B. Ma, R. Gao, Y. F. Zhu and Y. Qiu, "Polydisperse Spindle-Shaped ZnO Particles with Their Packing Micropores in the Photoanode for Highly Efficient Quasi-Solid Dye-Sensitized Solar Cells". *Advanced Functional Materials* **2010,** 20 (3), 437-444.
167. V. M. Guerin, J. Rathousky and T. Pauporte, "Electrochemical design of ZnO hierarchical structures for dye-sensitized solar cells". *Solar Energy Materials and Solar Cells* **2012,** 102.
168. V.-M. Guerin and T. Pauporte, "From nanowires to hierarchical structures of template-free electrodeposited ZnO for efficient dye-sensitized solar cells". *Energy & Environmental Science* **2011,** 4 (8), 2971-2979.
169. V. M. Guerin, J. Elias, T. T. Nguyen, L. Philippe and T. Pauporte, "Ordered networks of ZnO-nanowire hierarchical urchin-like structures for improved dye-sensitized solar cells". *Physical Chemistry Chemical Physics* **2012,** 14 (37), 12948-12955.
170. Fenghua Zhao, Jian-Guo Zheng, Xianfeng Yang, Xiuyan Li, Jing Wang, Fuli Zhao, Kam Sing Wong, Chaolun Lianga and M. Wu, "Complex ZnO nanotree arrays with tunable top, stem and branch structures". *Nanoscale* **2010,** 2, 1674–1683.
171. W. Chen, H. F. Zhang, I. M. Hsing and S. H. Yang, "A new photoanode architecture of dye sensitized solar cell based on ZnO nanotetrapods with no need for calcination". *Electrochem. Commun.* **2009,** 11 (5), 1057-1060.
172. X. Y. Wang, Z. P. Tian, T. Yu, H. M. Tian, J. Y. Zhang, S. K. Yuan, X. B. Zhang, Z. S. Li and Z. G. Zou, "Effective electron collection in highly (110)-oriented ZnO porous nanosheet framework photoanode". *Nanotechnology* **2010,** 21 (6), 285311.

173. M. Quintana, T. Edvinsson, A. Hagfeldt and G. Boschloo, "Comparison of dye-sensitized ZnO and TiO2 solar cells: Studies of charge transport and carrier lifetime". *Journal of Physical Chemistry C* **2007,** 111 (2), 1035-1041.
174. E. Galoppini, J. Rochford, H. H. Chen, G. Saraf, Y. C. Lu, A. Hagfeldt and G. Boschloo, "Fast electron transport in metal organic vapor deposition grown dye-sensitized ZnO nanorod solar cells". *Journal of Physical Chemistry B* **2006,** 110 (33), 16159-16161.
175. N. Memarian, I. Concina, A. Braga, S. M. Rozati, A. Vomiero and G. Sberveglieri, "Hierarchically Assembled ZnO Nanocrystallites for High-Efficiency Dye-Sensitized Solar Cells". *Angewandte Chemie-International Edition* **2011,** 50 (51).
176. J. Piris, N. Kopidakis, D. C. Olson, S. E. Shaheen, D. S. Ginley and G. Rumbles, "The locus of free charge-carrier generation in solution-cast Zn1-xMgxO/Poly(3-hexylthiophene) Bilayers for photovoltaic applications". *Advanced Functional Materials* **2007,** 17 (18).
177. B. D. Yuhas, D. O. Zitoun, P. J. Pauzauskie, R. R. He and P. D. Yang, "Transition-metal doped zinc oxide nanowires". *Angewandte Chemie-International Edition* **2006,** 45 (3), 420-423.
178. A. De Souza Gonc?alves, M. R. Davolos, N. Masaki, S. Yanagida, A. Morandeira, J. R. Durrant, J. N. Freitas and A. F. Nogueira, "Synthesis and characterization of ZnO and ZnO:Ga films and their application in dye-sensitized solar cells". *Dalton Transactions* **2008,** (11), 1487-1491.
179. N. Ye, J. J. Qi, Z. Qi, X. M. Zhang, Y. Yang, J. Liu and Y. Zhang, "Improvement of the performance of dye-sensitized solar cells using Sn-doped ZnO nanoparticles". *Journal of Power Sources* **2010,** 195 (17), 5806-5809.
180. S. Yun, J. Lee, J. Chung and S. Lim, "Improvement of ZnO nanorod-based dye-sensitized solar cell efficiency by Al-doping". *Journal of Physics and Chemistry of Solids* **2010,** 71 (12), 1724-1731.
181. O. Lupan, T. Pauporte, B. Viana, V. V. Ursaki, I. M. Tiginyanu, V. Sontea and L. Chow, "UV-Blue and Green Electroluminescence from Cu-Doped ZnO Nanorod Emitters Hydrothermally Synthesized on p-GaN". *Journal of Nanoelectronics and Optoelectronics* **2012,** 7 (7), 712-718.
182. V. Dhas, S. Muduli, W. Lee, S. H. Han and S. Ogale, "Enhanced conversion efficiency in dye-sensitized solar cells based on ZnO bifunctional nanoflowers loaded with gold nanoparticles". *Applied Physics Letters* **2008,** 93 (24).
183. H. H. Chen, A. Du Pasquier, G. Saraf, J. Zhong and Y. Lu, "Dye-sensitized solar cells using ZnO nanotips and Ga-doped ZnO films". *Semiconductor Science and Technology* **2008,** 23 (4).
184. Viruntachar Kruefu, Eric Peterson, Chanitpa Khantha, Chawarat Siriwong, Sukon Phanichphant and D. L. Carroll, "Flame-made niobium doped zinc oxide nanoparticles in bulk heterojunction solar cells". *Appl. Phys. Lett.* **2010,** 97, 053302.
185. J. Owen, M. S. Son, K. H. Yoo, B. D. Ahn and S. Y. Lee, "Organic photovoltaic devices with Ga-doped ZnO electrode". *Applied Physics Letters* **2007,** 90 (3).
186. K. S. Shin, K. H. Lee, H. H. Lee, D. Choi and S. W. Kim, "Enhanced Power Conversion Efficiency of Inverted Organic Solar Cells with a Ga-Doped ZnO Nanostructured Thin Film Prepared Using Aqueous Solution". *Journal of Physical Chemistry C* **2010,** 114 (37), 15782-15785.
187. J. H. Park, K. J. Ahn, K. I. Park, S. I. Na and H. K. Kim, "An Al-doped ZnO electrode grown by highly efficient cylindrical rotating magnetron sputtering for low cost organic photovoltaics". *Journal of Physics D-Applied Physics* **2010,** 43 (11).
188. K. Keis, E. Magnusson, H. Lindstrom, S. E. Lindquist and A. Hagfeldt, "A 5% efficient photo electrochemical solar cell based on nanostructured ZnO electrodes". *Solar Energy Materials and Solar Cells* **2002,** 73 (1), 51-58.
189. Y. Chiba, A. Islam, Y. Watanabe, R. Komiya, N. Koide and L. Y. Han, "Dye-sensitized solar cells with conversion efficiency of 11.1%". *Jpn. J. Appl. Phys. Part 2 - Lett. Express Lett.* **2006,** 45 (24-28), L638-L640.
190. N. A. Anderson, X. Ai and T. Q. Lian, "Electron injection dynamics from Ru polypyridyl complexes to ZnO nanocrystalline thin films". *Journal of Physical Chemistry B* **2003,** 107 (51), 14414-14421.
191. I. Gonzalez-Valls, Y. Yu, B. Ballesteros, J. Oro and M. Lira-Cantu, "Synthesis conditions, light intensity and temperature effect on the performance of ZnO nanorods-based Dye sensitized solar cells". *Journal of Power Sources* **2011,** 196, 6609–6621.

192. S. H. Ko, D. Lee, H. W. Kang, K. H. Nam, J. Y. Yeo, S. J. Hong, C. P. Grigoropoulos and H. J. Sung, "Nanoforest of Hydrothermally Grown Hierarchical ZnO Nanowires for a High Efficiency Dye-Sensitized Solar Cell". *Nano Letters* **2011,** 11 (2), 666-671.
193. J. S. Bendall, L. Etgar, S. C. Tan, N. Cai, P. Wang, S. M. Zakeeruddin, M. Graetzel and M. E. Welland, "An efficient DSSC based on ZnO nanowire photo-anodes and a new D-pi-A organic dye". *Energy & Environmental Science* **2011,** 4 (8), 2903-2908.
194. P. Ruankham, L. Macaraig, T. Sagawa, H. Nakazumi and S. Yoshikawa, "Surface Modification of ZnO Nanorods with Small Organic Molecular Dyes for Polymer-Inorganic Hybrid Solar Cells". *Journal of Physical Chemistry C* **2011,** 115 (48), 23809-23816.
195. M. Quintana, T. Marinado, K. Nonomura, G. Boschloo and A. Hagfeldt, "Organic chromophore-sensitized ZnO solar cells: Electrolyte-dependent dye desorption and band-edge shifts". *Journal of Photochemistry and Photobiology a-Chemistry* **2009,** 202 (2-3), 159-163.
196. X. Jiang, K. M. Karlsson, E. Gabrielsson, E. M. J. Johansson, M. Quintana, M. Karlsson, L. Sun, G. Boschloo and A. Hagfeldt, "Highly Efficient Solid-State Dye-Sensitized Solar Cells Based on Triphenylamine Dyes". *Advanced Functional Materials* **2011,** 21 (15), 2944-2952.
197. L. Ke, S. Bin Dolmanan, L. Shen, P. K. Pallathadk, Z. Zhang, D. M. Y. Lai and H. Liu, "Degradation mechanism of ZnO-based dye-sensitized solar cells". *Solar Energy Materials and Solar Cells* **2010,** 94 (2), 323-326.
198. N. Mir, M. Salavati-Niasari and F. Davar, "Preparation of ZnO nanoflowers and Zn glycerolate nanoplates using inorganic precursors via a convenient rout and application in dye sensitized solar cells". *Chemical Engineering Journal* **2012,** 181.
199. M. Wang, C. Huang, Y. Cao, Q. Yu, Z. Deng, Y. Liu, Z. Huang, J. Huang, Q. Huang, W. Guo and J. Liang, "Dye-sensitized solar cells based on nanoparticle-decorated ZnO/TiO(2) core/shell nanorod arrays". *Journal of Physics D-Applied Physics* **2009,** 42 (15).
200. T. Bora, H. H. Kyaw, S. Sarkar, S. K. Pal and J. Dutta, "Highly efficient ZnO/Au Schottky barrier dye-sensitized solar cells: Role of gold nanoparticles on the charge-transfer process". *Beilstein Journal of Nanotechnology* **2011,** 2, 681-690.
201. J. Fan, Y. Hao, A. Cabot, E. M. J. Johansson, G. Boschloo and A. Hagfeldt, "Cobalt(II/III) Redox Electrolyte in ZnO Nanowire-Based Dye-Sensitized Solar Cells". *ACS applied materials & interfaces* **2013,** 5 (6), 1902-6.
202. G. Boschloo and A. Hagfeldt, "Characteristics of the Iodide/Triiodide Redox Mediator in Dye-Sensitized Solar Cells". *Accounts of Chemical Research* **2009,** 42 (11), 1819-1826.
203. L. E. Greene, M. Law, B. D. Yuhas and P. D. Yang, "ZnO-TiO2 core-shell nanorod/P3HT solar cells". *Journal of Physical Chemistry C* **2007,** 111 (50), 18451-18456.
204. D.-M. Tang, G. Liu, F. Li, J. Tan, C. Liu, G. Q. Lu and H.-M. Cheng, "Synthesis and Photoelectrochemical Property of Urchin-like Zn/ZnO Core-Shell Structures". *Journal of Physical Chemistry C* **2009,** 113 (25), 11035-11040.
205. Y. Z. Hao, J. Pei, Y. Wei, Y. H. Cao, S. H. Jiao, F. Zhu, J. J. Li and D. H. Xu, "Efficient Semiconductor-Sensitized Solar Cells Based on Poly(3-hexylthiophene)@CdSe@ZnO Core-Shell Nanorod Arrays". *Journal of Physical Chemistry C* **2010,** 114 (18), 8622-8625.
206. A. Irannejad, K. Janghorban, O. K. Tan, H. Huang, C. K. Lim, P. Y. Tan, X. Fang, C. S. Chua, S. Maleksaeedi, S. M. H. Hejazi, M. M. Shahjamali and M. Ghaffari, "Effect of the TiO(2) shell thickness on the dye-sensitized solar cells with ZnO-TiO(2) core-shell nanorod electrodes". *Electrochimica Acta* **2011,** 58, 19-24.
207. B.-R. Huang and J.-C. Lin, "Core-shell structure of zinc oxide/indium oxide nanorod based hydrogen sensors". *Sensors and Actuators B-Chemical* **2012,** 174, 389-393.
208. S. Khanchandani, S. Kundu, A. Patra and A. K. Ganguli, "Shell Thickness Dependent Photocatalytic Properties of ZnO/CdS Core-Shell Nanorods". *Journal of Physical Chemistry C* **2012,** 116 (44), 23653-23662.
209. Y.-F. Tu, Q.-M. Fu, J.-P. Sang, Z.-J. Tan and X.-W. Zou, "Effects of annealing temperature on the properties of ZnO/SnO2 core/shell nanorod arrays". *Materials Letters* **2012,** 86, 80-83.
210. C.-Z. Yao, B.-H. Wei, L.-X. Meng, H. Li, Q.-J. Gong, H. Sun, H.-X. Ma and X.-H. Hu, "Controllable electrochemical synthesis and photovoltaic performance of ZnO/CdS core-shell nanorod arrays on fluorine-doped tin oxide". *Journal of Power Sources* **2012,** 207, 222-228.

Chapter 2
ZnO Nanorods

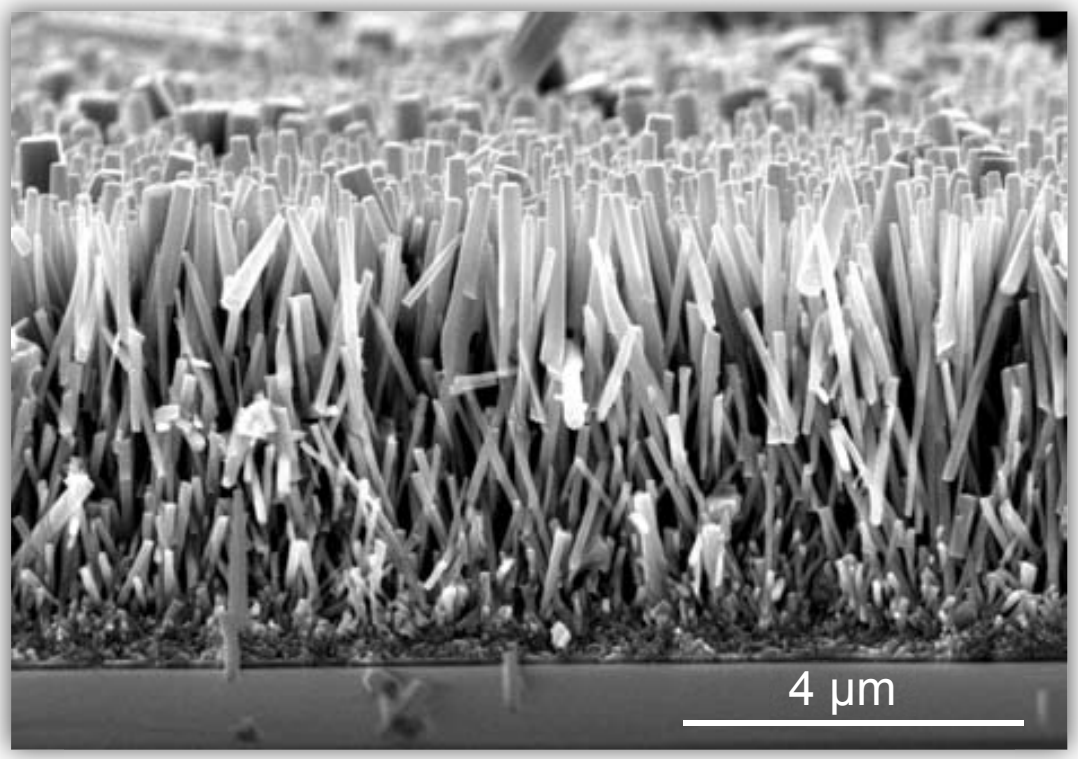

Chapter 2

ZnO Nanorods

2.1 Introduction

Oxide nanostructures in a vertically-aligned form are characterized by their highly efficient charge transport and charge carrier mobility. This distinctive up-standing nanoform provides low internal transport resistance (high resistance is usually observed in nanospheres or nanoparticle aggregates), reducing unfavourable recombination processes.[1, 2] Moreover, ID nanostructures enhance the interfacial active area between the oxide and organic semiconductors improving the amount of light harvested in the final excitonic solar cell (XSC). On the other hand, the application of ZnO presents important advantages with respect to TiO_2, the most used oxide in dye-sensitized solar cells (DSC). In general, ZnO's band gap (E_g~3.3 eV)[3] is similar to the TiO_2 band gap (E_g~3.2 eV)[4] and its conduction band edge is located at approximately the same energy level (-4.2 eV vs. vacuum).[5, 6] Yet, and the most important characteristic of all, is that only ZnO can be prepared by low-cost, solution processable and easy scalable synthesis techniques. ZnO fabrication can be made on almost any substrate in a wide variety of nanostructures and at large scale.[7] The latter makes ZnO highly compatible with printing techniques (like roll-to-roll, gravure printing, etc.) that are essential right now to cope with the low-cost photovoltaic requirements. Table 2.1 summarizes the photovoltaic values reported in the literature for DSCs applying the bare vertically-aligned ZnO NRs and NWs. Works applying not up-standing ZnO NRs, the co-existence of other semiconductor oxide (such as TiO_2) or other ZnO nanoforms (core-shell, nanoparticles, nanotetrapods, etc.) are not included in this table. As observed in Table 2.1, the majority of the research works describe the application of the ZnO NRs synthesized by the hydrothermal (HT) technique and applying the N719 commercial Dye. For easy comparison, the table is organized depending on the ZnO NR length. A large variety of NRs lengths are observed between 0.7 to 40 μm. Moreover, we have observed a discrepancy between the reported power conversion efficiencies (PCE) and the NR length that do not follow a direct relationship. The latter indicates that the solar cell performance is not only affected by the ZnO NR length, but it is probably the result between the contributions from several parameters. The highest PCE

applying ZnO NRs has been for long time 2.4% applying NRs of 1.9 μm in length.[8] The work was reported in 2005 by the group of M. Guo *et al.*[8] and that PCE was not reproduced or improved by any other group until recently. In 2010 and 2011 two works achieved similar results: A 2.3% PCE was reported applying 1 μm NR length and a new electrolyte,[9] and a second work was reported applying 7.9 μm ZnO NR length and a new organic dye.[10] A PCE value of 3.15%, the highest PCE reported for a DSC applying vertically-aligned ZnO NRs, have been reported by G. Y. Jung *et al.* with NRs of 0.7 μm in length.[11] A peculiar aspect in this work is the high short circuit current density (J_{sc}), 10.75 mA·cm^{-2}, which is an unusual value for ZnO NRs of less than 1 μm in length. This is an indication of a possible error during solar cell characterization.

Table 2.1 Literature review on vertically-aligned ZnO NRs and their application as electrodes in DSC. *HT: Hydrothermal, CVD: Chemical Vapour Deposition, MOCVD: Metal Organic Chemical Vapour Deposition, ECD: Electrochemical Deposition, PEI: Poliethileneimine.*

Film Thickness (μm)	Synthesis method	Dye	Light Intensity (mW/cm^2)	V_{oc} (V)	J_{sc} (mA·cm^{-2})	FF (%)	PCE (%)	Ref.
0.7	HT + PEI	N719	100	0.56	10.75	53	3.15	11
0.9	HT	N3	100	0.52	8.70	44	1.94	12
1.0	HT + PEI	Z907	100	0.72	6.40	49	2.30	9
1.0	HT	Rose Bengal	2	0.55	0.049	55	0.70	13
1.0	HT	Mulberry	50	0.23	2.90	30	0.41	14
1.8	HT	N719	-	0.47	4.79	32	0.71	15
1.9	HT	N3	42	0.55	5.18	36	2.40	8
2.0	MOCVD	Porphyrin based	-	-	-	-	0.60	16
2.0	ECD	N3	80	0.44	3.75	62	1.30	17
2.7	HT	N719	-	0.48	11.88	33	1.93	18
3.0	ECD	D149	100	0.53	2.52	37	0.49	19
3.0	Zn anodization	N719	100	0.76	3.60	53	1.40	20
3.0	HT	N719	100	0.55	2.50	42	0.60	21
3.2	MOCVD	N719	100	0.66	2.04	41	0.55	22
3.5	HT + CVD	N719	100	0.76	1.17	25	0.22	23
4.0	HT	N719	100	0.58	4.04	44	1.03	24
4.5	ECD	D149	100	0.61	3.28	33	0.66	25
4.6	HT	Mercurochrome	100	0.52	3.30	49	0.83	26
5.0	HT	N3	23.6	0.34	0.49	45	0.32	27
5.0	MOCVD	N719	100	0.82	1.20	61	0.60	28

5.0	HT	N719	100	0.50	3.80	30	0.70	29
5.0	HT + PEI	N719	100	0.76	2.44	38	0.70	30
5.0	ECD	D149	100	0.55	4.25	37	0.88	31
5.5	HT	Mercurochrome	100	0.44	2.15	47	0.45	32
7.0	HT	N719	100	0.55	1.50	40	0.42	33
7.2	HT	N719	-	0.66	2.59	41	0.71	34
7.9	HT + PEI	NKX-2883	100	0.58	7.30	55	2.30	10
8.0	HT	N719	100	0.67	1.30	32	0.30	35
9.0	HT	N719	100	0.54	2.25	59	0.72	36
9.3	HT	N719	100	0.73	1.13	31	0.26	37
10.0	HT	N719	100	0.64	5.37	49	1.69	38
10.0	HT	N719	100	0.65	5.51	38	1.37	39
10.0	HT	N719	85	0.72	3.96	20	0.66	40
10.0	HT	C220	100	0.52	5.49	43	1.25	41
11.0	HT	N719	100	0.63	4.50	36	1.00	42
11.0	HT	N3	80	0.55	9.07	34	2.21	43
12.9	HT + PEI	N719	100	0.47	4.31	43	0.87	44
13.0	HT + PEI	Mercurochrome	100	0.43	4.96	37	0.79	45
14.0	HT	N719	100	0.54	6.79	50	1.70	46
16.0	HT	N719	100	0.76	1.84	47	0.70	47
16.0	HT + PEI	N719	100	0.71	5.85	38	1.50	48
18.0	HT	N719	100	0.64	2.87	48	0.85	49
20.0	CVD	N719	85	0.80	1.97	39	0.73	40
20.0	HT	N719	100	0.64	4.13	42	1.12	50
20.0	HT	N719	100	0.77	2.96	65	1.47	51
33.0	HT	N719	100	0.67	9.30	34	2.10	52
40.0	HT + PEI	N719	100	0.69	4.26	42	1.30	53

In this chapter we present the preparation, optimization and characterization of vertically-aligned ZnO nanorod (NR) electrodes and their application in dye-sensitized solar cells (DSC). In chapter 1 section 1.3.1.1 the configuration and work mechanism of the DSC are defined, here we replace the nanoparticle oxide semiconductor for the ZnO NRs as represented in Figure 2.1a. The vertically-aligned ZnO NRs work as the electron transport material (ETM), a dye is applied as light harvesting material (LHM) and a liquid electrolyte as the hole transport material (HTL), as we can see in the band energy diagram of Figure 2.1b.[6, 54-57] We analysed the effect of different synthesis conditions that influence the final

ZnO NRs formation. We also analysed the effect of different ZnO NR morphologies, temperature, light irradiation, or the application of UV light on the photovoltaic performance of the DSCs.

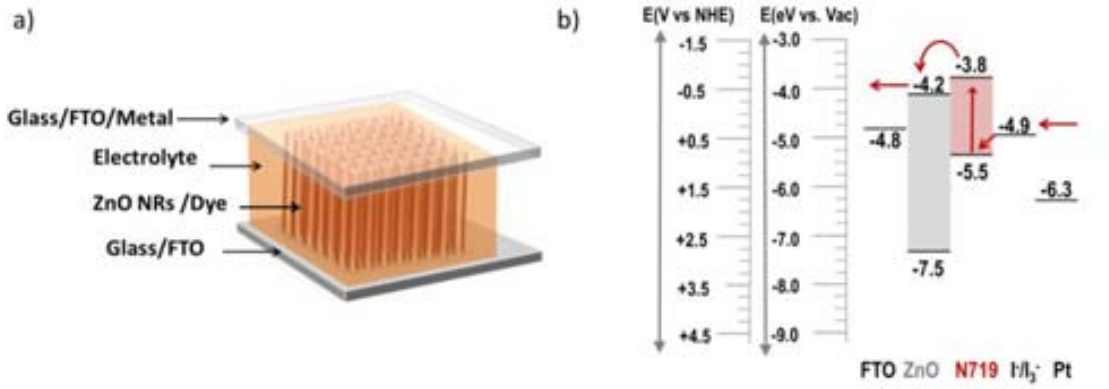

Figure 2.1 a) Schematic representation of a DSC applying ZnO nanorods (NR) as the electron transport material and b) the schematic representation band energy diagram vs. Vacuum, vs., NHE (Normal Hydrogen Electrode) and vs. SCE (Saturated Calomel Electrode) of a DSC with ZnO NRs, dye N719 a liquid electrolyte and a back metal contact of Pt.

2.2 Synthesis of Vertically-aligned ZnO NRs

Two types of transparent conducting oxide (TCO) substrates were analysed to grow the electrodes of ZnO nanorods (NR): indium doped tin oxide (ITO) and fluorine doped tin oxide (FTO). Our initial results indicate the same ZnO NR dimension can be obtained independently of the substrate used (FTO or ITO). Since the FTO can be annealed at higher temperatures (450°C) than ITO (350°C), it was chosen as the optimal substrate to prepare ZnO NRs for DSCs. Figure 2.2 shows a schematic representation of the steps required for the preparation of the ZnO NR electrodes. First, a ZnO buffer layer of about 80-100 nm thick is prepared on top of the TCO substrate by spin coating a sol-gel layer of ZnO and sintered at 450ºC for 2 h (heating ramp 3ºC/min). This buffer layer permits a better contact between the TCO and ZnO nanorods (NRs), it also eleiminates recombination processes produced by the direct interaction of the electrolyte with the FTO substrate. Next, a layer of ZnO NPs is deposited on the FTO/ZnO substrate, this layer of ZnO nanaoparticles is required as seeds for the posterior hydrothermal growth of ZnO NRs.[6, 58, 59]

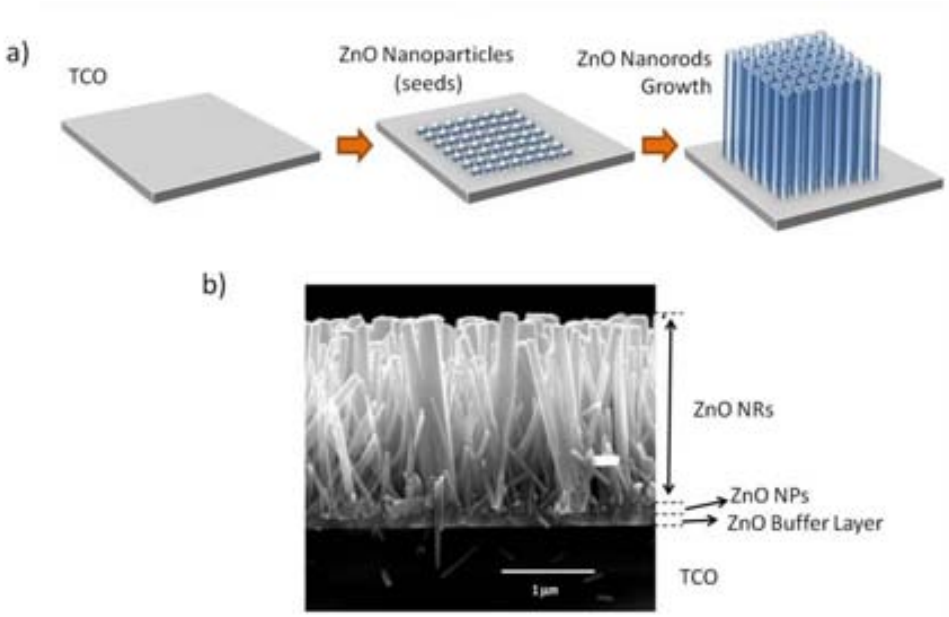

Figure 2.2 a) Schematic representation of the ZnO electrodes preparation: deposition of ZnO nanoparticles (NPs) by spin-coating and hydrothermal growth of ZnO NRs and b) SEM image of a ZnO NR electrode.

In order to improve the ZnO electrode properties we need vertically-aligned NRs with large active areas. One option to obtain the latter longer NRs with small diameters are needed. Therefore, many hydrothermal synthesis conditions were studied to control and optimize the ZnO electrodes: deposition layer of ZnO NPs, different distance between the substrate and the bottom of the reaction flask, different solution concentrations and growth time were studied.

2.2.1 Layer of ZnO nanoparticles

A layer of ZnO nanoparticles (NPs), used as seeds, were deposited on top of the ZnO buffer layer. The synthesis of the ZnO NPs was carried out by the method described by Pacholski *et al.,*[60] which consists on the hydrolysis of zinc acetate in basic media by reflux in methanol at 65°C for 2 hours. A white-cloudy solution containing the NPs was developed during synthesis. The NPs suspension was analysed by TEM at different periods of time. Figure 2.3 shows the NPs obtained at different reaction points, at early stages of the synthesis, the NPs presented a size between 5-7 nm (Figure 2.3a) and grow until reaching an homogeneous size of 10-12 nm after 2 hours of reflux (Figure 2.3b). By keeping the NPs

dispersion at room temperature we observed the agglomeration of the NPs after 4 hours at the end of the synthesis (Figure 2.3c), a behaviour also observed by M. Winterer *et al.*.[61] To avoid NP agglomeration, the synthesis of vertically-aligned Zn NRs was always carried out applying freshly-prepared NPs. In addition, every time before spin-coating, the NPs solution was filtered off with a 0.2 μm filter to avoid possible aggregates.[58]

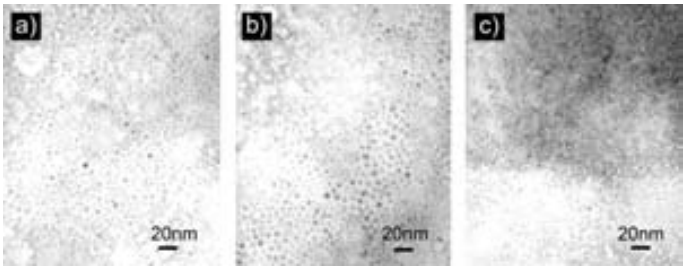

Figure 2.3 TEM images of the ZnO NPs solution at different points during and after the synthesis: a) at 30 min of reflux, b) at 2 h of reflux and c) at 4 hours after the synthesis was finished.

The layer ZnO NPs on the TCO/ZnO buffer layer act as nucleation points (seeds) for the formation of vertically aligned ZnO NRs. The effect of different ZnO NPs layer thicknesses were analysed on the obtained ZnO NRs. The ZnO NPs were deposited by spin coating, once deposited, the substrates were heated 150°C for 10 min between coatings. The ZnO NRs did not grow on substrates without the NPs layer, we observed only big aggregates of ZnO attached to the surface after 30 minutes and 1 hour synthesis growth time (Figure 2.4a and d). Increasing growth times increased the inhomogeneity of the ZnO deposition. The optimization of the NP layer deposition indicates that a minimum of three layers of ZnO nanoparticles are required in order to initiate the nucleation and growth of the NRs. Under these conditions, the formation of the NRs can clearly be observed after 1h (Figure 2.4b, c, e and f).

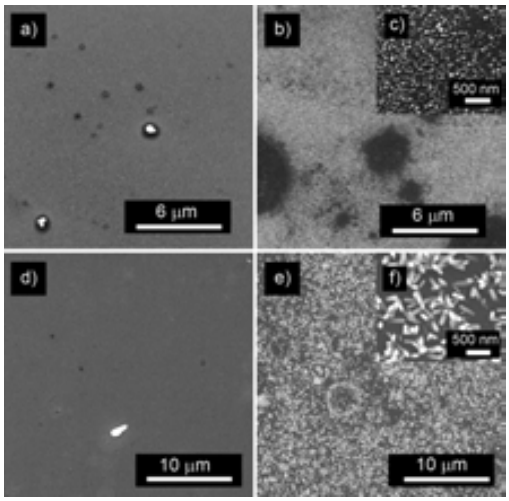

Figure 2.4 SEM images of ITO substrates without deposition of ZnO NPs grown for a) 30 min, d) 1 h and ITO substrates with 3 layers of ZnO NPs grown for b), c) 30 min and e), f) 1 h. (Hydrothermal growth with a 250 mL flask, distance from the bottom 6-8 cm).

Figure 2.5 shows vertically-aligned ZnO NR electrodes grown for 1.5 h applying 3, 6 and 9 layers of NPs. The NR density was calculated from SEM images and resulted in densities of $3.3 \cdot 10^9$ NR·cm^{-2}, $3.5 \cdot 10^9$ NR·cm^{-2} and $3.8 \cdot 10^9$ NR·cm^{-2} for 3, 6 and 9 NPs layer respectively. Similar NR-densities for the same HT synthesis have been reported earlier.[8, 62, 63] Diameters were also quite similar for all the ZnO NPs layers: between 70 nm - 80 nm. Taking into account the similar NR densities and diameters obtained by the application of 3 to 9 layers of NPs, we used 3 layers of NPs for all the ZnO electrodes preparation.

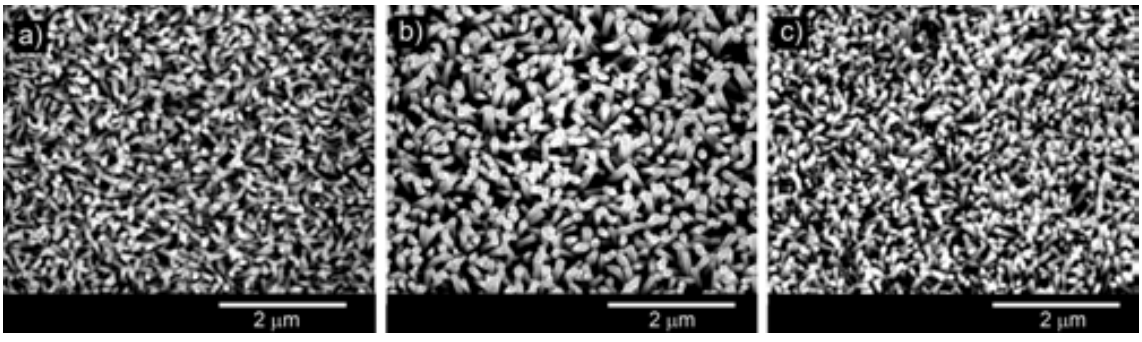

Figure 2.5 SEM images of ITO substrates with a) 3 layers, b) 6 layers and c) 9 layers of ZnO NPs grown for 1,5 h in a small flask of 10 mL, distance from the bottom 1 cm.

2.2.2 Distance between the substrate and the bottom of the reaction flask

ZnO NRs with different dimensions were obtained when the substrates were grown at different distances from the bottom of the flask.[64] For this reason, this distance was carefully optimized to obtain reproducible results. Figure 2.6 shows ZnO NRs grown at different distances between the flask's bottom and the ITO substrate: at 1 cm and at 7 cm. Two different flasks were used in each synthesis, one of 10 mL for 1 cm distance and the other was a PYREX® bottle of 250 mL for the 7 cm distance (Figure 2.6b). The length and the diameter of the ZnO NRs were drastically affected. Substrates closer to the bottom of the reaction flasks initiate NPs nucleation and NRs growth much earlier (Figure 2.6c, 30 min growth time) than the substrates placed at 7 cm distance (Figure 2.6d, 30 min growth time) and thus, longer NRs can be obtained at closer distances. On the other hand, NRs grown for 2 h at larger distances developed smaller diameters, of about ~20 nm (Figure 2.7b), in comparison with the ~70-80 nm diameter observed for NR grown at smaller distances (Figure 2.7a). Since we aim for small ZnO NRs diameters in order to cope with the electron diffusion length required in excitonic solar cells, ~20 nm,[64] thus, we fixed the NR growth distance between 6-8 cm.[58, 59, 64] For the latter, home-made plastic holders with 3 substrate positions at 6, 7 and 8 cm from the bottom of the flask were used to fix the TCO substrates up-side down during the hydrothermal growth.

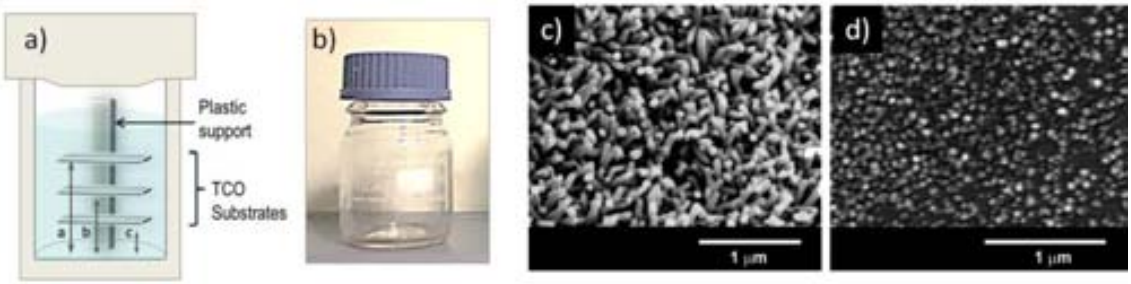

Figure 2.6 Synthesis of ZnO NR. a) Schematic representation of the reaction flask used for the synthesis of ZnO NRs on TCO substrates. The distance between the substrate and the bottom of the flask is indicated by a, b and c, b) Image of the large reaction bottle, c) SEM image of an ITO substrate with 3 layers of ZnO NPs grown for 30 minutes in a small flask of 10 mL, distance from the bottom 1 cm and d) in a big flask of 250 mL, distance 7 cm from the bottom.

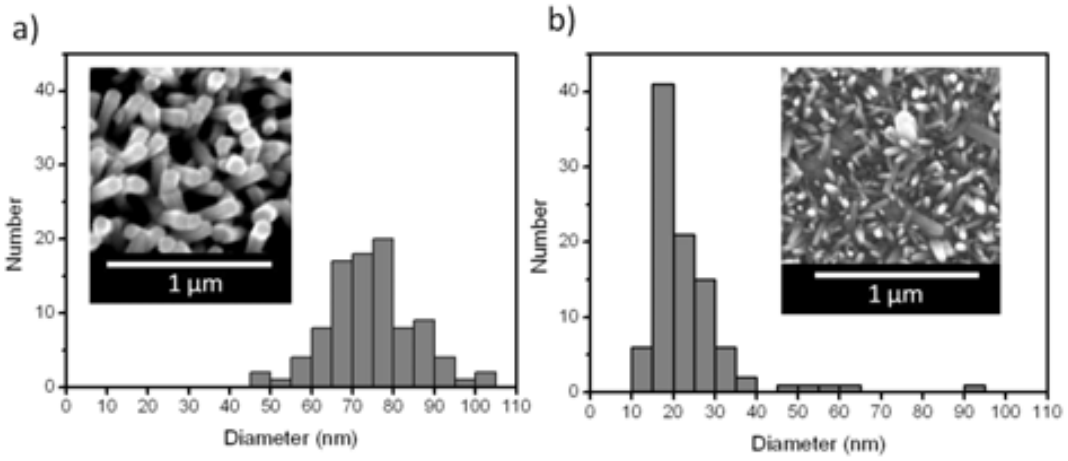

Figure 2.7 Diameter distribution for 2 h growth of ZnO NRs in a a) 10 mL flask, 1 cm distance and b) 250 mL flask, 7 cm distance and respective inset SEM images.

2.2.3 Effect of the hydrothermal solution concentration

The concentration of the reaction solution is another important parameter to control for the ZnO NR synthesis. We analysed two different concentrations a) 100 mM and b) 25 mM. Figure 2.8 shows the SEM images of the resulted ZnO grown on the substrate. Cubic and inhomogeneous ZnO nanostructures were formed for high concentrations, while the desired ZnO NRs were obtained at 25 mM concentrations (See Figure 2.8). We chose to work with a 25 mM equimolar solution of the reactants.[58]

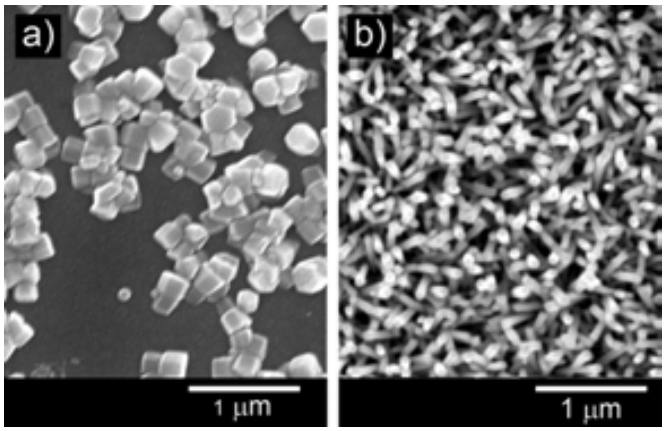

Figure 2.8 SEM images of ITO substrates with 3 layers of NPs and grown for 1,5 h using the reactants concentration of a) 100 mM and b) 25 mM. The reaction bottle was of 10 mL in volume and the used distance from the bottom to the substrate was 1 cm.

2.2.4 ZnO nanorod growth time

Our studies on the NRs length revealed that length is increased when increasing reaction time, as expected and in well agreement with already reported works.[35, 65] Growth times between 1 h to 28 h were applied changing the hydrothermal solution every 4-6 h. The ZnO NRs obtained were characterized by SEM and profilometry. Figure 2.9 shows the graphs of the length and diameters for the different growth times measured by SEM microscopy.[58, 59, 66]

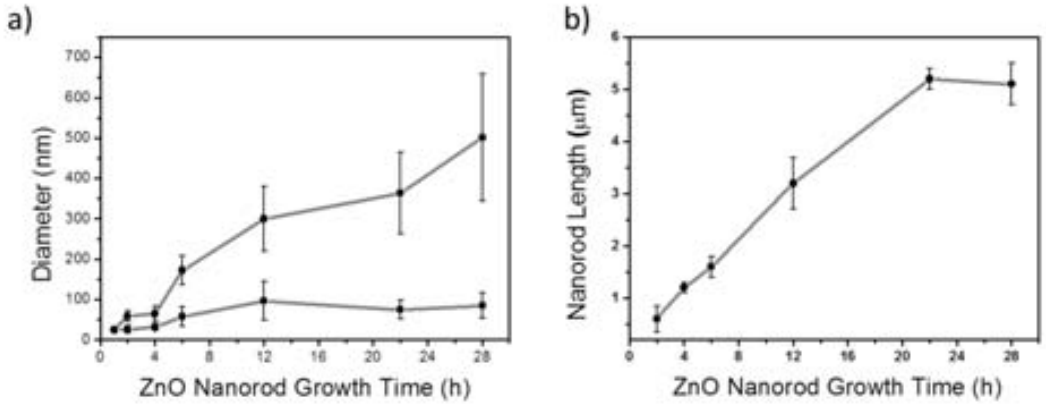

Figure 2.9 Variation of ZnO NRs dimensions with growth time a) diameter and b) length. Notice that two different NR diameters are present in a).

The NR lengths varied between 600 nm and 5.2 μm, for a 2 h and 22 h growth time respectively, with no variation in NR length between 22 h and 28 h growth time. Two different sizes of NR diameters were observed: small diameters between ~20 and ~80 nm were obtained for every growth time with and few larger diameters between 150-600 nm observed when increasing reaction time.[58] The diameters for the NRs grown at 28 h were the largest (see details in Figure 2.9). Another aspect to mention for the synthesis at 28 h was the presence of large amounts of broken NRs attached to the surface (some of them with huge dimensions). All the mentioned observations reveal that even changing the solution every 4-6 h we could not avoid the formation of NRs with large diameters, and this has been attributed to the nucleation between two or more NRs with time.

2.2.5 Optimum synthesis parameters to obtain vertically-aligned ZnO NRs.

All the above mentioned parameters have been optimized in order to obtain the best conditions for the synthesis of vertically-aligned ZnO electrodes. The optimized synthesis conditions finally obtained were:

a) Use of FTO substrate
b) Application of three layers of a fresh ZnO NPs solution
c) Distance between the substrate and the bottom of the reaction flask fixed at 6-8 cm
d) Low concentration of reactants of 25 mM

Once all the preparation parameters of the ZnO electrodes were optimized, and fixed for all the synthesis, the ZnO NR electrodes were characterized by SEM, TEM, profilometry, XRD, UV-vis and PL spectroscopies at different hydrothermal growth times.

2.3 ZnO NR characterization

2.3.1. ZnO NR dimensions, aspect ratio and electrode density by SEM microscopy analyses

The Scanning Electronic Microscopy (SEM) generates high-resolution images of the external ZnO NR morphology. The chemical composition of the sample can be also determined by the backscattered electrons (BSE) detector and the energy dispersive X-rays spectrocopy (EDS) detector. Figure 2.10 shows cross-sectional and top view SEM images of some NR electrodes grown for 6 h, 12 h, 22 h and 28 h. The lengths and diameters were measured and are depicted in the graphs of Figure 2.9. The NR density was measured from the SEM pictures for all the ZnO electrodes at different growth time: $2.6 \cdot 10^9$ NR·cm^{-2} (6 h), $2.2 \cdot 10^9$ NR·cm^{-2} (12 h), $1.7 \cdot 10^9$ NR·cm^{-2} (22 h), $1.5 \cdot 10^9$ NR·cm^{-2} (28 h). The NR electrode density decrease for longer NR growth times due to the formation of NRs with larger diameters. Figure 2.11 represents the NR density and aspect ratio for each ZnO NR length. The aspect-ratio is defined as the length of the NR divided by its diameter.[67, 68] Increasing the NR length also increased the aspect ratio, only the ZnO NRs grown for 28 h had a low aspect ratio than the electrodes grown for 22 h due to have the same NR length but with larger diameters.

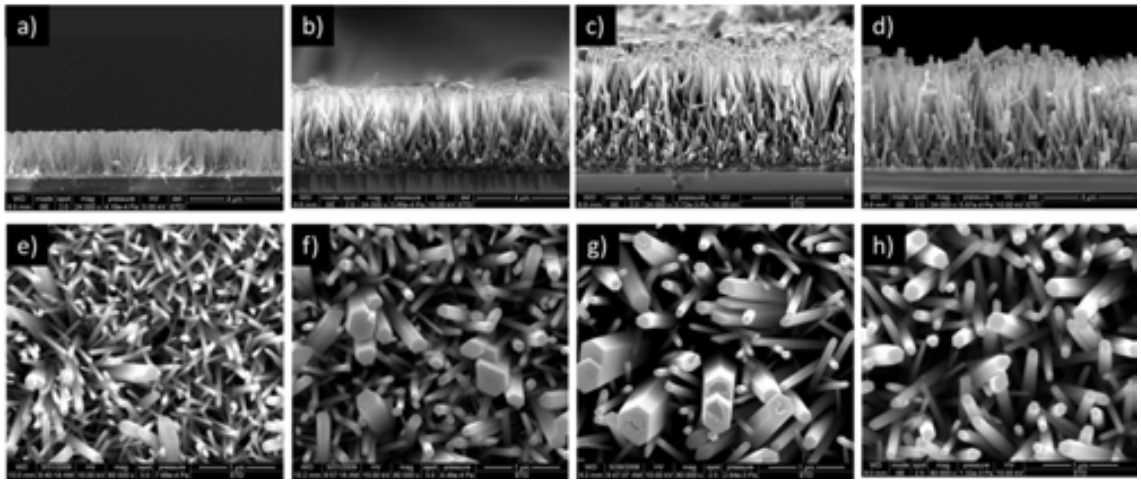

Figure 2.10 SEM images of cross section ZnO NR electrodes grown on FTO for a) 6 h, b) 12 h, c) 22 h, d) 28 h and top view electrodes grown for e) 6 h, f) 12 h, g) 22 h and h) 28 h.

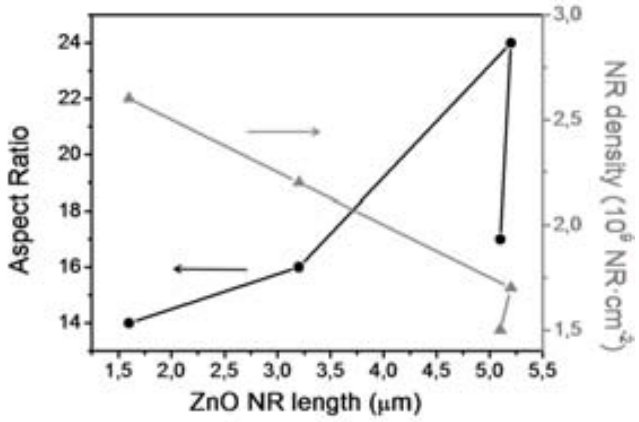

Figure 2.11 Aspect ratio (black circles) and NR density (grey triangles) for each ZnO NR length.

2.3.2. ZnO NR crystalline quality and composition by X-Ray diffraction (XRD) and Transmission Electron Microscopy (TEM) analyses

X-ray diffraction (XRD) is a non-destructive technique which gives information about the crystal structure, chemical composition and physical properties of materials and thin films. The transmission electron microscopy (TEM) can also reveal information about the crystal structure of the sample. Nevertheless, more useful information about the morphology and the chemical composition of the ZnO NRs can be obtained by this technique, especially with the careful application of the energy dispersive x-ray

spectroscopy (EDS) detector. XRD analysis for all the electrodes showed a hexagonal wurtzite structure for all ZnO NRs independently of the synthesis conditions or reaction time.[58, 66] The high intensity of the (0002) peak indicates preferential orientation due to the vertical growth of the NRs on the TCO substrate (Figure 2.12a). The as-prepared NRs were scratched from the electrodes and suspended in ethanol in order to carry out TEM analyses. TEM results confirmed the good crystallinity of the ZnO NRs and also the NR length observed previously by SEM (Figure 2.12b NR grown for 6 h, length 1.6 μm). The selected-area electron diffraction (SAED) pattern of the NR in Figure 2.12c, represents the plane with directions (0002) and (10-10) from the wurtzite structure where the NR growth is along the direction (0002) (Figure 2.12c).

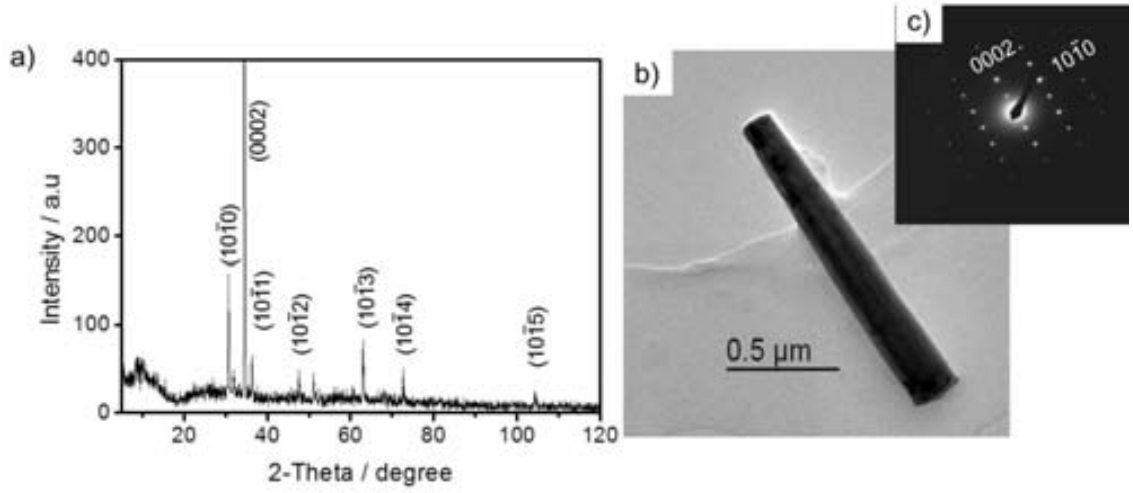

Figure 2.12 a) XRD pattern of ZnO nanorods grown on ITO, b) TEM image of a single ZnO NR of 6 h growth time and c) Selected-area electron diffraction (SAED) pattern of the ZnO NR.

2.3.3. Photoluminescence (PL) and Time resolved photoluminescence (TRPL)

Room temperature photoluminescence (PL) spectroscopy reveals the optical properties, providing information about the defects on the surface and core of the ZnO NRs. The PL spectra of the ZnO NR electrodes obtained with a UV laser excitation at 325 nm is presented in Figure 2.13a. This PL spectra presented two peaks one at ~380 nm called the Near Band Edge (NBE) and the other broader band, called the orange band, at ~640 nm.[69] As explained in section 1.4.1.2, the orange band is related to the quantity of ZnO defects present in the sample. The PL analyses performed to the ZnO NRs indicate that the intensity of both peaks varies for each ZnO NR electrode. The relation between the orange

band and the NBE depending on the NR growth time was calculated as shown in Figure 2.13b. An increase of the orange band/NBE ratio is observed when increasing ZnO NR growth time, an indication that the surface defects increase when the NR length increases.

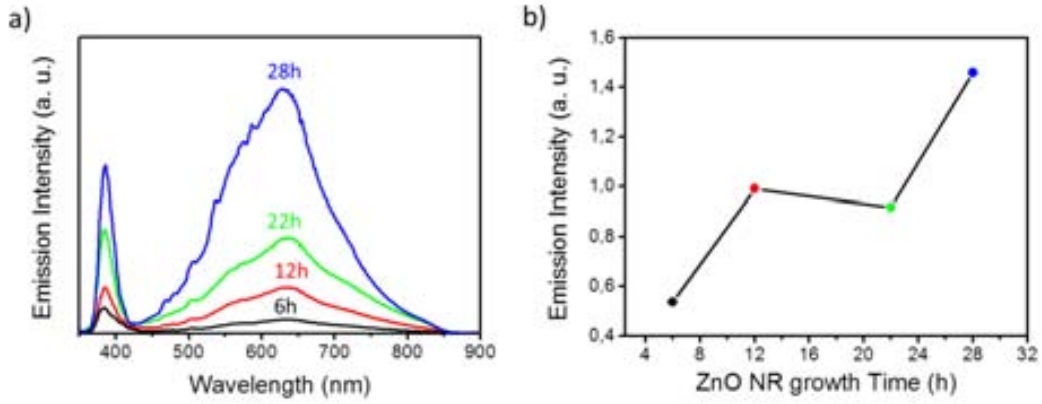

Figure 2.13 a) Room temperature PL spectrum for ZnO NRs electrodes grown at 6 h, 12 h, 22 h and 28 h and b) Intensity ratios for orange band peak/NBE peak of the PL spectra of the ZnO NRs electrodes grown at different growth times.

Time Resolved Photoluminescence analyses (TRPL) of the ZnO NRs electrodes with and without the N719 dye were performed in order to study the lifetime of the free excitons. The ZnO NR electrodes (grown for 6 h, 12 h, 22 h and 28 h) were measured with a micro-photoluminescence setup to guarantee that only a couple of nanorods were excited within the laser spot, avoiding inhomogeneous broadening in the PL spectra. Figure 2.14a shows the TRPL of the ZnO NR electrode grown for 6 h (black line). All the other electrodes (grown for 12 h, 22 h and 28 h) had a similar spectra. The measured absolute lifetime values for the different ZnO NR electrodes in function of the NR length are represented in Figure 2.14b. The lifetimes of the free excitons in the ZnO NRs are between 25 and 80 ps. The longer lifetime is for the 22 h growth time electrode, the others (6 h, 12 h and 28 h) had a similar lifetime around 25-30 ps (see Figure 2.14b black line). These free exciton lifetimes are similar with other reported lifetimes, between 40 and 160 ps for ZnO NRs prepared with other synthesis techniques,[70, 71] while the bulk samples are 300-400 ps, almost an order of magnitude higher.[72] The latter is probably due to the presence of surface states in the NRs, which act as alternative recombination sites.[70] A curious aspect is the similar trend of the lifetimes in function of the NR lengths compared with the aspect ratio also in function of NR length in Figure 2.11 (black line). Both graphs presented a higher lifetime and aspect ratio for the ZnO NRs grown for 22 h.

When the dye N719 was adsorbed on the ZnO NR electrode, the lifetime of the free excitons was reduced for all the ZnO NR electrodes and all the electrodes presented the same lifetime, 20 ps (Figure 2.14b grey line). This lifetime reduction is due to the incorporation of other recombination channels when the dye is applied. The measured experimental lifetime is a combination of a radiative recombination (the emitted photon) and non-radiative (transfer processes to the shell or to the dye) as show in equation 2.1. The application of the dye makes the non-radiative recombination fast (not negligible) and, thus, the experimental effective lifetime decreases.[73-77]

$$\frac{1}{\tau_{exp}} = \frac{1}{\tau_{rad}} + \frac{1}{\tau_{non-rad}} \qquad (2.1)$$

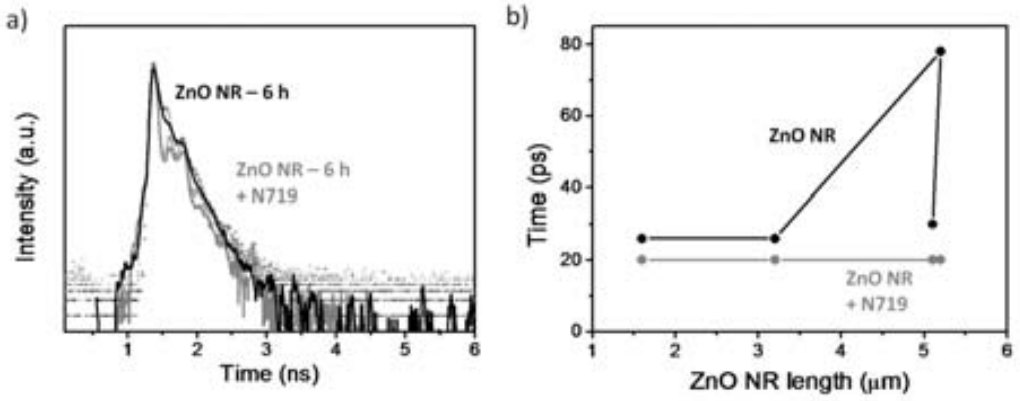

Figure 2.14 a) Time resolved photoluminescence TRPL of a ZnO NR electrode grown for 6h (black line) and after immersion of the electrode in a N719 dye solution for 2h (grey line). The excitation energy of the laser was set to 4.66 eV (266 nm) at 300 K. b) Lifetime of the free excitons as a function of the ZnO NR length measured from the ZnO electrodes grown for 6 h, 12 h, 22 h and 28 h (black line) and the same electrodes with the dye N719 (grey line).

2.4 Application in Dye-sensitized Solar Cells

The application of the ZnO NRs electrodes in DSCs is presented in this section. The experimental condutions for the preparation of the solar cell has been described under experimental section chaper 6, section 6.6. In general, the ruthenium (II) complex dye, $(Bu_4N)_2Ru(debpyH)_2(NCS)$, also known as N-719 was used as sensitizer, the I_3/I^- electrolyte (from Solaronix) was introduced in the solar cell after the devices were sealed with a surlin thermal adhesive placed in direct contact with the Pt counter-electrode (See Figure 2.15 for a schematic representation). We have noticed that many preparation and testing parameters influence the final solar cell performance. Environmental conditions such as relative humidity (RH %) or temperature are important factors. Other factors are also significant considering that ZnO properties can be modified by them like synthesis methods,[78-83] synthesis temperature,[8, 84] testing atmosphere (air, vacuum),[85-88] or illumination.[89-92] Therefore, in order to obtain the maximum performance of the solar cells, the following parameters were studied: thermal treatment, dye loading time, effect of the Pt counter-electrode, NR length, application of different dyes, effect of the UV-light, temperature, light intensity and also long term stability tests.

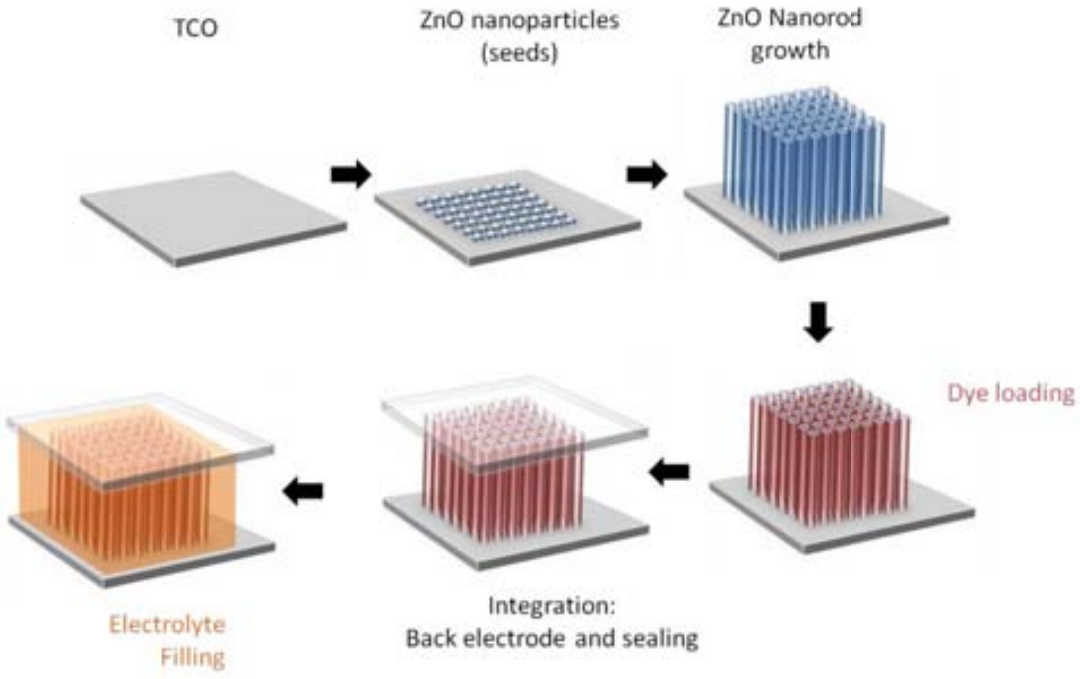

Figure 2.15 Schematic representation of all the steps for the DSC preparation applying ZnO NRs.

2.4.1 Effect of thermal treatment

Our initial results show that DSC performance improves after sintering the as-prepared ZnO NRs electrodes at 450°C for 30 min. Power conversion efficiency was observed to increase from 0.41% up to 0.53%, V_{oc} registered slight changes from 0.43 V to 0.47 V and J_{sc} improved from 2.2 mA/cm^2 to 3.4 mA/cm^2, see Figure 2.16 (for ZnO NRs of ~1.6 μm length, 30 min immersion time in dye solution, Pt counter electrode from solaronix ~50 nm thick). Improvement after thermal treatment has been related to the decrease of defects, e.g. oxygen vacancies (O_{vac})[3, 93] usually observed in amorphous oxides.[94] The incorporation of oxygen during thermal treatment is well-known to modify optical properties of semiconductor oxides affecting photovoltaic properties. Oxygen vacancies (or deep donor states) act as traps for electrons[95] and thus, as recombination centres[96] reducing the power conversion efficiency of the device.[97] As a consequence, the optical band gap of these materials is very sensitive to oxygen incorporation which in turn, could be the responsible for the increase observed for V_{oc}.[86, 87, 98] Our electrodes were then systematically treated in air at 450°C for 30 minutes before being applied in DSCs.

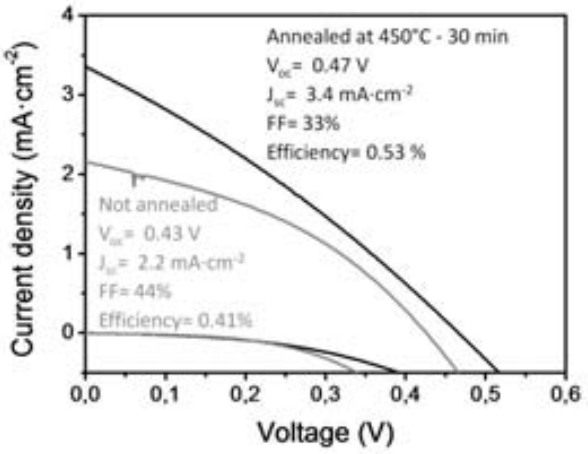

Figure 2.16 Current-Voltage graph of two DSCs applying ZnO NRs grown for 6h (1.6 μm length), dye-loaded for 30 min and using the Pt counter-electrode from Solaronix 50 nm thick. One ZnO electrode was annealed at 450°C for 30 min before the DSC was prepared (black line) and the other was not annealed (grey line)

2.4.2 Effect of the platinum counter-electrode

The counter electrode (CE) consists of a platinized TCO that is placed on top of the ZnO electrode fixed with a polymer sealant for the suitable extraction of photo generated

charge carriers in the device. The need of a platinized TCO is due to the inefficient reduction of the triiodide into iodide on plain TCO due to their high over potential. Platinum acts as catalyst for this reduction to take place and also reduces charge recombination at the working electrode TCO/electrolyte.[99] Two types of Pt CE were prepared, the first one made from a Pt-paste (T/SP), and the other was prepared by electron beam physical vapour deposition (EBPVD). Our first DSCs were prepared with the Pt catalyst paste (T/SP), commercially available from Solaronix, made by the doctor blade technique on FTO substrates. The annealing process at 450ºC for 30 minutes results in a transparent Pt-CE. One layer of tape was used to fix the FTO substrates and then deposit the Pt paste by doctor blade as described under the experimental section 6.6 (chapter 6). A ~50 nm Pt layer thickness was obtained (measured by AFM). We observed that using 2 layers of tape in the doctor blade process results in a layer of ~60 nm of Pt, which improves the performance of DSCs. The Pt electrode made by the EBPVD produces a metallic Pt-CE. Table 2.2 shows the best DSC data measured for electrodes of ~1.6 μm ZnO NRs length (6 h growth time) and 2 h of dye loading time with N719 using different Pt-CEs. All the cells presented an increase on the performance after some hours of being prepared. The latter effect will be explained in detail in the section 2.5.3 since it is related to the UV light.

Table 2.2 Solar cell parameters obtained with electrodes of ~1.6 μm ZnO NRs, DLT of 2 h and electrolyte AN50 at start and at maximum performance. 100 mW·cm^{-2} (AM 1.5) light intensity and 72°C. Active area ~0.20 cm^2.

Measure	Pt-CE type and thickness		V_{oc} (V)	J_{sc} (mA/cm^2)	FF (%)	PCE (%)	R_{sh} (Ω·cm^2)	R_s (Ω·cm^2)
At start	Pt-catalyst T/SP	50 nm	0.45	1.92	41	0.35	1009	87
		60 nm	0.48	2.73	41	0.53	604	70
	EBPVD	150 nm	0.49	2.02	38	0.38	1708	85
		100 nm	0.46	2.95	43	0.58	516	54
		50 nm	0.42	2.72	37	0.43	466	66
		20 nm	0.48	2.76	38	0.50	455	66
At max.	Pt-catalyst T/SP	50 nm	0.53	1.98	45	0.47	1713	71
		60 nm	0.53	2.67	41	0.61	2318	68
	EBPVD	150 nm	0.53	1.82	46	0.45	2010	82
		100 nm	0.56	2.67	45	0.67	703	66
		50 nm	0.55	2.46	48	0.65	1434	66
		20 nm	0.60	2.33	48	0.66	2111	71

The best DSC performance was obtained with Pt deposited by the EBPVD, with electrode thickness below 100 nm. In the case of DSCs applying the Pt prepared by doctor blade deposition, the best performance was achieved with an electrode thickness of 60 nm. The latter DSCs presented similar PCEs around 0.6% (at maximum performance). The values of the series resistance (R_s) were observed to decrease for the highest DSC photovoltaic response. This is attributed to the improvement in the interface CE/electrolyte that permits less recombination processes and also an increase in the current density (J_{sc}). In the case of the shunt resistance (R_{sh}) we did not observed well agreement with respect to the DSC PCEs, probably due to the presence of other internal recombination processes in the cell. All the R_{sh} values increase at maximum performance corresponding with the increase of FF and V_{oc}. Figure 2.17 represents the JV-curves at start (black line) and maximum performances (grey line) for all the 6 types of Pt-CE studied. From the JV curves we can see how the FF improves for the cells measured after three days stored in the dark at room temperature. Our results indicate that it is important to specify the type of Pt-CE used when reporting DSCs data.

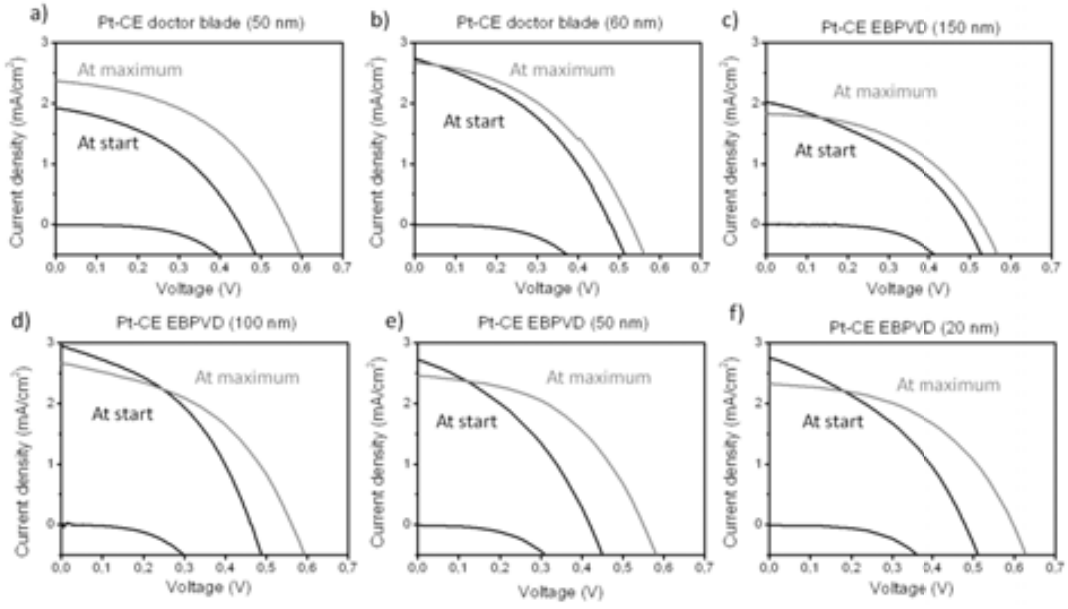

Figure 2.17 DSCs JV-curves with ZnO electrodes of ~1.6 μm ZnO NRs, DLT of 2 h, electrolyte AN50 and Pt-CE of a) doctor blade 50 nm, b) doctor blade 60 nm thickness, c) EBPVD 150 nm, d) EBPVD 100 nm, e) EBPVD 50 nm and f) EBPVD 20 nm. They were measured at 100 mW·cm^{-2} (AM 1.5) light intensity and 72°C. Active area ~0.20 cm^2.

2.4.3 Optimization of the dye loading time

The adsorption of the dye onto the ZnO electrode is a critical parameter that must be carefully controlled for optimal photovoltaic performance. An optimal immersion time of the ZnO electrode into the dye solution can avoid dye aggregation and the consequent loss of photovoltaic response. The dye loading time (DLT) depends on the amount of semiconductor oxide to be covered by the dye and thus, it depends on ZnO NRs length. Therefore the dye immersion time for the different ZnO NR electrodes was optimized as follows: ZnO NR electrodes with NR lengths of 1.6 μm (6 h growth time), 3.2 μm (12 h growth time), 5.2 μm (22 h growth time) and 5.1 μm (28 h growth time) were immersed in a 0.5 mM dye N719 solution between 10 min and 16 h. After each dye loading time the ZnO/Dye electrode was used to assemble a complete DSC and analyse its PCE. Figure 2.18 shows the DSC power conversion efficiencies obtained applying the different dye loading times for each ZnO NR electrode. In general, we observed that the photovoltaic performance increased when the dye loading time increased until a maximum point, which is the optimum dye loading time. Longer immersion times resulted in the decrease of performance due to dye agglomeration. The dye N719 has 2 acid groups that interact with the Zn^{2+} producing the formation of aggregates.[100, 101] An effect also observed for other Ru-based dyes such as N3.[102, 103]

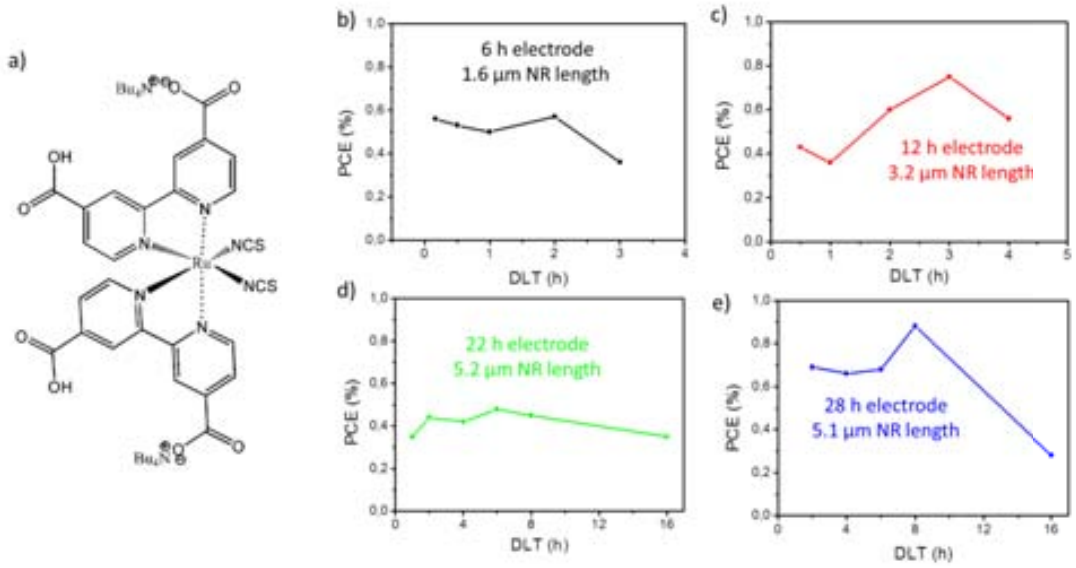

Figure 2.18 a) Organic molecular structure of the dye N719 and DSC power conversion efficiency at different dye loading times (DLT) for ZnO NR electrodes grown at b) 6 h, c) 12 h, d) 22 h and e) 28 h. All the cells were measured at 100 $mW \cdot cm^{-2}$ (AM 1.5) light intensity and 72°C. Pt counter electrode from Solaronix (~50 nm thickness). Active area ~0.20 cm^2.

The optimum DLTs were: 2 h, 3 h, 6 h and 8 h for ZnO NRs lengths of ~1.6 μm, ~3.2 μm, ~5.2 μm and ~5.1 μm respectively (Figure 2.19).[58, 66] A singular aspect was the different optimum DLTs observed for similar ZnO NR lengths of ~5.2 μm (grown at 22 h) and ~5.1 μm (grown at 28 h). Optimum DLT of 6 h and 8 h were obtained respectively. The latter result is attributed to the presence of big NR diameters in the electrode prepared at 28 h (Figure 2.9) thus, requiring a longer DLT. Different temperatures (room temperature, 60°C and 100°C) were also tested during the dye-loading process. However, the photovoltaic performance was not observed to improve for higher temperatures.

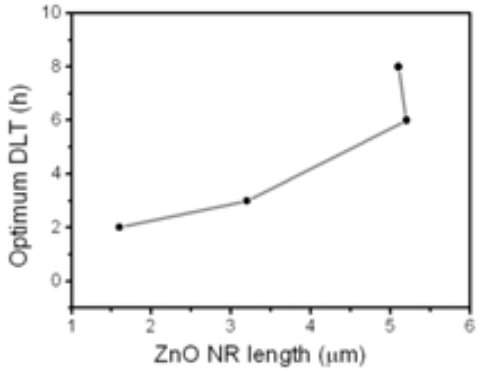

Figure 2.19 Optimum dye loading times (DLT) carried out at room temperature, for ZnO NR electrodes depending on the NR length.

2.4.4 Effect of ZnO nanorod length

In order to analyse the effect of the ZnO NR length, several DSCs were fabricated with ZnO NR of different lengths, the solar cells were all prepared under the same conditions: ZnO electrode thermal treatment at 450ºC/30 min, 0.5 mM N719 dye solution concentration, electrolyte AN50, Pt-CE doctor blade 60 nm. The dye loading times were those obtained after the optimization described in Section 2.4.3. The average photovoltaic properties of the best 5 cells (out of a set of 12 cells) from each ZnO NR length are detailed in Table 2.3. Values are shown at the start of the measurement and after 3 days of being kept in the dark at room temperature. Figure 2.20a represents the power conversion efficiency versus the NR length and the improvement of the photovoltaic performance after 3 days. Longer ZnO NRs have higher efficiencies due to the higher surface area of the oxide which permits

to adsorb more dye. The amount of dye adsorbed on the oxide was measured by the dye desorption method, which consist on the separation of the two electrodes, followed by the immersion of the ZnO-dye electrode in an aqueous basic solution of 0.1 mM KOH. The dye desorption took place after one hour, then the solution turned into a pink colour due to the presence of the N719 dye at the same time that the ZnO electrode turned colourless.[104] The quantity of dye adsorbed on the ZnO electrode was determined by UV-vis analysis of the desorbed dye solution applying the lambert-beer law. The results were corrected by the active area of the DSC (Figure 2.20b). ZnO electrodes grown for 22 h and 28 h have similar NR lengths at around 5 μm and yielded similar efficiencies (~0.9%). However, the 28 h electrode had more dye adsorbed owing to the longer dye immersion time optimized at 8 h, in contrast to the 6 h for the 22h electrode. High quantity of dye adsorbed on the 28 h electrode allowed also higher J_{sc} values, however, presented lower FF (Table 2.3). The latter was due to the presence of more charge recombination indicated by the shunt resistances (R_{sh}) (Figure 2.20b). Increasing the NR length, decreases the R_{sh} which is an indication of larger internal loss due to charge recombination.[58] This result was also supported by the photoluminescence measurements where longer NRs show higher intensity of the orange band, an indication of the higher amount of ZnO surface defects (see Figure 2.13).

Table 2.3 Performance of DSCs made with vertically-aligned ZnO NRs (average of 5). Effect of the ZnO NRs growth time on solar cell efficiency. 1.5 A.M., 1000 W/m^2, active area ~ 0.20 cm^2. Sun simulator lamp temperature 72°C. Pt CE from Solaronix (~60 nm thickness). *DLT = Dye loading time

	NR Growth Time (h)	NR Length (μm)	DLT* (h)	V_{oc} (V)	J_{sc} (mA/cm^2)	FF (%)	PCE (%)	Max PCE (%)
At start	6	1.6±0.2	2	0.49 ± 0.04	2.30 ± 0.34	44 ± 1	0.46 ± 0.05	0.53
	12	3.2±0.5	3	0.49 ± 0.02	3.98 ± 0.32	41 ± 1	0.73 ± 0.05	0.80
	22	5.1±0.2	6	0.52 ± 0.06	3.53 ± 0.22	43 ± 2	0.78 ± 0.08	0.86
	28	5.0±0.4	8	0.54 ± 0.05	3.92 ± 0.46	38 ± 5	0.79 ± 0.06	0.88
At max	6	1.6±0.2	2	0.55 ± 0.03	2.23 ± 0.31	44 ± 3	0.56 ± 0.04	0.60
	12	3.2±0.5	3	0.54 ± 0.03	3.59 ± 0.61	41 ± 1	0.80 ± 0.09	0.87
	22	5.1±0.2	6	0.54 ± 0.04	3.83 ± 0.30	44 ± 1	0.92 ± 0.10	1.01
	28	5.0±0.4	8	0.58 ± 0.05	4.12 ± 0.50	39 ± 3	0.89 ± 0.09	1.01

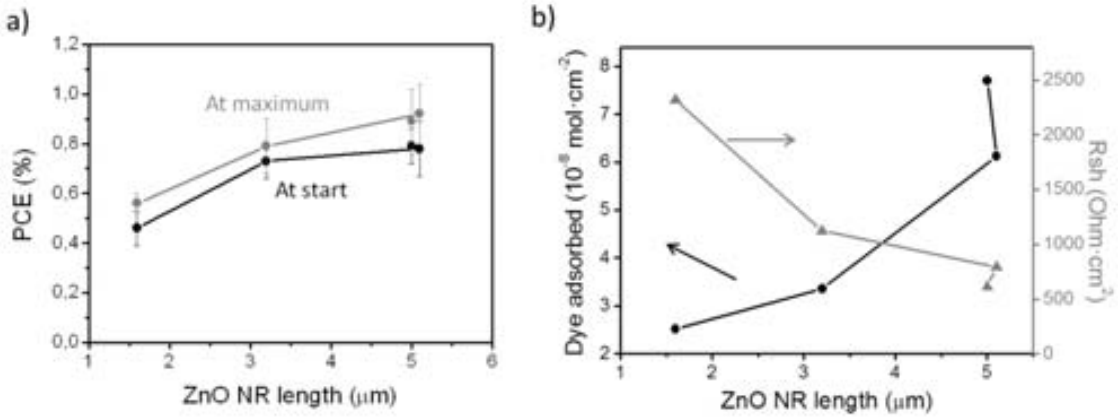

Figure 2.20a) Average performance of DSCs (of 5) showing the effect of the ZnO NRs length on the performance. Measured at 100 mW·cm^{-2} (AM 1.5) light intensity and 72°C. Active area ~0.20 cm^2. Pt-CE from Solaronix (~60 nm thickness) and b) N719 dye adsorbed and shunt resistances (R_{sh}) on the ZnO NRs electrode with different NR lengths.

Figure 2.21 shows the JV-curves and IPCE graphs for the best cells obtained for each NR length. IPCE data from our cells usually show 2 peaks, one is attributed to ZnO at ~370 nm and the other corresponds to the dye at ~500 nm. The dye N719 has two absorption peaks one at ~ 390 nm and the other at ~ 520 nm. The effect of the dye on the DSC performance is usually related to the peak at ~500 nm.

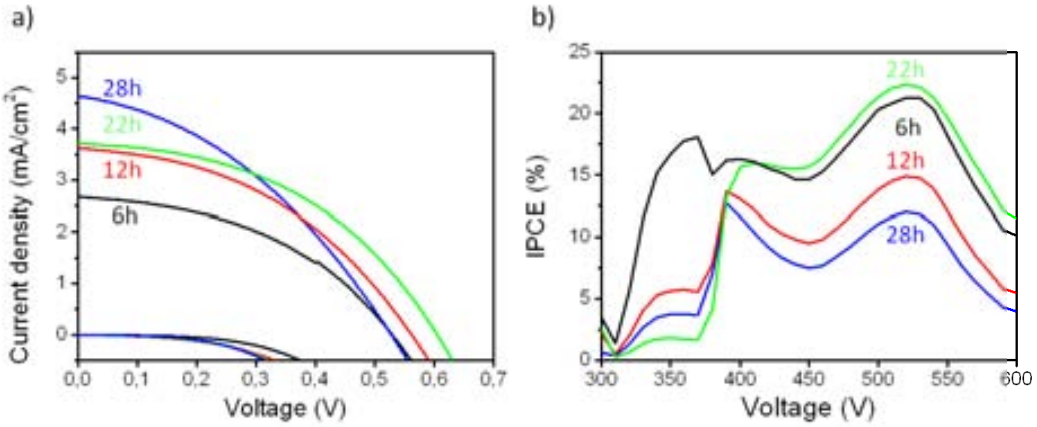

Figure 2.21 a) JV-curves for DSCs with ZnO NRs grown at 6 h, 12 h, 22 h and 28 h at maximum performance (after 3 days) and b) IPCE spectra for the same cells. 100 mW·cm^{-2} (AM 1.5) light intensity and 72°C. Active area ~0.20 cm^2. Pt-CE from Solaronix (~60 nm thickness).

2.4.5 Comparison of different dyes

Ru (II) complex dyes such as N719 or N3 have protons from carboxyl groups that dissolve the ZnO forming [Zn^{2+}-dye] aggregates and reduce the solar cell performance. In addition, ruthenium is a rare and expensive metal.[100, 103] For this reason metal-free sensitizers are very attractive for ZnO DSCs. Many research groups are developing new organic dyes with higher extinction coefficients that produce high light-harvesting yield.[31, 105-109] The modification of the dye molecular structure and the anchoring groups, allows the improvement of the solar cell properties. The ideal dye should have the excited state redox potential close to the energy of the conduction band edge of the ZnO and a strong conjugation across the chromophore and anchoring groups from the dye to provide effective charge transport and higher conversion efficiency.[110, 111] The stability of the dye is another factor to take into account to design a good sensitizer since organic dyes are more instable than Ru(II) complexes for their side reactions such as formation of excited triplet states and unstable radicals.[112] Novel sensitizers such as coumarin,[113] heptamethine cyanine,[105] indoline,[106,114] xanthene,[115] polyene thyophene[109,116] and squarylium[117] have been reported in DSCs. Some commercial organic dyes, one indoline (D149) and three xanthene (Eosin Y, Eosin B and Mercurochrome) were tested and compared with N719 in our ZnO NRs DSCs. Figure 2.22 shows the molecular structures of the dyes analysed.

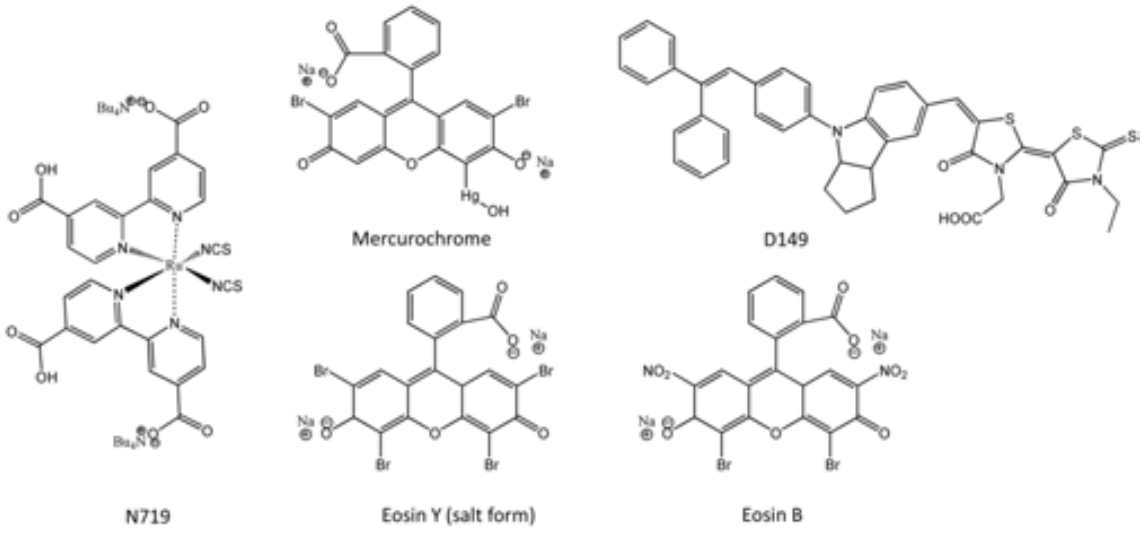

Figure 2.22 Molecular structures of N719, Mercurochrome, D149, Eosin Y and Eosin B dyes analysed in this work.

The photovoltaic parameters of the best DSCs applying the different dyes electrodes of ~1.6 μm ZnO NRs length (6 h growth time) are shown in Table 2.4. Dye loading time (DLT) of 2 h was applied in all cases. Increasing DLT up to 24 h did not show any improvement in DSC performance. Performance improvement, typically observed with time when the N719 dye is used, was not observed for any organic dye. The photovoltaic performance improved depending on the dye applied as follows: N719 > D149 > Mercurochrome > Eosin Y > Eosin B. The solvents used to dissolve the dyes were: ethanol (for N719, Eosin Y and Eosin B), methanol (for Mercurochrome) and acetonitrile (ACN)/tert-buthyl alcohol (^{t}BuOH) 1:1 (for D149), applying a constant concentration of 0.5 mM. The dye D149 had very low performances using the electrolyte AN50, when a new electrolyte was used (0.6 M BMII, 0.03 M I_2 and 0.1 M GuSCN in ACN/valeronitrile 85:15)[9] the cells showed an improvement in the photovoltaic response (Table 2.4). The later indicates the positive effect of ionic liquids in this type of solar cells, which is known to confer chemical stability to ZnO. Nevertheless, the study of DSC applying ionic liquids is out of the scope of this thesis work. Figure 2.23 depicts the current-voltage curves and IPCE spectra for the cells in Table 2.4. The peak at ~530 nm (related to the dye) corresponded with the current densities (J_{sc}) of the cells (Figure 2.23). A high current density was obtained with D149 dye but the FF was much lower than N719, thus DSCs with D149 had higher recombination wich is evident in the low value of shunt resistance R_{sh} claculated from the IV-curve (Table 2.4). The dye N719 has the best value of R_s (the lowest) and Mercurochrome has the best value of R_{sh} (the highest).

Table 2.4 Effect of different dyes on the performance of DSCs made with ZnO NRs electrodes of ~1.6 μm length (6 h growth time) and 2 h DLT. Measured at start at 100 mW·cm^{-2} (AM 1.5) light intensity and 72°C. Active area ~0.2 cm^2. [a]Electrolyte: 0.6 M BMII, 0.03 M I_2 and 0.1 M GuSCN in acetonitrile-valeronitrile (85:15). Pt-CE from Solaronix (~50 nm thickness).

Dye	V_{oc} (V)	J_{sc} (mA·cm^{-2})	FF (%)	PCE (%)	R_{sh} (Ω·cm^2)	R_s (Ω·cm^2)
N719	0.504	2.17	40	0.44	768	92
Mercurochrome	0.480	0.71	47	0.16	2803	166
Eosin B	0.356	0.36	42	0.05	1968	305
Eosin Y	0.449	0.39	40	0.07	1681	302
D149	0.451	0.48	46	0.10	2686	272
	0.484[a]	2.35[a]	31[a]	0.35[a]	276[a]	110[a]

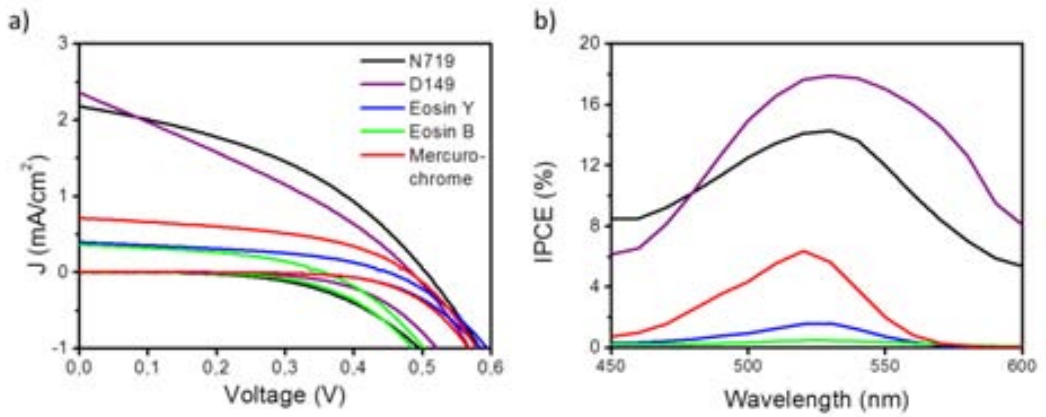

Figure 2.23 a) Current-Voltage curves and b) IPCE graphs of DSCs with ~1.6 μm ZnO NR length and different dyes (2 h DLT). Dyes: N719 (black line), D149 (purple line), Eosin Y (blue line), Eosin B (green line) and Mercurochrome (red line). 100 mW·cm^{-2} (AM 1.5) light intensity and 72°C. Active area ~0.20 cm^2. Pt-CE from Solaronix (~50 nm thickness).

2.5. Specific photovoltaic analysis

2.5.1. Effect of incident light intensity

The photovoltaic response of all XCS, such as TiO_2-based DSC[118] or polymer solar cells,[119] show a dependence on the incident light intensity. When light intensity increases, an increase on the open circuit voltage (V_{oc}) is observed. This effect has been attributed to the increase on charge generation rate producing a large chemical potential.[118] An increase on the V_{oc} for higher incident light intensities is also observed in ZnO DSCs suggesting the same effect detected in TiO_2. In this section we analysed several solar cells made with ZnO NRs at different light intensities, temperature and with or without the application of an UV-filter. The analyses were carried out in a home-made solar cell described in the chapter 6- Experimental Methods, section 6.6.

Our results showed changes in V_{oc} from 0.58 V to 0.62 V when light intensity was modified from 1000 W· cm^{-2} up to 1500 W· cm^{-2}. Below 1000 W· cm^{-2} the values of V_{oc} were almost unchanged. Current densities (J_{sc}) increased linearly with light intensity, as was expected, due to the presence of more amount of photons reaching the solar cell. Only FF values were shown to decrease slightly with light intensity, with variation between 2 and 3% (Figure 2.24).[58]

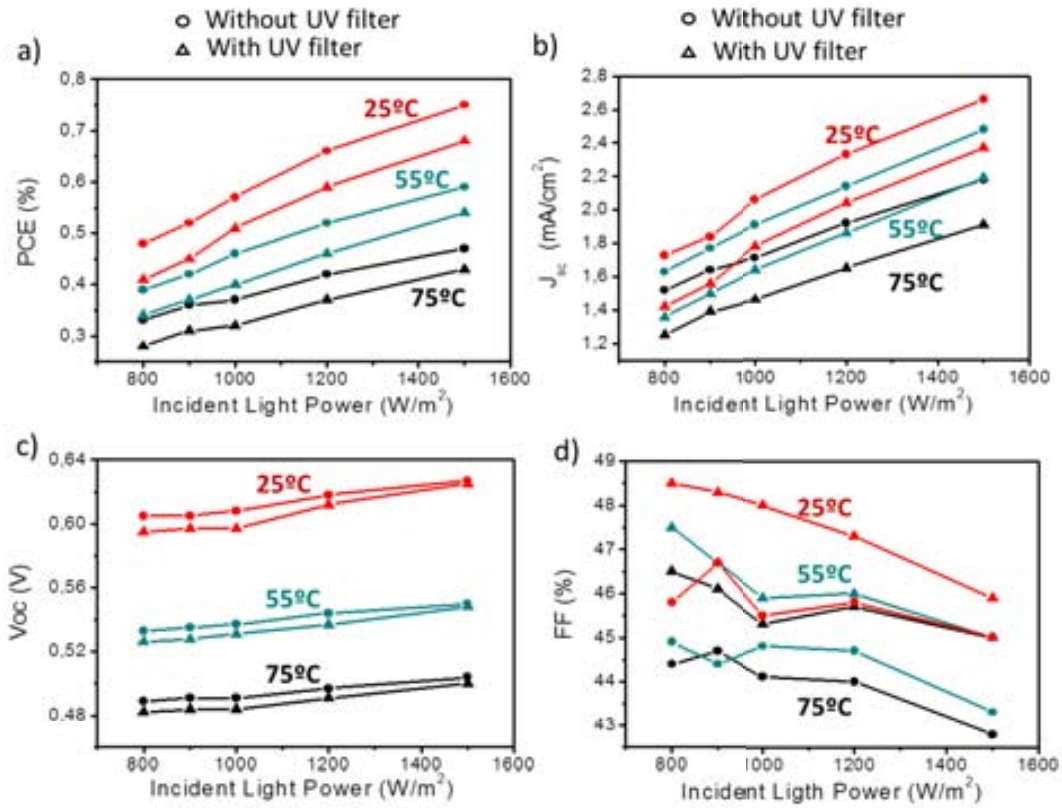

Figure 2.24 Effect of ZnO-DSC with different light intensities (800-1000 W·cm^{-2}), at different temperatures (25°C, 55°C and 75°C) and also with and without UV-filter (<400 nm). a) PCE, b) J_{sc}, c) V_{oc} and d) FF. Devices prepared with ZnO NR electrodes grown at 6 h (~1.6 μm) and 2 h DLT in N719. Active area ~0.15-0.25 cm^2. Pt-CE from Solaronix (~50 nm thickness).

2.5.2. Effect of temperature

Temperature is expected to affect the diffusion of electrons and thus current density and power conversion efficiency of the final DSCs.[120-124] We have observed contradictory results reported in the literature, some groups observed almost null effect of temperature in DSCs based in TiO_2 when low levels of irradiation were applied,[120] other groups demonstrated that values of V_{oc} are reduced when temperature increases.[122] Comparison between DSC applying TiO_2 and ZnO should be carefully made since the properties of both oxides are highly different and the variation of their properties with temperature can vary from material to material. The history behind each electrode (synthesis conditions, thermal treatments, oxide quality, etc.) can also introduce variations to the DSC performance with temperature.

In this work, we present the study of the effect of temperature on vertically-aligned ZnO NR-based DSCs using the home-made holder described in chapter 6, section 6.6. In general, we observed a decrease in photovoltaic response when temperature increases from 25°C to 75°C. Figure 2.24 shows the changes observed with temperature on PCE, J_{sc}, V_{oc}, and FF for our DSCs. The most drastic effect was observed in V_{oc}, which decreased from ~0.6 V to ~0.48 V when temperature was raised. A similar trend was observed for J_{sc}, however, below 55°C some cells maintained almost unchanged the J_{sc} and some other showed a slightly decrease. At higher temperatures (55°C-75°C) the J_{sc} decrease was accentuated (Figure 2.24 and Figure 2.25). The latter effect is attributed to the efficient electron diffusion observed in semiconductor oxides as temperature increases but at higher temperatures the charge recombination is stronger than the beneficial effect of diffusion.[121, 125] IPCE analyses showed this effect, the peak of ZnO at ~350 nm decreases with the increase of the temperature but the peak at ~520 nm related to the dye had a different behaviour, the IPCE was constant until 55°C and decreased at higher temperatures (Figure 2.26). A slightly variation on FF between 2 and 3% was also observed since is directly related to V_{oc} and J_{sc}.[58]

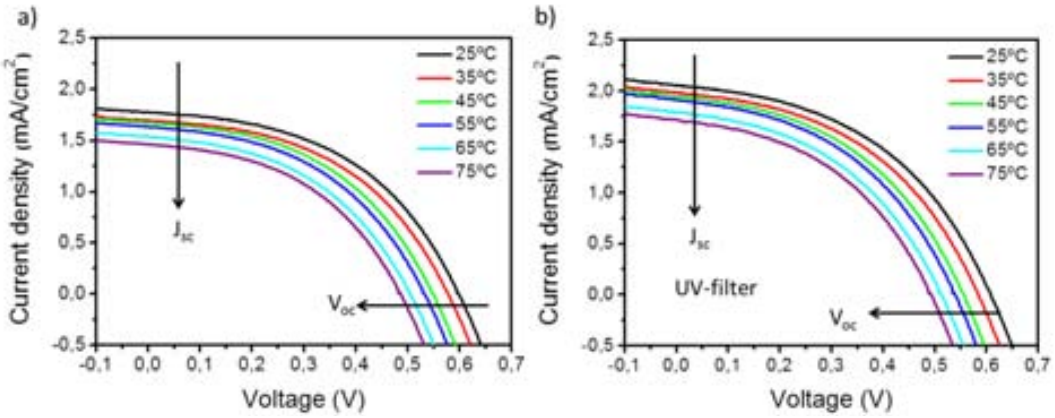

Figure 2.25 J-V curves for ZnO NRs DSCs grown for 6h (~1.6 μm) and 2 h DLT in N719. Measured at different temperatures a) without UV-filter and b) with a UV-filter (<400 nm). 100 mW·cm^{-2} (AM 1.5). Active area ~0.20 cm^2. Pt-CE from Solaronix (~50 nm thickness).

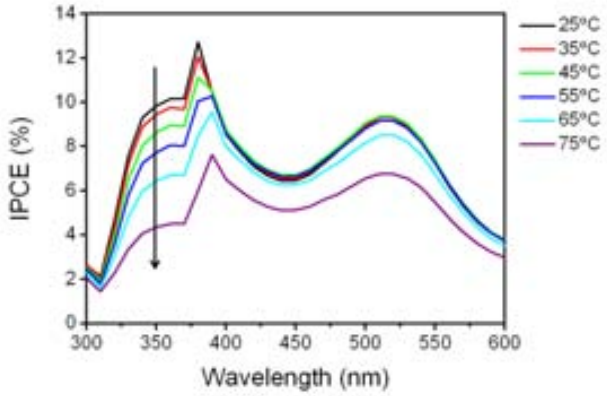

Figure 2.26 Variation of IPCE with temperature for a DSC of NRs grown for 6 h (~1.6 μm) and 2 h DLT in N719. Pt-CE from Solaronix (~50 nm thickness).

2.5.3. Effect of UV-light

In order to study the effect of the UV-light on the ZnO NR-DSCs, we measured the cells with and without an UV filter that cuts the light below 400 nm. As expected, lower J_{sc} values were obtained when using the filter since less light hit the DSCs, a 5% less that corresponds to UV light. The same effect with different light intensities and temperatures was observed when a UV filter was used compared with the ZnO-NRs DSCs applying UV-light (Figure 2.24 and Figure 2.25). Nevertheless, UV light is known to be destructive for TiO_2-based DSCs since oxygen migrates from the semiconductor oxide photo generating holes that accelerate the oxidation of the dye.[85, 126] An opposite behaviour has been reported for ZnO-based DSC and organic solar cells where the ZnO is applied as buffer layer, where UV light seems to promote the physisorption/chemisorption of organic molecules (polymers or dyes) on the ZnO semiconductor, improving the photovoltaic performance of the solar cells, at least initially.[90-92, 127] Therefore, three cells with similar performances were used to study the UV light effect with time, two were analysed at 1000 $W{\cdot}m^2$ (one with and the other without the UV-filter) and the third one at 1800 $W{\cdot}m^2$ without UV-filter. Figure 2.27a show the response of the 3 cells at different periods of time while keeping the devices in the dark between measurements. Cells irradiated with UV light presented a similar trend: an initial increase in PCE (~20% for 1000 $W{\cdot}m^{-2}$ and ~40% for 1800 $W{\cdot}m^{-2}$), followed by a stabilization period of about 180 h and, finally, a decrease in solar cell performance after the first ~200 h of testing. The behaviour of the sample with the UV-filter presented a good stability with null efficiency variation for the

first 50 h of testing. Table 2.5 represents the DSCs data from Figure 2.27a at start and maximum (after 3 days) efficiency.[66]

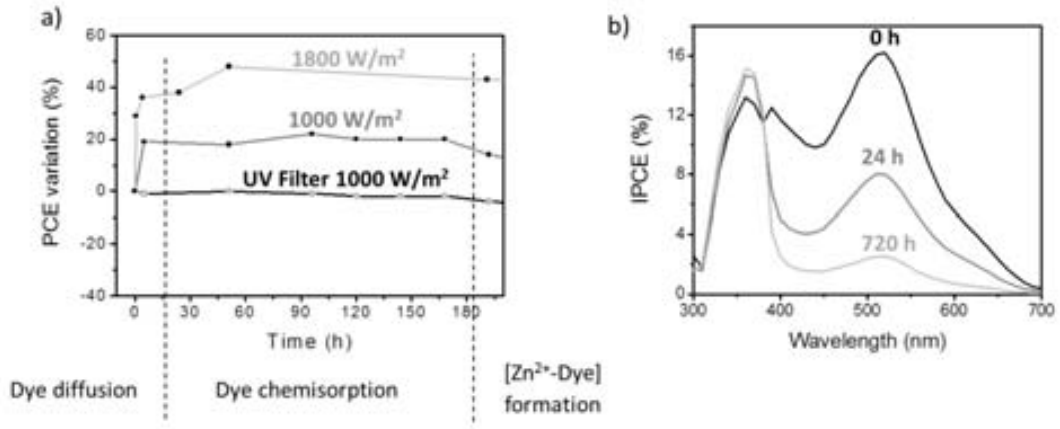

Figure 2.27 Vertically-aligned ZnO electrodes grown for 6 h and sealed DSCs. a) Power conversion efficiency (PCE) variation with time and b) IPCE spectra for the same sealed cell at different periods of time: freshly prepared (0 h), after efficiency increased (24 h) and completely degraded (720 h). Pt CE from Solaronix (~50 nm thickness).

Table 2.5 Effect of UV light on ZnO NRs-based DSC. NRs were grown for 6 h and analysed as sealed DSC. Devices analysed at 72º C. Active area of 0.2 cm^2 . Values obtained for each device at start and at maximum efficiency observed during lifetime studies. Pt CE from Solaronix (~50 nm thickness).

	Sample	Light intensity (W/m^2)	V_{oc} (V)	J_{sc} (mA/cm^2)	FF (%)	Eff (%)
At start	No Filter	1800	0.519	3.02	33	0.52
	No Filter	1000	0.508	2.20	36	0.41
	UV Filter	1000	0.486	1.30	43	0.27
At max	No Filter	1800	0.612	3.22	38	0.75
	No Filter	1000	0.535	2.34	39	0.49
	UV Filter	1000	0.514	1.23	42	0.27

Several series of measurements resulted in different IPCE values due to some irreproducibility (showed as error bars in Figure 2.20a and Table 2.3). Other groups have also reported the same effect.[100] The IPCE analyses for a DSC at different periods of time: freshly prepared (0 h), once the efficiency increased after 24 h and once the device was completely degraded at 720 h show a slight initial increase of the ~370 nm peak (related to ZnO), which stabilizes with time, and a gradual disappearance of the peak at ~520 nm (related to the dye) (Figure 2.27b). To understand these IPCE changes and correlate the processes with the solar cell performance and lifetime, we decided to work with solutions of dye N719 and ZnO NRs to study the interaction between them and exclude the

possibility of external effects like the presence of electrolyte. Three solutions of dye N719 and ZnO NRs with the same concentration, 0.002 g of ZnO NRs scratched from an electrode surface (grown for 6h) in 3 ml of a 0.01 mM dye N719 in absolute ethanol was divided in 3 parts. The solutions were kept sealed (in air) in 3 UV-cuvettes under constant stirring during the time the experiment took place (about 1 week). One solution was kept in the dark all the time (a) as reference, the other two were irradiated under the sun simulator at 1000 $W \cdot m^{-2}$ with a UV-filter (b) and without (c). UV-vis absorption analyses were performed at different periods of time, between 0h to 192h (Figure 2.28). Samples (b) and (c) were kept in the dark between experiments and subjected to irradiation under the sun simulator for 5 min before each UV-vis absorption measurement. Figure 2.28 shows the UV-vis spectra of the 3 solutions and for comparison purposes the UV-vis absorption spectra of the dye and the ZnO suspension are also included. The dye N719 has two absorption bands, one at ~380 nm and the other at ~525 nm, attributed to metal-to-ligand charge transfer, specifically the absorption at ~380 nm which corresponds to intraligand (π-π^*) charge transfer transition[126] and the ZnO NRs absorb at ~375 nm (Figure 2.28). At the start of the experiment, the two absorption bands initially observed, stay unaltered for a period of about 24 h for the sample kept in the dark (Figure 2.28a). The sample (b) irradiated with the filter, the maximum peat at ~525 nm increases slightly and stabilizes for about 24 h (Figure 2.28b). The sample (c) irradiated without the UV filter presented the absorption bands unaffected for only 5 h and then the maximum at ~380 nm starts to increase in intensity while the peak at ~525 nm remains unchanged. After 24 h, all the samples registered a sudden blue-shift of the peak at ~525 nm to ~505 nm until the complete suppression of the peak and this effect was faster when UV-light was irradiated, sample (c). A similar behaviour was reported by Keis *et al.* who defined these processes as steps between agglomeration, dissolution and [Zn^{2+}-dye] complex formation.[100] The latter is clearly represented in Figure 2.29 where the two peaks are displayed separately in function of time. The suppression of the ~525 nm peak was observed for the 3 dispersions, and is linked to the formation of a deprotonated form, weak electron coupling and the detachment of the SCN-group of the N719 dye.[128, 129] Both absorption peaks were suppressed with time for TiO_2 –N719 in reported work.[128, 129] However, in our case, the peak at ~380 nm did not disappeared, initially increases and then stabilizes with time due to the ZnO dissolution and a formation of a new compound: [Zn^{2+}-dye] complex. In addition, the peak at ~380 nm slightly shifted to lower wavelengths approaching the ZnO maximum at ~375 nm which supports the formation of a new [Zn^{2+}-dye] complex.[66] Our

results confirm that even storage of the solar cells in the dark can lead to degradation of the ZnO with time. The interaction of the dye N719 with ZnO NRs seem to take place in 3 well-defined steps: dye diffusion, dye chemisorption and complex [Zn^{2+}-dye] formation, represented in Figure 2.27a. UV-light irradiation permits a faster interaction between the dye and the ZnO (increasing the initial efficiency) but faster degradation of the cell was also observed. Without UV-light irradiation the latter process also takes place, but in a slower mode. The latter was also observed by other groups.[130]

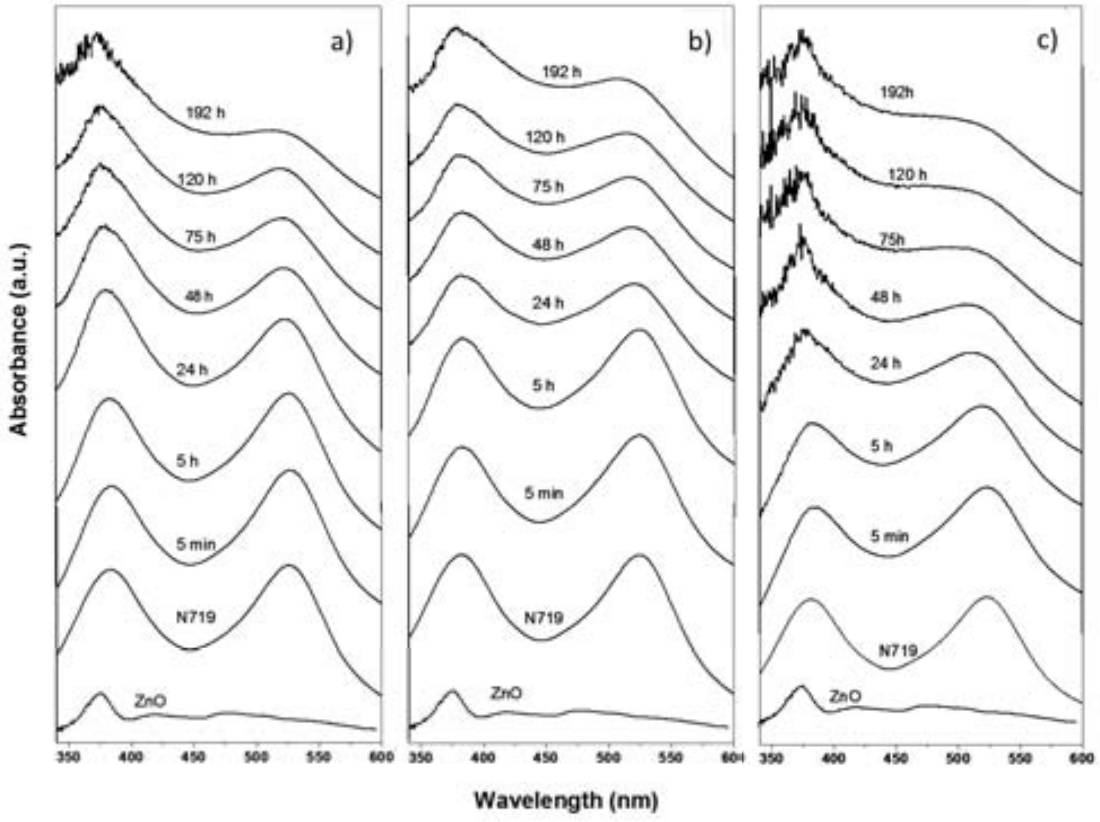

Figure 2.28 UV-vis spectra of a dye N719/ZnO nanorod dispersion: (a) kept in the dark, (b) irradiated under sun simulator at 1000 $W \cdot m^{-2}$ using a UV filter (<400 nm) and (c) irradiated at 1000 $W \cdot m^{-2}$ without filter.

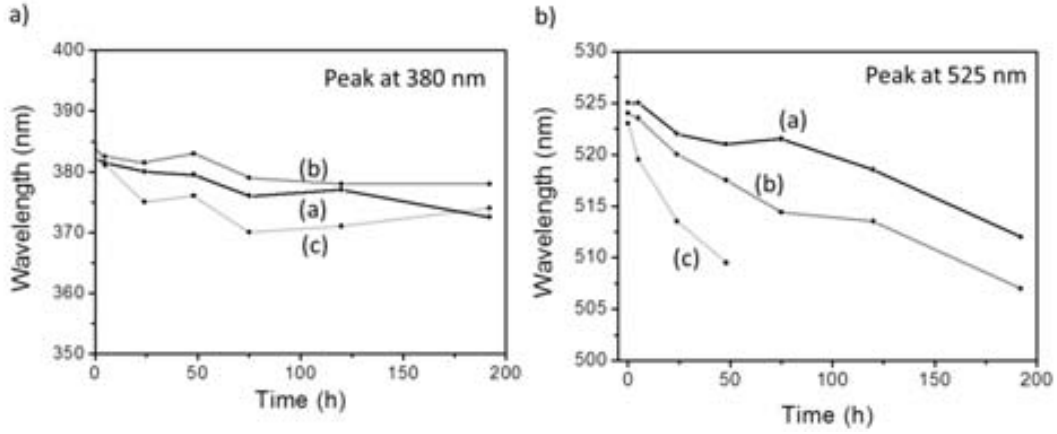

Figure 2.29 Evolution of the UV-vis absorption bands of N719/ZnO NRs dispersion with time. a) Absorption band at ~380 nm and b) absorption band at ~525 nm. Sample (a) dark, sample (b) no UV light irradiation and sample (c) UV light irradiation.

2.5.4. Long term stability analyses

Long-term stability analyses of the DSC were carried out at 45ºC and 1000 W/m^2. Figure 2.30 shows the degradation process for all the parameters from a DSC with ~5 μm ZnO NR length. After 40 h of irradiation the J_{sc} shows a faster degradation but V_{oc} was almost constant during all the measurement (Figure 2.30a and b). On the other hand, the efficiency of the cell decreased exponentially (Figure 2.30d). In order to study the latter effect, vertically-aligned ZnO NRs were scratched from an electrode and suspended in an ethanolic solution containing the dye N719, the mixture was stirred for one month. A pink solid was observed in the solution with time. The solid was centrifuged and washed with ethanol before analysed. TEM studies of the solid in the solution showed a slight degradation of the ZnO NRs, the formation of a very thin shell organic layer covering all the NRs was observed (Figure 2.31a and b). EDS analyses indicate the presence of ruthenium from the dye in the shell. The effect of the electrolyte was analysed by adding some drops of electrolyte in the dye N719/ZnO NRs solution, several pieces of aggregates appeared over the sample (Figure 2.31c). These results show that the dissolution of the dye is not only due to the interaction between the dye and ZnO but also by the effect imposed by the electrolyte. SEM images of the aggregate are in Figure 2.31d and e. TGA analyses of the aggregate showed the presence of a highly hygroscopic solid, which weight loss was less than 1% (organic matter) below 550°C.[58]

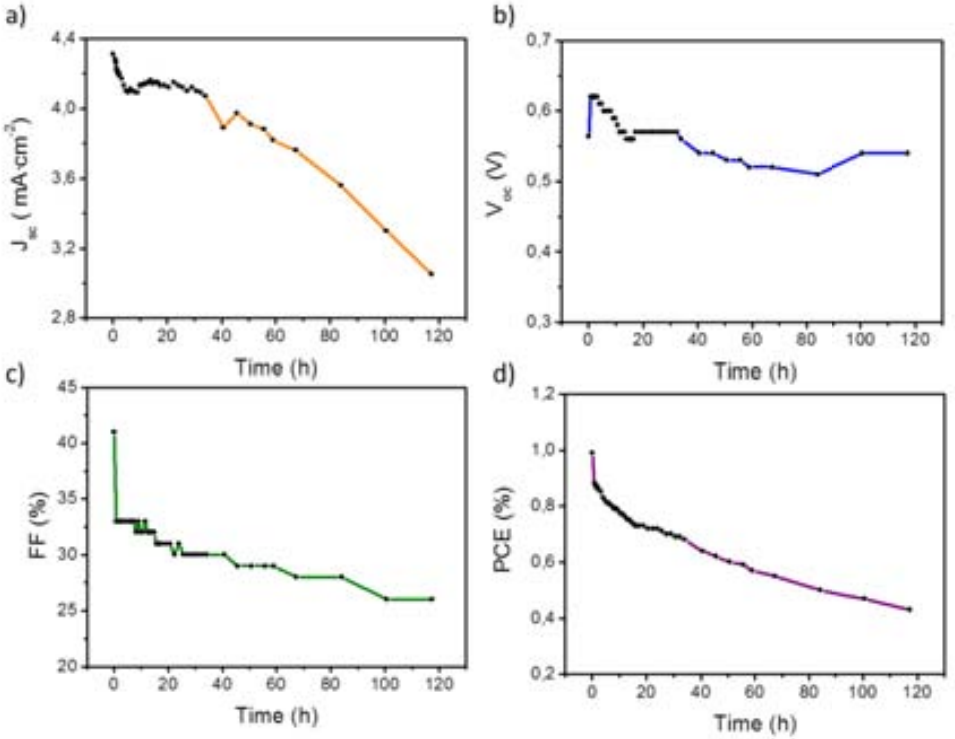

Figure 2.30 Continuous irradiation carried out at 1000 W·m^{-2} for a DSC with ~5 μm ZnO NRs length (22 h growth time). Effect of a) J_{sc}, b) V_{oc}, c) FF and d) PCE with time. Pt CE from Solaronix (~50 nm thickness).

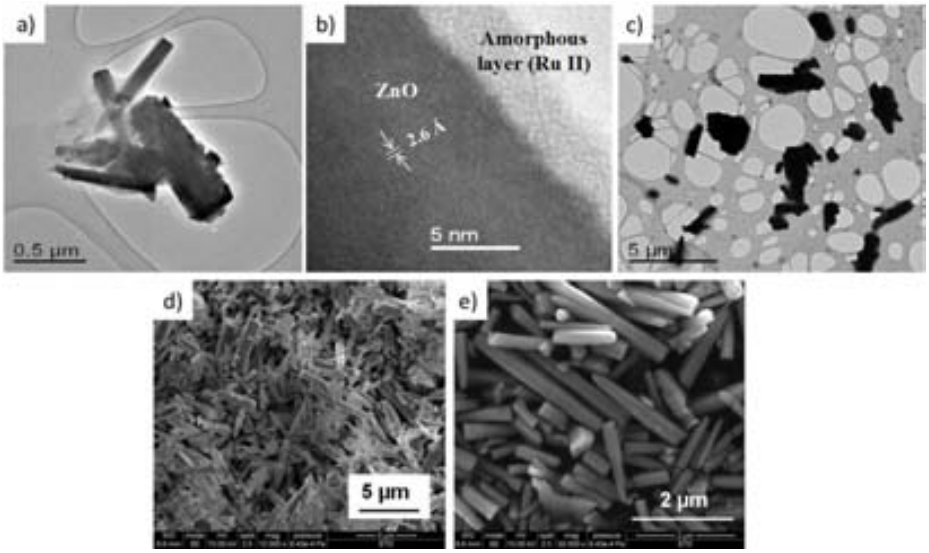

Figure 2.31 FE-TEM images. a) Solution of ZnO NRs and N719 dye, b) High-magnification image of one ZnO NR from the solution a), c) solution of ZnO NRs with N719 dye and electrolyte. FE-SEM images of d) big aggregates from the solution dye N719-ZnO NRs and e) higher magnification of the image d).

2.6 Conclusions

In this chapter we have prepared and optimized vertically-aligned ZnO NRs electrodes on TCO substrates. All the synthesis conditions were studied and fixed to have reproducible results. The optimal conditions for the synthesis of vertically-aligned ZnO NRs electrodes are:

a) FTO substrates
b) three layers of ZnO NPs deposition
c) 25 mM equimolar concentration of the hydrothermal solution
d) 6-8 cm NR growth distance of the substrates from the bottom of the flask
e) NR growth time between 2 h and 28 h.

The electrodes prepared with different NRs lengths were characterized by SEM, TEM, profilometer, XRD, UV-vis absorption and PL measurements. Our results shows that all the ZnO NRs present good crystallinity with an hexagonal wurtzite structure, the NR length and diameter increased when the growth time increases. The PL peak that corresponds to the orange band at ~650 nm increases with NR length, an indication of the increment of the surface defects and directly associated with recombination processes.

The application of the ZnO NR electrodes in DSCs was also optimized. We carried out the analyses of different testing parameters that play a crucial role on the final solar cell performance: electrode thermal treatment, platinum counter electrode, dye loading time, NR length, comparison with different dyes, light intensity, temperature, UV-light and long term stability analyses. Different solar cell performances were observed when various Pt-CE were used. The power conversion efficiencies increased when the electrodes were annealed at 450°C for 30 min and longer NR lengths were applied, moreover, longer dye loading times were needed. Increasing the light intensity and temperature affects the series and shunt resistances of the devices reducing the final solar cell efficiency. UV-light irradiation produced an increase of ~20% of efficiency from the start of the measurements for 1000 $W \cdot m^{-2}$ and ~40% for 1800 $W \cdot m^{-2}$ when no UV light was irradiated, no variance from the initial performance was observed. All the devices degraded with time but in a faster way when UV light was applied. The study of the interaction between N719 dye and ZnO NRs by UV-vis absorption and IPCE measurements was confirmed to take place in 3 well-defined steps: dye diffusion, dye chemisorption and

[Zn^{2+}-dye] complex formation. Analysis of lifetime under continuous irradiation at 1 Sun (1000 $W \cdot m^{-2}$) revealed the total dissolution of ZnO NRs after several hours.

2.7 References

1. Q. Zhang, S. Yodyingyong, J. Xi, D. Myers and G. Cao, "Oxide nanowires for solar cell applications". *Nanoscale* **2012,** 4 (5), 1436-1445.
2. Q. F. Zhang, C. S. Dandeneau, X. Y. Zhou and G. Z. Cao, "ZnO Nanostructures for Dye-Sensitized Solar Cells". *Advanced Materials* **2009,** 21 (41), 4087-4108.
3. U. Ozgur, Y. I. Alivov, C. Liu, A. Teke, M. A. Reshchikov, S. Dogan, V. Avrutin, S. J. Cho and H. Morkoc, "A comprehensive review of ZnO materials and devices". *Journal of Applied Physics* **2005,** 98 (4).
4. W.-J. Yin, S. Chen, J.-H. Yang, X.-G. Gong, Y. Yan and S.-H. Wei, "Effective band gap narrowing of anatase TiO2 by strain along a soft crystal direction". *Applied Physics Letters* **2010,** 96 (22).
5. M. Gratzel, "Photoelectrochemical cells". *Nature* **2001,** 414 (6861), 338-344.
6. Y. Xu and M. A. A. Schoonen, "The absolute energy positions of conduction and valence bands of selected semiconducting minerals". *American Mineralogist* **2000,** 85 (3-4), 543-556.
7. Z. L. Wang, "Nanostructures of zinc oxide". *Materials Today* **2004,** 7 (6), 26-33.
8. M. Guo, P. Diao, X. D. Wang and S. M. Cai, "The effect of hydrothermal growth temperature on preparation and photoelectrochemical performance of ZnO nanorod array films". *Journal of Solid State Chemistry* **2005,** 178 (10), 3210-3215.
9. Y. Xie, P. Joshi, S. B. Darling, Q. L. Chen, T. Zhang, D. Galipeau and Q. Q. Qiao, "Electrolyte Effects On Electron Transport and Recombination at ZnO Nanorods for Dye-Sensitized Solar Cells". *Journal of Physical Chemistry C* **2010,** 114 (41), 17880-17888.
10. Q. Huang, L. Fang, X. Chen and M. Saleem, "Effect of polyethyleneimine on the growth of ZnO nanorod arrays and their application in dye-sensitized solar cells". *Journal of Alloys and Compounds* **2011,** 509 (39), 9456-9459.
11. J. J. Kim, K. S. Kim and G. Y. Jung, "Fabrication of flexible dye-sensitised solar cells with photoanodes composed of periodically aligned single crystalline vertical ZnO NRs by utilising a direct metal transfer method". *Journal of Materials Chemistry* **2011,** 21 (21), 7730-7735.
12. P. Uthirakumar, J. H. Kang, S. Senthilarasu and C.-H. Hong, "The different types of ZnO materials on the performance of dye-sensitized solar cells". *Physica E-Low-Dimensional Systems & Nanostructures* **2011,** 43 (9), 1746-1750.
13. B. Pradhan, S. K. Batabyal and A. J. Pal, "Vertically aligned ZnO nanowire arrays in Rose Bengal-based dye-sensitized solar cells". *Solar Energy Materials and Solar Cells* **2007,** 91 (9), 769-773.
14. M. Thambidurai, N. Muthukumarasamy, D. Velauthapillai, N. S. Arul, S. Agilan and R. Balasundaraprabhu, "Dye-sensitized ZnO nanorod based photoelectrochemical solar cells with natural dyes extracted from Ixora coccinea, Mulberry and Beetroot". *Journal of Materials Science-Materials in Electronics* **2011,** 22 (11), 1662-1666.
15. J. Chung, J. Lee and S. Lim, "Annealing effects of ZnO nanorods on dye-sensitized solar cell efficiency". *Physica B-Condensed Matter* **2010,** 405 (11), 2593-2598.
16. E. Galoppini, J. Rochford, H. H. Chen, G. Saraf, Y. C. Lu, A. Hagfeldt and G. Boschloo, "Fast electron transport in metal organic vapor deposition grown dye-sensitized ZnO nanorod solar cells". *Journal of Physical Chemistry B* **2006,** 110 (33), 16159-16161.
17. Z. Liu, Y. Li, C. Liu, J. Ya, W. Zhao, L. E, D. Zhao and L. An, "Performance of ZnO dye-sensitized solar cells with various nanostructures as anodes". *Solid State Sciences* **2011,** 13 (6).
18. C.-H. Chao, C.-H. Chan, J.-J. Huang, L.-S. Chang and H.-C. Shih, "Manipulated the band gap of 1D ZnO nano-rods array with controlled solution concentration and its application for DSSCs". *Current Applied Physics* **2011,** 11 (1), S136-S139.
19. V.-M. Guerin and T. Pauporte, "From nanowires to hierarchical structures of template-free electrodeposited ZnO for efficient dye-sensitized solar cells". *Energy & Environmental Science* **2011,** 4 (8), 2971-2979.

20. Z. Z. Yang, T. Xu, Y. S. Ito, U. Welp and W. K. Kwoko, "Enhanced Electron Transport in Dye-Sensitized Solar Cells Using Short ZnO Nanotips on A Rough Metal Anode". *Journal of Physical Chemistry C* **2009,** 113 (47), 20521-20526.
21. S. H. Lee, S. H. Han, H. S. Jung, H. Shin, J. Lee, J. H. Noh, S. Lee, I. S. Cho, J. K. Lee and J. Kim, "Al-Doped ZnO Thin Film: A New Transparent Conducting Layer for ZnO Nanowire-Based Dye-Sensitized Solar Cells". *Journal of Physical Chemistry C* **2010,** 114 (15), 7185-7189.
22. A. Du Pasquier, H. H. Chen and Y. C. Lu, "Dye sensitized solar cells using well-aligned zinc oxide nanotip arrays". *Applied Physics Letters* **2006,** 89 (25), 253513.
23. Y. F. Hsu, Y. Y. Xi, A. B. Djuris?ic and W. K. Chan, "ZnO nanorods for solar cells: Hydrothermal growth versus vapor deposition". *Applied Physics Letters* **2008,** 92 (13), 133507.
24. N. Karst, G. Rey, B. Doisneau, H. Roussel, R. Deshayes, V. Consonni, C. Ternon and D. Bellet, "Fabrication and characterization of a composite ZnO semiconductor as electron transporting layer in dye-sensitized solar cells". *Materials Science and Engineering B-Advanced Functional Solid-State Materials* **2011,** 176 (8), 653-659.
25. O. Lupan, V. M. Guerin, I. M. Tiginyanu, V. V. Ursaki, L. Chow, H. Heinrich and T. Pauporte, "Well-aligned arrays of vertically oriented ZnO nanowires electrodeposited on ITO-coated glass and their integration in dye sensitized solar cells". *Journal of Photochemistry and Photobiology a-Chemistry* **2010,** 211 (1), 65-73.
26. J. J. Wu, G. R. Chen, H. H. Yang, C. H. Ku and J. Y. Lai, "Effects of dye adsorption on the electron transport properties in ZnO-nanowire dye-sensitized solar cells". *Applied Physics Letters* **2007,** 90 (21), 213109.
27. H. Gao, G. Fang, M. Wang, N. Liu, L. Yuan, C. Li, L. Ai, J. Zhang, C. Zhou, S. Wu and X. Zhao, "The effect of growth conditions on the properties of ZnO nanorod dye-sensitized solar cells". *Materials Research Bulletin* **2008,** 43 (12), 3345-3351.
28. A. J. Cheng, Y. Tzeng, Y. Zhou, M. Park, T. H. Wu, C. Shannon, D. Wang and W. Lee, "Thermal chemical vapor deposition growth of zinc oxide nanostructures for dye-sensitized solar cell fabrication". *Applied Physics Letters* **2008,** 92 (9), 092113
29. Z. H. Chen, Y. B. Tang, C. P. Liu, Y. H. Leung, G. D. Yuan, L. M. Chen, Y. Q. Wang, I. Bello, J. A. Zapien, W. J. Zhang, C. S. Lee and S. T. Lee, "Vertically Aligned ZnO Nanorod Arrays Sentisized with Gold Nanoparticles for Schottky Barrier Photovoltaic Cells". *Journal of Physical Chemistry C* **2009,** 113 (30), 13433-13437.
30. Y. Tian, C. Hu, Q. Wu, X. Wu, X. Li and M. Hashim, "Investigation of the fill factor of dye-sensitized solar cell based on ZnO nanowire arrays". *Applied Surface Science* **2011,** 258 (1), 321-326.
31. E. Guillen, E. Azaceta, L. M. Peter, A. Zukal, R. Tena-Zaera and J. A. Anta, "ZnO solar cells with an indoline sensitizer: a comparison between nanoparticulate films and electrodeposited nanowire arrays". *Energy & Environmental Science* **2011,** 4 (9), 3400-3407.
32. C. H. Ku and J. J. Wu, "Chemical bath deposition of ZnO nanowire-nanoparticle composite electrodes for use in dye-sensitized solar cells". *Nanotechnology* **2007,** 18 (50), 505706.
33. C. Y. Jiang, X. W. Sun, K. W. Tan, G. Q. Lo, A. K. K. Kyaw and D. L. Kwong, "High-bendability flexible dye-sensitized solar cell with a nanoparticle-modified ZnO-nanowire electrode". *Applied Physics Letters* **2008,** 92 (14), 143101.
34. A. Yengantiwar, R. Sharma, O. Game and A. Banpurkar, "Growth of aligned ZnO nanorods array on ITO for dye sensitized solar cell". *Current Applied Physics* **2011,** 11 (1), S113-S116.
35. J. B. Baxter, A. M. Walker, K. van Ommering and E. S. Aydil, "Synthesis and characterization of ZnO nanowires and their integration into dye-sensitized solar cells". *Nanotechnology* **2006,** 17 (11), S304-S312.
36. W. G. Yang, F. R. Wan, S. W. Chen and C. H. Jiang, "Hydrothermal Growth and Application of ZnO Nanowire Films with ZnO and TiO2 Buffer Layers in Dye-Sensitized Solar Cells". *Nanoscale Research Letters* **2009,** 4 (12), 1486-1492.
37. J. Jung, J. Myoung and S. Lim, "Effects of ZnO nanowire synthesis parameters on the photovoltaic performance of dye-sensitized solar cells". *Thin Solid Films* **2012,** 520 (17), 5779-5789.
38. P. Charoensirithavorn and S. Yoshikawa, "Controllable synthesis of ZnO nanorod arrays via simple solution-based method". *Zinc Oxide and Related Materials* **2007,** 957, 225-228.

39. M. H. Lai, M. W. Lee, G.-J. Wang and M. F. Tai, "Photovoltaic Performance of New-Structure ZnO-nanorod Dye-Sensitized Solar Cells". *International Journal of Electrochemical Science* **2011,** 6 (6), 2122-2130.
40. M. H. Lai, A. Tubtimtae, M. W. Lee and G. J. Wang, "ZnO-Nanorod Dye-Sensitized Solar Cells: New Structure without a Transparent Conducting Oxide Layer". *International Journal of Photoenergy* **2010**, 497095.
41. J. S. Bendall, L. Etgar, S. C. Tan, N. Cai, P. Wang, S. M. Zakeeruddin, M. Graetzel and M. E. Welland, "An efficient DSSC based on ZnO nanowire photo-anodes and a new D-pi-A organic dye". *Energy & Environmental Science* **2011,** 4 (8), 2903-2908.
42. C. Y. Jiang, X. W. Sun, G. Q. Lo, D. L. Kwong, J. X. Wang and Fc, "Improved dye-sensitized solar cells with a ZnO-nanoflower photoanode". *Applied Physics Letters* **2007,** 90 (26), 263501.
43. R. S. Mane, W. J. Lee, C. D. Lokhande, B. W. Cho and S. H. Han, "Controlled repeated chemical growth of ZnO films for dye-sensitized solar cells". *Current Applied Physics* **2008,** 8 (5), 549-553.
44. W. Yang, Y. Wang, Q. Zhen and W. Shi, "Effect of growth time on morphology and photovoltaic properties of ZnO nanowire array films". *Rare Metals* **2011,** 30 (6), 676-680.
45. S. M. Mahpeykar, J. Koohsorkhi and H. Ghafoori-Fard, "Ultra-fast microwave-assisted hydrothermal synthesis of long vertically aligned ZnO nanowires for dye-sensitized solar cell application". *Nanotechnology* **2012,** 23 (16), 165602.
46. Y. F. Gao, M. Nagai, T. C. Chang and J. J. Shyue, "Solution-derived ZnO nanowire array film as photoelectrode in dye-sensitized solar cells". *Crystal Growth & Design* **2007,** 7, 2467-2471.
47. A. Al-Hajry, A. Umar, Y. B. Hahn and D. H. Kim, "Growth, properties and dye-sensitized solar cells - applications of ZnO nanorods grown by low-temperature solution process". *Superlattices and Microstructures* **2009,** 45 (6), 529-534.
48. M. Law, L. E. Greene, J. C. Johnson, R. Saykally and P. D. Yang, "Nanowire dye-sensitized solar cells". *Nature Materials* **2005,** 4 (6), 455-459.
49. S. H. Ko, D. Lee, H. W. Kang, K. H. Nam, J. Y. Yeo, S. J. Hong, C. P. Grigoropoulos and H. J. Sung, "Nanoforest of Hydrothermally Grown Hierarchical ZnO Nanowires for a High Efficiency Dye-Sensitized Solar Cell". *Nano Letters* **2011,** 11 (2), 666-671.
50. J. X. Wang, C. M. L. Wu, W. S. Cheung, L. B. Luo, Z. B. He, G. D. Yuan, W. J. Zhang, C. S. Lee and S. T. Lee, "Synthesis of Hierarchical Porous ZnO Disklike Nanostructures for Improved Photovoltaic Properties of Dye-Sensitized Solar Cells". *Journal of Physical Chemistry C* **2010,** 114 (31), 13157-13161.
51. A. Wagner, A. Behrends, A. Waag and A. Bakin, "Two step deposition method with a high growth rate for ZnO nanowire arrays and its application in photovoltaics". *Thin Solid Films* **2012,** 520 (14), 4637-4641.
52. C. K. Xu, P. Shin, L. L. Cao and D. Gao, "Preferential Growth of Long ZnO Nanowire Array and Its Application in Dye-Sensitized Solar Cells". *Journal of Physical Chemistry C* **2010,** 114 (1), 125-129.
53. J. J. Qiu, X. M. Li, F. W. Zhuge, X. Y. Gan, X. D. Gao, W. Z. He, S. J. Park, H. K. Kim and Y. H. Hwang, "Solution-derived 40 mu m vertically aligned ZnO nanowire arrays as photoelectrodes in dye-sensitized solar cells". *Nanotechnology* **2010,** 21 (19), 195602.
54. F. De Angelis, S. Fantacci, E. Mosconi, M. K. Nazeeruddin and M. Graetzel, "Absorption Spectra and Excited State Energy Levels of the N719 Dye on TiO2 in Dye-Sensitized Solar Cell Models". *Journal of Physical Chemistry C* **2011,** 115 (17), 8825-8831.
55. Z. Cao, P. Nandhikonda, A. Penuela, S. Nance and A. D. Heagy, "N-Aryl Arenedicarboximides as Tunable Panchromatic Dyes for Molecular Solar Cells". *International Journal of Photoenergy* **2010**.
56. M. K. Nazeeruddin, F. De Angelis, S. Fantacci, A. Selloni, G. Viscardi, P. Liska, S. Ito, T. Bessho and M. Gratzel, "Combined experimental and DFT-TDDFT computational study of photoelectrochemical cell ruthenium sensitizers". *Journal of the American Chemical Society* **2005,** 127 (48), 16835-16847.
57. A. J. Said, G. Poize, C. Martini, D. Ferry, W. Marine, S. Giorgio, F. Fages, J. Hocq, J. Boucle, J. Nelson, J. R. Durrant and J. Ackermann, "Hybrid Bulk Heterojunction Solar Cells Based on P3HT

and Porphyrin-Modified ZnO Nanorods". *Journal of Physical Chemistry C* **2010,** 114 (25), 11273-11278.
58. I. Gonzalez-Valls, Y. Yu, B. Ballesteros, J. Oro and M. Lira-Cantu, "Synthesis conditions, light intensity and temperature effect on the performance of ZnO nanorods-based Dye sensitized solar cells". *Journal of Power Sources* **2011,** 196, 6609–6621.
59. I. Gonzalez-Valls and M. Lira-Cantu, "Effect of testing conditions on the photovoltaic performance of ZnO-based dye sensitized solar cells". In *Vi Encuentro Franco-Espanol De Quimica Y Fisica Del Estado Solido - Vi Rencontre Franco-Espagnole Sur La Chimie Et La Physique De L Etat Solide*, J. J. Carvajal,M. AguiloandF. Diaz, Eds. **2010**; Vol. 8, pp 28-32.
60. C. Pacholski, A. Kornowski and H. Weller, "Self-assembly of ZnO: From nanodots, to nanorods". *Angewandte Chemie-International Edition* **2002,** 41 (7), 1188-1191.
61. M. Ali and M. Winterer, "ZnO Nanocrystals: Surprisingly 'Alive'". *Chemistry of Materials* **2010,** 22 (1), 85-91.
62. T. Ma, M. Guo, M. Zhang, Y. J. Zhang and X. D. Wang, "Density-controlled hydrothermal growth of well-aligned ZnO nanorod arrays". *Nanotechnology* **2007,** 18 (3), 035605.
63. R. Tena-Zaera, J. Elias and C. Lévy-Clément, "ZnO nanowire arrays: Optical scattering and sensitization to solar light". *Applied Physics Letters* **2008,** 93 (23), 233119.
64. I. Gonzalez-Valls and M. Lira-Cantu, "Vertically-aligned nanostructures of ZnO for excitonic solar cells: a review". *Energy & Environmental Science* **2009,** 2 (1), 19-34.
65. L. E. Greene, M. Law, J. Goldberger, F. Kim, J. C. Johnson, Y. F. Zhang, R. J. Saykally, P. D. Yang and Qp, "Low-temperature wafer-scale production of ZnO nanowire arrays". *Angewandte Chemie-International Edition* **2003,** 42 (26), 3031-3034.
66. I. Gonzalez-Valls and M. Lira-Cantu, "Dye sensitized solar cells based on vertically-aligned ZnO nanorods: effect of UV light on power conversion efficiency and lifetime". *Energy & Environmental Science* **2010,** 3 (6), 789-795.
67. C. J. Murphy and N. R. Jana, "Controlling the aspect ratio of inorganic nanorods and nanowires". *Advanced Materials* **2002,** 14 (1).
68. B. Cheng and E. T. Samulski, "Hydrothermal synthesis of one-dimensional ZnO nanostructures with different aspect ratios". *Chemical Communications* **2004,** (8), 986-987.
69. O. Lupan, T. Pauporte, I. M. Tiginyanu, V. V. Ursaki, H. Heinrich and L. Chow, "Optical properties of ZnO nanowire arrays electrodeposited on n- and p-type Si(1 1 1): Effects of thermal annealing". *Materials Science and Engineering B-Advanced Functional Solid-State Materials* **2011,** 176 (16), 1277-1284.
70. J. S. Reparaz, F. Gueell, M. R. Wagner, G. Callsen, R. Kirste, S. Claramunt, J. R. Morante and A. Hoffmann, "Recombination dynamics in ZnO nanowires: Surfaces states versus mode quality factor". *Applied Physics Letters* **2010,** 97 (13).
71. J. S. Reparaz, F. Gueell, M. R. Wagner, A. Hoffmann, A. Cornet and J. R. Morante, "Size-dependent recombination dynamics in ZnO nanowires". *Applied Physics Letters* **2010,** 96 (5).
72. R. Heitz, C. Fricke, A. Hoffmann and I. Broser, "PICOSECOND ENERGY-TRANSFER BETWEEN EXCITONS AND DEFECTS IN II-IV SEMICONDUCTORS". *Proceedings of the 16th International Conference on Defects in Semiconductors, Pts 1-3* **1992,** 83, 1241-1246.
73. M. R. Wagner, G. Callsen, J. S. Reparaz, J. H. Schulze, R. Kirste, M. Cobet, I. A. Ostapenko, S. Rodt, C. Nenstiel, M. Kaiser, A. Hoffmann, A. V. Rodina, M. R. Phillips, S. Lautenschlaeger, S. Eisermann and B. K. Meyer, "Bound excitons in ZnO: Structural defect complexes versus shallow impurity centers". *Physical Review B* **2011,** 84 (3).
74. B. K. Meyer, J. Sann, S. Eisermann, S. Lautenschlaeger, M. R. Wagner, M. Kaiser, G. Callsen, J. S. Reparaz and A. Hoffmann, "Excited state properties of donor bound excitons in ZnO". *Physical Review B* **2010,** 82 (11).
75. Y. Kawakami, K. Omae, A. Kaneta, K. Okamoto, T. Izumi, S. Saijou, K. Inoue, Y. Narukawa, T. Mukai and S. Fujita, "Radiative and nonradiative recombination processes in GaN-based semiconductors". *Physica Status Solidi a-Applications and Materials Science* **2001,** 183 (1), 41-50.
76. S. K. Zhang, H. Lu, W. B. Wang, B. B. Das, N. Okoye, M. Tamargo and R. R. Alfano, "Radiative and nonradiative recombination processes in ZnCdSe/ZnCdMgSe multi-quantum-wells". *Journal of Applied Physics* **2007,** 101 (2).

77. J. Nissfolk, K. Fredin, A. Hagfeldt and G. Boschloo, "Recombination and transport processes in dye-sensitized solar cells investigated under working conditions". *Journal of Physical Chemistry B* **2006,** 110 (36), 17715-17718.
78. M. H. Huang, S. Mao, H. Feick, H. Q. Yan, Y. Y. Wu, H. Kind, E. Weber, R. Russo and P. D. Yang, "Room-temperature ultraviolet nanowire nanolasers". *Science* **2001,** 292 (5523), 1897-1899.
79. J. Elias, R. Tena-Zaera and C. Lévy-Clément, "Effect of the chemical nature of the anions on the electrodeposition of ZnO nanowire arrays". *Journal of Physical Chemistry C* **2008,** 112 (15), 5736-5741.
80. J. J. Wu and S. C. Liu, "Low-temperature growth of well-aligned ZnO nanorods by chemical vapor deposition". *Advanced Materials* **2002,** 14 (3), 215-+.
81. T. Yoshida, J. B. Zhang, D. Komatsu, S. Sawatani, H. Minoura, T. Pauporte, D. Lincot, T. Oekermann, D. Schlettwein, H. Tada, D. Wohrle, K. Funabiki, M. Matsui, H. Miura and H. Yanagi, "Electrodeposition of Inorganic/Organic Hybrid Thin Films". *Advanced Functional Materials* **2009,** 19 (1), 17-43.
82. L. Vayssieres, "Growth of arrayed nanorods and nanowires of ZnO from aqueous solutions". *Advanced Materials* **2003,** 15 (5), 464-466.
83. K. Govender, D. S. Boyle, P. B. Kenway and P. O'Brien, "Understanding the factors that govern the deposition and morphology of thin films of ZnO from aqueous solution". *Journal of Materials Chemistry* **2004,** 14 (16), 2575-2591.
84. Z. Y. Huang, C. F. Chai and B. Q. Cao, "Temperature-dependent emission shifts of peanutlike ZnO microrods synthesized by a hydrothermal method". *Crystal Growth & Design* **2007,** 7 (9), 1686-1689.
85. M. Lira-Cantu, F. C. Krebs and Dl, "Hybrid solar cells based on MEH-PPV and thin film semiconductor oxides (TiO2, Nb2O5, ZnO, CeO(2)and CeO2-TiO2): Performance improvement during long-time irradiation". *Solar Energy Materials and Solar Cells* **2006,** 90 (14), 2076-2086.
86. M. Lira-Cantu, K. Norrman, J. W. Andreasen, N. Casan-Pastor and F. C. Krebs, "Detrimental effect of inert atmospheres on hybrid solar cells based on semiconductor oxides". *Journal of the Electrochemical Society* **2007,** 154 (6), B508-B513.
87. M. Lira-Cantu and P. Gomez-Romero, "Electrochemical and chemical syntheses of the hybrid organic-inorganic electroactive material formed by phosphomolybdate and polyaniline. Application as cation-insertion electrodes". *Chemistry of Materials* **1998,** 10 (3), 698-704.
88. S.-E. Ahn, H. J. Ji, K. Kim, G. T. Kim, C. H. Bae, S. M. Park, Y.-K. Kim and J. S. Ha, "Origin of the slow photoresponse in an individual sol-gel synthesized ZnO nanowire". *Applied Physics Letters* **2007,** 90 (15).
89. Y. Shapira, S. M. Cox and D. Lichtman, "CHEMISORPTION, PHOTODESORPTION AND CONDUCTIVITY MEASUREMENTS ON ZNO SURFACES". *Surface Science* **1976,** 54 (1), 43-59.
90. G. Kenanakis, E. Stratakis, K. Vlachou, D. Vernardou, E. Koudoumas and N. Katsarakis, "Light-induced reversible hydrophilicity of ZnO structures grown by aqueous chemical growth". *Applied Surface Science* **2008,** 254 (18), 5695-5699.
91. X. J. Feng, L. Feng, M. H. Jin, J. Zhai, L. Jiang and D. B. Zhu, "Reversible super-hydrophobicity to super-hydrophilicity transition of aligned ZnO nanorod films". *Journal of the American Chemical Society* **2004,** 126 (1), 62-63.
92. S. N. Das, J. H. Choi, J. P. Kar and J. M. Myoung, "Tunable and reversible surface wettability transition of vertically aligned ZnO nanorod arrays". *Applied Surface Science* **2009,** 255 (16), 7319-7322.
93. M. K. Nowotny, L. R. Sheppard, T. Bak and J. Nowotny, "Defect chemistry of titanium dioxide. application of defect engineering in processing of TiO2-based photocatalysts". *Journal of Physical Chemistry C* **2008,** 112 (14), 5275-5300.
94. A. Moustaghfir, E. Tomasella, S. Ben Amor, M. Jacquet, J. Cellier and T. Sauvage, "Structural and optical studies of ZnO thin films deposited by rf magnetron sputtering: influence of annealing". *Surface & Coatings Technology* **2003,** 174, 193-196.
95. X. J. Wang, L. S. Vlasenko, S. J. Pearton, W. M. Chen and I. A. Buyanova, "Oxygen and zinc vacancies in as-grown ZnO single crystals". *Journal of Physics D-Applied Physics* **2009,** 42 (17).

96. D. C. Olson, S. E. Shaheen, R. T. Collins and D. S. Ginley, "The effect of atmosphere and ZnO morphology on the performance of hybrid poly(3-hexylthiophene)/ZnO nanofiber photovoltaic devices". *Journal of Physical Chemistry C* **2007,** 111 (44), 16670-16678.
97. X. Q. Wei, Z. G. Zhang, M. Liu, C. S. Chen, G. Sun, C. S. Xue, H. Z. Zhuang and B. Y. Man, "Annealing effect on the micro structure and photoluminescence of ZnO thin films". *Materials Chemistry and Physics* **2007,** 101 (2-3), 285-290.
98. M. Lira-Cantu, M. K. Siddiki, D. Munoz-Rojas, R. Amade and N. I. Gonzalez-Pech, "Nb-TiO2/polymer hybrid solar cells with photovoltaic response under inert atmosphere conditions". *Solar Energy Materials and Solar Cells* **2010,** 94 (7), 1227-1234.
99. D. Fu, X. L. Zhang, R. L. Barber and U. Bach, "Dye-Sensitized Back-Contact Solar Cells". *Advanced Materials* **2010,** 22 (38), 4270-+.
100. K. Keis, J. Lindgren, S. E. Lindquist and A. Hagfeldt, "Studies of the adsorption process of Ru complexes in nanoporous ZnO electrodes". *Langmuir* **2000,** 16 (10), 4688-4694.
101. E. Guillen, F. Casanueva, J. A. Anta, A. Vega-Poot, G. Oskam, R. Alcantara, C. Fernandez-Lorenzo and J. Martin-Calleja, "Photovoltaic performance of nanostructured zinc oxide sensitised with xanthene dyes". *Journal of Photochemistry and Photobiology a-Chemistry* **2008,** 200 (2-3), 364-370.
102. T. P. Chou, Q. Zhang and G. Cao, "Effects of dye loading conditions on the energy conversion efficiency of ZnO and TiO2 dye-sensitized solar cells". *Journal of Physical Chemistry C* **2007,** 111 (50), 18804-18811.
103. H. Horiuchi, R. Katoh, K. Hara, M. Yanagida, S. Murata, H. Arakawa and M. Tachiya, "Electron injection efficiency from excited N3 into nanocrystalline ZnO films: Effect of (N3-Zn2+) aggregate formation". *Journal of Physical Chemistry B* **2003,** 107 (11), 2570-2574.
104. N. R. Neale, N. Kopidakis, J. van de Lagemaat, M. Gratzel and A. J. Frank, "Effect of a coadsorbent on the performance of dye-sensitized TiO2 solar cells: Shielding versus band-edge movement". *Journal of Physical Chemistry B* **2005,** 109 (49), 23183-23189.
105. A. Otsuka, K. Funabiki, N. Sugiyama, H. Mase, T. Yoshida, H. Minoura and M. Matsui, "Design and synthesis of near-infrared-active heptamethine-cyanine dyes to suppress aggregation in a dye-sensitized porous zinc oxide solar cell". *Chemistry Letters* **2008,** 37 (2), 176-177.
106. E. Hosono, Y. Mitsui and H. S. Zhou, "Metal-free organic dye sensitized solar cell based on perpendicular zinc oxide nanosheet thick films with high conversion efficiency". *Dalton Transactions* **2008,** (40), 5439-5441.
107. D. P. Hagberg, T. Marinado, K. M. Karlsson, K. Nonomura, P. Qin, G. Boschloo, T. Brinck, A. Hagfeldt and L. Sun, "Tuning the HOMO and LUMO energy levels of organic chromophores for dye sensitized solar cells". *Journal of Organic Chemistry* **2007,** 72 (25), 9550-9556.
108. P. Qin, H. Zhu, T. Edvinsson, G. Boschloo, A. Hagfeldt and L. Sun, "Design of an organic chromophore for p-type dye-sensitized solar cells". *Journal of the American Chemical Society* **2008,** 130 (27), 8570-+.
109. G. Boschloo, T. Marinado, K. Nonomura, T. Edvinsson, A. G. Agrios, D. P. Hagberg, L. Sun, M. Quintana, C. S. Karthikeyan, M. Thelakkat and A. Hagfeldt, "A comparative study of a polyene-diphenylaniline dye and Ru(dcbpy)2(NCS)2 in electrolyte-based and solid-state dye-sensitized solar cells". *Thin Solid Films* **2008,** 516 (20), 7214–7217.
110. H. M. Nguyen, R. S. Mane, T. Ganesh, S. H. Han and N. Kim, "Aggregation-Free ZnO Nanocrystals Coupled HMP-2 Dye of Higher Extinction Coefficient for Enhancing Energy Conversion Efficiency". *Journal of Physical Chemistry C* **2009,** 113 (21), 9206-9209.
111. D. P. Hagberg, T. Edvinsson, T. Marinado, G. Boschloo, A. Hagfeldt and L. Sun, "A novel organic chromophore for dye-sensitized nanostructured solar cells". *Chemical Communications* **2006,** (21), 2245-2247.
112. R. M. El-Shishtawy, "Functional Dyes, and Some Hi-Tech Applications". *International Journal of Photoenergy* **2009**.
113. K. Hara, T. Sato, R. Katoh, A. Furube, Y. Ohga, A. Shinpo, S. Suga, K. Sayama, H. Sugihara and H. Arakawa, "Molecular design of coumarin dyes for efficient dye-sensitized solar cells". *Journal of Physical Chemistry B* **2003,** 107 (2), 597-606.

114. T. Horiuchi, H. Miura, K. Sumioka and S. Uchida, "High efficiency of dye-sensitized solar cells based on metal-free indoline dyes". *Journal of the American Chemical Society* **2004,** 126 (39), 12218-12219.
115. E. Guillen, C. Fernandez-Lorenzo, R. Alcantara, J. Martin-Calleja and J. A. Anta, "Solvent-free ZnO dye-sensitised solar cells". *Solar Energy Materials and Solar Cells* **2009,** 93 (10), 1846-1852.
116. R. Katoh, A. Furube, S. Mori, M. Miyashita, K. Sunahara, N. Koumura and K. Hara, "Highly stable sensitizer dyes for dye-sensitized solar cells: role of the oligothiophene moiety". *Energy & Environmental Science* **2009,** 2 (5), 542-546.
117. A. Otsuka, K. Funabiki, N. Sugiyama and T. Yoshida, "Dye sensitization of ZnO by unsymmetrical squaraine dyes suppressing aggregation". *Chemistry Letters* **2006,** 35 (6), 666-667.
118. T. Trupke, P. Wurfel and I. Uhlendorf, "Dependence of the photocurrent conversion efficiency of dye-sensitized solar cells on the incident light intensity". *Journal of Physical Chemistry B* **2000,** 104 (48), 11484-11488.
119. J. A. Barker, C. M. Ramsdale and N. C. Greenham, "Modeling the current-voltage characteristics of bilayer polymer photovoltaic devices". *Physical Review B* **2003,** 67 (7), 075205
120. H. J. Snaith, L. Schmidt-Mende, M. Gratzel and M. Chiesa, "Light intensity, temperature, and thickness dependence of the open-circuit voltage in solid-state dye-sensitized solar cells". *Physical Review B* **2006,** 74 (4).
121. M. Toivola, L. Peltokorpi, J. Halme and P. Lund, "Regenerative effects by temperature variations in dye-sensitized solar cells". *Solar Energy Materials and Solar Cells* **2007,** 91, 1733-1742.
122. M. Berginc, U. O. Krasovec, M. Jankovec and M. Topic, "The effect of temperature on the performance of dye-sensitized solar cells based on a propyl-methyl-imidazolium iodide electrolyte". *Solar Energy Materials and Solar Cells* **2007,** 91 (9), 821-828.
123. L. Andrade, S. M. Zakeeruddin, M. K. Nazeeruddin, H. A. Ribeiro, A. Mendes and M. Gratzel, "Influence of Sodium Cations of N3 Dye on the Photovoltaic Performance and Stability of Dye-Sensitized Solar Cells". *Chemphyschem* **2009,** 10 (7), 1117-1124.
124. K. Ocakoglu, F. Yakuphanoglu, J. R. Durrant and S. Icli, "The effect of temperature on the charge transport and transient absorption properties of K27 sensitized DSSC". *Solar Energy Materials and Solar Cells* **2008,** 92 (9), 1047-1053.
125. L. M. Peter, A. B. Walker, G. Boschloo and A. Hagfeldt, "Interpretation of apparent activation energies for electron transport in dye-sensitized nanocrystalline solar cells". *Journal of Physical Chemistry B* **2006,** 110 (28), 13694-13699.
126. H. G. Agrell, J. Lindgren and A. Hagfeldt, "Degradation mechanisms in a dye-sensitized solar cell studied by UV-VIS and IR spectroscopy". *Solar Energy* **2003,** 75 (2), 169-180.
127. R. D. Sun, A. Nakajima, A. Fujishima, T. Watanabe and K. Hashimoto, "Photoinduced surface wettability conversion of ZnO and TiO2 thin films". *Journal of Physical Chemistry B* **2001,** 105 (10), 1984-1990.
128. M. K. Nazeeruddin, S. M. Zakeeruddin, R. Humphry-Baker, M. Jirousek, P. Liska, N. Vlachopoulos, V. Shklover, C. H. Fischer and M. Gratzel, "Acid-base equilibria of (2,2 '-bipyridyl-4,4 '-dicarboxylic acid)ruthenium(II) complexes and the effect of protonation on charge-transfer sensitization of nanocrystalline titania". *Inorganic Chemistry* **1999,** 38 (26), 6298-6305.
129. K. Nonomura, Y. Xu, T. Marinado, D. P. Hagberg, R. Zhang, G. Boschloo, L. Sun and A. Hagfeldt, "The Effect of UV-Irradiation (under Short-Circuit Condition) on Dye-Sensitized Solar Cells Sensitized with a Ru-Complex Dye Functionalized with a (diphenylamino)Styryl-Thiophen Group". *International Journal of Photoenergy* **2009**.
130. F. Verbakel, S. C. J. Meskers and R. A. J. Janssen, "Surface modification of zinc oxide nanoparticles influences the electronic memory effects in ZnO-polystyrene diodes". *Journal of Physical Chemistry C* **2007,** 111 (28), 10150-10153.